GAS DISCHARGES CONFINED BY METALLIC WALLS

Natalie Anne Ridge

A Thesis Submitted for the Degree of PhD
at the
University of St Andrews

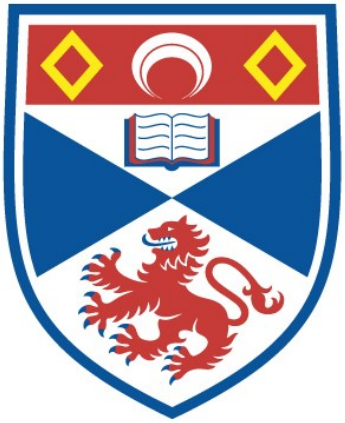

1992

GAS DISCHARGES CONFINED BY METALLIC WALLS.

A THESIS PRESENTED BY
NATALIE ANNE RIDGE
TO THE UNIVERSITY OF ST. ANDREWS
FOR THE DEGREE OF
DOCTOR OF PHILOSOPHY.
MAY 1991.

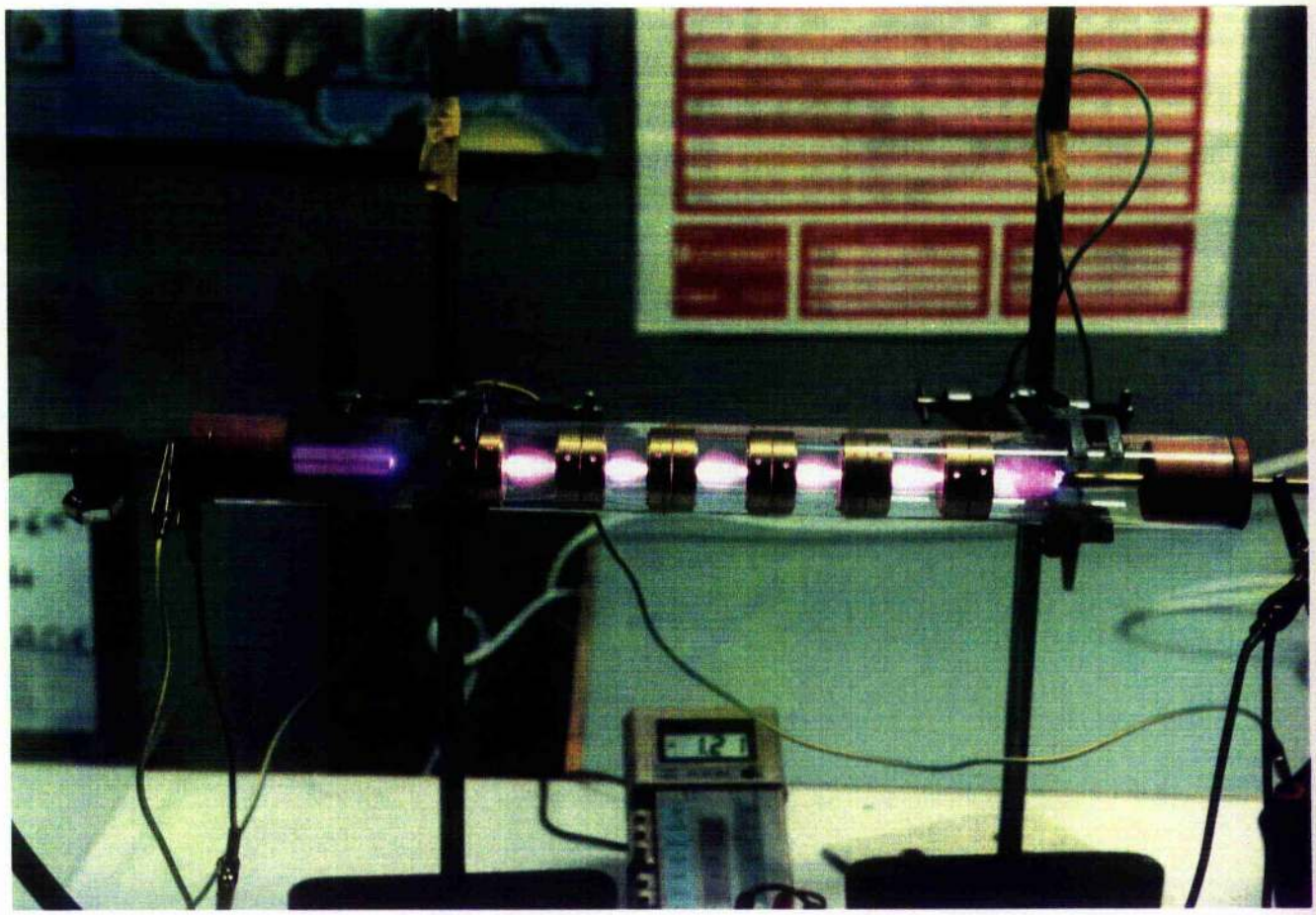

Glow discharge in air, confined by brass 'plugs'. (Chapter 7.)
The positive column is pink and the negative glow is purple.

COPYRIGHT

DECLARATION

I, Natalie Anne Ridge, hereby certify that this thesis has been composed by myself, that it is a record of my own work, and that it has not been accepted in partial or complete fulfilment of any other degree or professional qualification.

Signed Date 27th May 1991

I was admitted to the Faculty of Science of the University of St. Andrews under Ordinance General No 12 in October 1985 and as a candidate for the degree of Ph.D. in October 1986.

Signed Date 27th May 1991

CERTIFICATE.

I hereby certify that the candidate has fulfilled the conditions of the Resolution and Regulations appropriate to the Degree of Ph.D.

Signature of Supervisor Date

27 May 91

ACKNOWLEDGEMENTS

I would like especially to thank Arthur Maitland for his support, encouragement, and financial acumen throughout this work. Also all the technicians in the Mechanical and Electronic Workshops for their expert advice, and Frits for his glass blowing skills. Thanks to all the rest of LASER 1/AM, especially Andy, Graeme, Ian, Chris and Ewan, to the "boys" from EEV and to David and Peter for doing the proof-reading. I also wish to say thank you for the encouragement given by my parents and brothers, and to Tony for being patient with me. I am grateful to the SERC for their funding, to EEV for their generous contributions to the research and to Dave Parkes.

AUTHOR'S CAREER

The author was born in Burnley, Lancashire in 1962. She attended Southport High School for Girls from 1973 to 1980. In 1984 she obtained a B.Sc. in Astronomy, Astrophysics, and Physics at the University of St. Andrews. In 1985 she attended the taught M.Sc. in Optoelectronic and Laser devices, given jointly by the Universities of St. Andrews and Heriot-Watt, and graduated in 1986. She then began work on a Ph.D. degree in the Physics department of the University of St. Andrews. Since 1988 she has worked as a Research Assistant, funded by RSRE. Natalie is an Associate Member of the Institute of Physics.

DEDICATION

I dedicate this thesis to

Mum, Dad, Andrew, Michael

and to Tony.

Thank you.

ABSTRACT

This thesis describes experimental and theoretical aspects of low pressure gas discharges confined by metallic walls. Simple considerations predict that the current between the anode and the cathode of a discharge tube which contains isolated cylindrical metal segments is conducted through the metal. Under certain conditions, however, a glow discharge may form along the axis of the tube: conduction occurs along the path which results in the lowest sustaining voltage.

The energy losses at insulating and conducting walls in the region of the positive column are investigated theoretically for rare gas discharges at high current densities. The energy losses are found to be greater when the walls are conducting, resulting in a higher axial electric field.

A possible criterion for the maximum length of a metal segment is proposed. The maximum length may be defined as the length at which the radial electric field in the positive ion sheath at one end of a metal segment is equal to the breakdown field.

A relationship between the maximum length of a metal segment and the tube radius and pressure has been derived. The form of this relationship agrees qualitatively with experimental results.

Measurements of the anode-cathode breakdown voltage of a gas in a tube containing metal segments of small bore are presented. The anode-cathode breakdown voltage is found to

be approximately equal to the sum of the breakdown voltages of the inter-segment and electrode-segment gaps. When the system is operating on the left of the Paschen minimum, the anode-cathode breakdown voltage may be increased by the addition of metal segments in such away as to reduce the effective gap. Individually the product's of pressure and inter-segment gap (pd) are less than the product $(pd)_{min}$ at the Paschen minimum. Hence, the anode-cathode breakdown voltage will increase as the number of gaps (and segments) increases and pd decreases.

Discharges in dual-bore (alternate narrow and wide bore) metal tubes have been investigated. The anode-cathode breakdown voltages and sustaining voltages of low current density discharges, confined by dual-bore tubes of various lengths, are shown to depend upon the system geometry.

A laser system using dual-bore metal discharge tubes, has been designed and tested for producing high current densities in rare gas - metal vapour mixtures.

CONTENTS

CHAPTER 1.

INTRODUCTION.

1.1) Introduction.

The discharges considered in this work are wall stabilised gas discharges. The positive column is the region of interest. The main difference between insulating and conducting walled tubes, in the region of the positive column, is shown in figure (2.1). In insulating tubes the wall potential relative to the plasma/sheath boundary is constant (section 2.2). In a tube with conducting walls, this is not the case, as the metal assumes an equipotential relative to the cathode. The potential difference across the sheath decreases (for conducting walls), as the potential of the plasma (relative to the anode), becomes more negative on moving from the anode end to the cathode end of the metal segment.

1.2) History.

Work on discharges in tubes with conducting walls began in the early part of the century. John Zeleny (1938) published work in which he compared the appearance of glow discharges, in hydrogen and air, in insulating and conducting tubes. The conducting tubes were formed of cylinders of fine mesh brass gauze, contained within a glass tube which acted as the vacuum envelope. Wires attached to the cylinders allowed measurements of tube potential and of

the current between adjacent cylinders. Other probes allowed the measurement of potential between striae. He noted that the diameter of the striae at the cathode end were nearly equal to the cylinder diameter and that the diameter of the striae progressivly decrease towards the anode end. This decrease in diameter of the striae is due to an increase in the thickness of the positive ion sheath (see section 2.8). The diameter also depends on the magnitude of the current, and decreases as the current decreases. The striae became more closely spaced towards the anode end which is indicative of an increase in the axial electric field.

In one experiment Zeleny observed the discharge as the current was increased, at constant pressure and with only a slight variation in the discharge voltage. Initially all the current flowed through the tube walls. Discharges were observed between the anode and the adjacent end of the cylinder and between the cathode and the other end of the cylinder. On increasing the current, a point of instability was reached whereby the current split between the walls and the gas. The onset of instability occured when the potential fall in the gas along the axis of the gauze cylinder was equal to the sum of the two falls at the surface of the metal. Eventually the glow extended down the whole cylinder. Current measurements indicated that only a small fraction of the current then flowed through the walls of the cylinder.

There seems to have been little interest in metal walled tubes for the next 25 years or so, until the advent of the argon ion laser. It was found that as higher powers were reached, quartz and ceramic tubes suffered

deterioration, sometimes catastrophic, due to ion bombardment and/or poor thermal shock qualities. It became necessary to look at other materials. The most obvious choices were metals. Metals have good thermal conductivities and thermal shock properties, and are less easily damaged by sputtering, which in this case leads only to the transport of material, rather than decomposition.

J.D Rigden (1965) was the first to report using a demountable, segmented metal discharge tube for an argon ion laser, closely followed by Labuda et al. (1965). Rigden built a tube of fourteen aluminium discs, each of 12.5 mm length, with a 3 mm hole, for the discharge, at the centre. Twelve holes, situated around the central hole, were used for water cooling and for bolting the structure together. The discs were insulated from each other by inserting 0.5 mm thick Delrin gaskets. Water and vacuum seals were made with Viton A O-rings. The tube was operated continuously for 20 hours on one fill of argon. A current of 30 amps produced an output power of 800 milliwatts. Higher powers could be obtained for only short periods due to overheating of the anode glass-to-metal seal.

Labuda et al.(1965) note that there is a possibility of operating the tubes at a high enough temperature for cooling via radiation to occur. They also show that the total electron current and ion current to a conducting wall is zero. The wall assumes a negative potential with respect to the plasma, and is separated from it by a positive ion sheath. They suggest two factors which may limit the maximum usable length of a metal segment. Firstly, that the

thickness of the sheath should not exceed the bore radius, and secondly that the voltage drop along the axis should not exceed that necessary for cold cathode formation. Under the operating conditions encountered in the argon ion laser, the maximum length is found experimentally to be 5 cm for a 1 mm bore tube.

Results indicated no difference in potential drop, or threshold current in combinations of 1 mm and 2 mm bore, segmented tubes (segment length not given, though probably 25 mm). The most successful design was one of 3 inch diameter vacuum-fired molybdenum discs contained within a quartz envelope, cooled by thermal radiation. A large diameter, large emissivity, and good thermal conductivity are desirable to operate tubes with radiative cooling. Two tubes were constructed of total length 25 cm and 1 and 2 mm bores. These tubes were operated at 10 and 40 amps, respectively, producing output powers of 0.25 and 1.0 watt. The currents used were twice the safe value normally passed through quartz tubes. Sputtering problems were encountered due to the potential drops between adjacent segments.

Paananen et al. (1965) used metal and coated metal. Metal segments were used which were insulated from one another by O-rings, glass or ceramic washers, contained within a quartz envelope. The segments had extra holes bored in them to provide an internal gas return. This design eventually yielded a unit whereby metal and ceramic sections were brazed together to form the vacuum jacket. The other method that was pursued was the use of long aluminium tubes

coated with aluminium oxide.

There appears to be little difference in general operation between these metal-walled tubes, and those with insulating walls. The only difference of note is difficulty in initiating a discharge when conducting walls are used. This difficulty is due to lack of field penetration into the segments.

J.V. Parker (1967) reported the use of a segmented metal structure to produce a reliable 2 watt argon ion laser, and compared its operating characteristics with those of conventional tubes.

Hernqvist and Fendley (1967) produced the first theory associated with a tube with conducting walls. They used Tonks-Langmuir free-fall theory, and energy balance considerations for a tube with insulating walls, to calculate a relationship between the axial field X, and the tube radius, in a conventional argon ion discharge. They went on to show that the average plasma-wall potential is larger when metal segments are used. Conversely, for short segments of length L, (provided $eXL/kT_e < 2$, where T_e is the electron temperature.), the increase in the axial electric field over that in a ceramic tube is less than 2 %. They also compared tantalum, molybdenum and high purity graphite segments, of length 9 mm and bore 1.2 mm, in the same argon discharge column, at a current of 5 amps. The life test lasted 10 hours. Laser operation ceased due to obstruction of the bore. The tantalum segments had been widened at the anode end and had, by material deposition, been narrowed at the cathode end. The molybdenum segments showed a small

amount of similar damage. The graphite was undamaged, except in the vicinity of the metal segments, where material build up occured from metal sputtered off the adjacent segments. This is due to the high sputtering threshold and low sputtering yield of graphite.

Further theoretical work by Maitland (1969), calculates the maximum length of a metal segment in an established DC discharge. This is achieved by equating the electron and ion currents to the tube walls (see section (2.3.1)) using a constant ion current model, and assuming that no part of the segment should become positive. The criterion is that the plasma-wall potential difference at the cathode end becomes zero. He finds

$$d_{max} = (kT_e/eX)(2m_+/\pi m_e)^{1/2},$$

which for argon becomes

$$d_{max} = 1.86 \times 10^{-2}(T_e/X),$$

where X is the axial electric field, and T_e is the electron temperature.

The maximum length of a metal segment, as a function of external electric and magnetic fields applied to the segments, was discussed. An axial magnetic field reduces the maximum segment length attainable. Biasing the segments electrically did not appear to be advantageous (but see Stangeby and Allen, 1971, on the "Plasma state current amplifier."). Negative biasing would lead to damage of the

segments by ion bombardment and positive biasing could lead to ionisation of the neutral gas in the sheath region, thus causing breakdown. The problems of discharge initiation were also discussed. Two remedies suggested were the application of RF fields (60 GHz for a 4 mm bore), and the use of a plasma jet as a cathode, as preionisers.

Maitland and Cornish (1972) measured the electron temperatures in a segmented aluminium, argon ion laser. They used two of the segments as a floating double probe. Electron temperatures of $2 - 6 \times 10^4$ K were measured at pressures of 0.1 - 1.0 torr and current densities of 70 - 300 amps/cm^2. They concluded, from the probe characteristics, that the ion current density at the tube walls should be governed by a Boltzmann factor rather than have a constant value.

Further work by Cornish and Maitland (1975) compared various ion current models, which are a function of the potential across the positive ion sheath between the plasma and the walls. In each case (apart from the constant ion current model) the total current to the wall was greater for a conducting wall than for an insulating wall of the same length. This implies that the electric field must increase in order to maintain particle continuity. They obtained expressions for the field, and found that in the limit, as the length of the conducting wall decreases, the expressions for the axial fields in ceramic and metal tubes become equal. Using the ion wall current with a Boltzmann dependence, they calculated the maximum length of a metal segment.

For argon this is

$$d_{max} = 3.3 \times 10^{-4}(T_e/X).$$

This is much smaller than the value calculated using a constant ion wall current. These two expressions represent the two extremes that are likely to be encountered. (The constant ion current model is considered throughout this work).

More recent work by Clark and Maitland (1987), concerns the use of metal tubes in copper vapour lasers (CVL). Generally alumina tubes are used for discharge confinement. These cause problems due to outgassing of contaminants, which reduce the output power. Tube sag may also occur through overheating. Refractory metals have higher softening points and do not contaminate the discharge. In this case, rolls of molybdenum foil, held by alumina rings, provide the discharge boundary. They are contained within an alumina tube, which is not in direct contact with the plasma. Concentric molybdenum "tubes" are placed within each other, with zirconia felt sandwiched between the foil to provide insulation. Further layers of foil may be added, to reduce the diameter without altering the thermal conductivity, and obtain the optimum output power.

A novel, low temperature CVL, reported by Livingstone and Maitland (1989), is constructed out of copper cylinders, insulated from each other by alumina rings and contained in a quartz tube with a pyrex water jacket. Copper is made in situ, by flowing a mixture of helium or neon with

chlorine or bromine, slowly through the tube. The CuBr/CuCl produced then dissociates in the discharge to give free copper. Output powers in the region of 18 W (Cl_2) - 22 W (Br_2) have been obtained.

References.

J. Zeleny. "On the role of tube walls, and surface and space charges in electrical discharges through rarefied gases." Journal of the Franklin Institute. 226, 1938, p 35.

J.D. Rigden. " A metallic plasma tube for ion lasers." IEEE J. Quant. Elec., Vol. QE-1, 1965, p 221.

E.F. Labuda, E.I. Gordon, R.C. Miller. "Continuous-duty argon ion lasers". IEEE J. Quant. Elec., Vol. QE-1, No. 6, 1965, p 273.

R.A. Paananen, A.Adams Jr., D.T. Wilson. "Characteristics of metal wall ionised argon lasers." NEREM Record, 1965, p 238.

J.V. Parker. "Metal apperture lasers" 13th Annual International Electron Devices Meeting, October 18-20 1967.

K.G. Hernqvist, J.R. Fendley Jr. "Construction of long life argon lasers." IEEE J. Quant. Elec., Vol. QE-3, No. 2, 1967, p 66.

A. Maitland. "Theory of segmented metal discharge tubes for argon lasers." J. Phys D, Appl. Phys., Vol 4, 1971, p 907.

A. Maitland, J.C.L. Cornish. "Electron temperatures in a segmented-metal argon-ion laser." J. Phys. D, Appl. Phys., Vol 5, 1972, p 1807.

P.C. Stangeby, J.G. Allen. "Plasma state current amplifier." Nature Physical Science, Vol 233, Sep 1971, p 26.

J.C.L. Cornish, A. Maitland. "High current discharges in segmented metal tubes." J. Phys. D, Appl. Phys., Vol 6, 1973, p 1899.

G.L. Clark, A. Maitland. "A copper vapour laser using metallic walls for discharge confinement." J. Phys. E, Sci. Instrum., 20, 1987, p 80.

E.S. Livingstone, A. Maitland. "A low temperature, segmented metal, copper vapour laser." J. Phys. E, Sci. Instrum., 22, 1989, p 63.

CHAPTER 2.

THE THEORY OF SEGMENTED METAL DISCHARGE TUBES.

2.1) Introduction.

The discharge tube considered consists of a vacuum envelope within which there is an anode and a cathode. The tube imposes the boundary conditions and determines the current density of a discharge established between the electrodes. The tube generally consists of insulating material, such as quartz or alumina, but these have maximum wall temperatures of about 1000°C and 1800°C, respectively. When the noble gas ion lasers (Ar^+, Kr^+, Ne^+) were first tested it was found that the output power attainable was limited, not by power supply problems, but by tube failure.

At the high current densities at which rare-gas ion lasers operate (> 500 amps/cm^2), ceramic tubes may start to deteriorate. Material decomposition occurs due to ion bombardment. Decomposition products can lead to cathode poisoning and discharge tubes with very short lifetimes. Sheindlin and Asinovskii (1963) produced (non-laser) gas discharges in tubes containing metal sections. The first published work of a segmented metal tube applied to a laser discharge was by J D Rigden (1965).

Metals have advantages over ceramics in that they have better heat exchange properties, that is, they are able to dissipate large powers without deterioration, and they are less likely to crack (at high temperatures) due to thermal shock. Ion bombardment does not lead to material

decomposition as it does with ceramic tubes, and the sputtered metal is merely transfered by the gas to another part of the tube. Metals are also far more robust and can be machined easily to any chosen geometry.

Metal discharge tubes necessarily consist of segments separated by insulators. The use of metal to confine the discharge allows higher current densities with higher gas temperatures to be obtained. It is shown below that the segments have a maximum usable length, which if exceeded results in the discharge running through the metal of the segments and through randomly sited arcs between them. At lengths less than the maximum it is possible to run a discharge in the gas along the axis of the segments. It has been found experimentally that the maximum segment length increases as the radius of the segment increases.

2.2) Potentials in the discharge tube.

Figure (2.1a) shows the potential distribution, in the positive column (Appendix 1), along the axis of a ceramic (insulator) discharge tube. A radial potential gradient is produced by ambipolar diffusion of electrons and ions towards the walls (Appendix 1.). As the tube is electrically isolated from external sources of potential (floating), the net charge of the particles arriving at the wall must be zero in the steady state. When the discharge is first initiated, the electrons, because of their higher mobility, arrive at the wall first, charging it negatively. The positive ions then establish a space charge sheath between

the plasma and the wall. Only the fastest electrons are now able to reach the wall, and this electron current is equal to the ion current. A ceramic tube has low electrical conductivity, therefore charge neutralisation at the surface may only be affected at points very close to where the charges arrive, so the local electron and ion currents at the wall are constrained to be equal.

In the case of a segmented metal tube, figure (2.1b), the above constraint on the local electron and ion currents is not applicable. In this case it is the total currents to the whole segment which are the same. The segment attains a negative potential with respect to the plasma, as in the case of a ceramic tube, but because the segment is made of metal, an equipotential surface is produced relative to the cathode (earth) potential. However, the potential relative to the plasma is not constant along the length of the segment. There is a net flow of electrons to the metal at the cathode end of the segment and a net flow of ions at the anode end. There is a boundary region, that is a thin line, at which the ion and electron currents are equal and at this line the segment has the same potential $V_{w\infty}$, with respect to the plasma, that a ceramic walled tube would have.

2.3) The constant ion current model.(Maitland 1971)

2.3.1) The wall currents.

We may assume that the ion current density at the wall is determined solely by the rate of arrival of ions at the sheath edge, as there are no ionising collisions within the sheath. The sheath thickness is small (less than 0.1 mm under argon ion laser discharge conditions), and we may take the sheath area as approximately equal to the area of the wall. The electron density assumes a Boltzmann distribution within the sheath leading to an overall positively charged region adjacent to the tube walls. This leads to the ion current model of Chen (1965).

The mean thermal velocity of a particle is given by,

$$v = (8kT/\pi m)^{1/2}. \qquad (2.3.1)$$

The ion current density, j_+, is given by,

$$j_+ = (en/2)(kT_e/m_+)^{1/2}. \qquad (2.3.2)$$

and the electron current density, j_-, by,

$$j_- = (env_-/4)\exp(-|eV|/kT_e), \qquad (2.3.3)$$

where n is the electron/ion number density at the sheath-plasma boundary (ignoring any pre-sheath region) and V is the potential of the wall relative to the plasma. (See

Appendix 3 for theory relating the ion current to the electron temperature T_e.)

The electron and ion currents to a floating collector of small dimensions are equal. Consequently, in the case of a ceramic tube, we find from equations (2.3.2) and (2.3.3) that the wall potential V_w is given by,

$$|V_w| = (kT_e/2|e|)\log_e(2m_+/\pi m_e). \qquad (2.3.4)$$

For argon, $|V_w|_{Ar}$ is $4.6\times10^{-4}T_e$.

The ion current is independent of the segment potential, and it may be assumed that the ion current to a metal segment is the same at all points along its length. For a metal segment of length L, we must equate the total electron and ion currents to the segment. From (2.3.2) and (2.3.3) we find,

$$(enL/2)((kT_e)/m_+)^{1/2} = (nev_e/4)\int_0^L \exp(-|eV(x)|/kT_e)dx. \qquad (2.3.5)$$

We define $|V(x)|$ as the potential of the segment relative to the plasma, at the point x. The point x=0 is taken as the anode end of the segment and the point x=L as the cathode end. Thus, we may write $|V(x)|$ as,

$$|V(x)| = |V(0)| - |X|x, \qquad (2.3.6)$$

where X is the axial electric field, assumed constant within the plasma. (Observations of glow discharges indicate an increase in the axial electric field towards the anode end

of the segment, due to an increase in thickness of the positive ion sheath (see section 2.8). In a high current density discharge the sheath thickness is a lot less than the tube radius. In this case the increase in sheath thickness has a negligible effect on the field, and as a first approximation we may assume a constant electric field along the length of the segment.)

Integrating equation (2.3.5) with

$$d|V(x)| = -|X|dx,$$

and the limits $|V(0)|$ and $|V(L)| = |V(0)|-L|X|$, we get,

$$(\pi m_e/2m_+)^{1/2}(c|X|L) = \exp(-|cV(0)|)\{\exp(|cXL|)-1\}, \quad (2.3.7)$$

where c is given by, $c=e/kT_e$.

2.3.2) Maximum length of a metal segment in an established DC discharge.

We may estimate the maximum length of a segment by setting V(L)=0. In the case under consideration (Argon ion laser), the ion temperature is of the order of 1eV (Kitaeva et al. 1970). If the segment acquires a positive potential of this order, the ion current is likely to be reduced to zero, and the electron and ion currents to the walls would no longer be equal. Thus, we may state the criterion that the maximum length of a metal segment is such that, no part of the segment should become positive with respect to the plasma.

The point where the segment and the plasma have the same potential (relative to the cathode), gives the maximum segment length, the ion sheath thickness is now zero and the segment is in direct contact with the plasma.
From equation (2.3.6) we find $|V(0)|=|X|L_{max}$ and substituting this into (2.3.7), we get,

$$1+|cX|L_{max}(\pi m_e/2m_+)^{1/2}\exp(|cX|L_{max}) = \exp(|cX|L_{max}). \quad (2.3.8)$$

Equation (2.3.8) is of the form $1+ZA\exp(Z)=\exp(Z)$ and since we have $ZA\exp(Z)>>1$, the expression may be reduced to $Z=1/A$. Therefore, we can write,

$$L_{max} = (kT_e/|eX|)(2m_+/\pi m_e)^{1/2}, \quad (2.3.9)$$

which gives the maximum segment length for an established axial discharge. Equation (2.3.9) shows that the maximum segment length is dependent on the electron temperature and the axial electric field in the plasma. Experiment shows that the lengths obtained are only correct to an order of magnitude.

2.3.3) Equivalence of wall potentials in ceramic and metal tubes.

We may substitute for V(0) in equation (2.3.7) from (2.3.6) and we obtain,

$$\exp(|c|[|V(x)|+x|X|]) = M(\exp(Y) - 1)/Y, \quad (2.3.10)$$

where $Y=|cX|L$, and $M=(2m_+/\pi m_-)^{1/2}$. The value of M is approximately 216 for Argon. From (2.3.4) and (2.3.10) we can find the position x, along a metal segment where we have V(x) equal to V_w, provided we know the lengths of the segments, the axial electric field and the electron temperature. Thus we find,

$$x/L = \log_e\{(\exp(Y) - 1)/Y\}/Y, \qquad (2.3.11)$$

which is plotted in figure (2.2). (See Appendix 8 for the case where the electron temperatures, of discharges in metal and ceramic tubes, are not the same.) The points are calculated from the data given in table (2.1), page 25 (Cornish and Maitland 1973). It can be seen from figure (2.2) that x/L is always greater than or equal to 0.5. In other words, the point along the segment at which its potential relative to the plasma is equivalent to that of a ceramic tube, is always closer to the cathode end of the segment than the anode end. Figure (2.3) shows this for the case $T_e=39\times10^3$K, L=2.5cm and X=456V/m, (point(2) in figure (2.2)).

[To show that equation (2.3.11) goes to 0.5 as Y goes to 0. When Y is small we may expand the exponential in (2.3.11) to give,

$$x/L \approx \log_e\{1 + Y + Y^2/2 + \ldots - 1)/Y\}/Y,$$

$$\approx \log_e\{1 + Y/2 + \ldots\}/Y.$$

Expanding the logarithm,

$$x/L \approx (Y/2)/Y = 0.5 \quad].$$

2.4) The Energy Balance equation.

For the case of the high current density DC discharges under consideration, Hernqvist and Fendley (1967) assumed that the major energy loss to the system is from electrons and ions losing their kinetic and ionisation energies to the walls. They used this assumption to obtain an energy balance equation, in the positive column of the discharge, for a tube with insulating walls. We have estimated the electron and ion number densities in the plasma by equating the energy input to the energy lost at the walls; initially in the case of a ceramic tube and then for a metal tube. This shows that the energy input to a discharge in a metal tube is always greater than or equal to that in a ceramic tube, at the same pressure and current.

In equilibrium, we have

power input = power lost to the walls.

The major energy losses to the walls are:-
eV_w' is the kinetic energy delivered to the wall by each ion after falling through the sheath, and includes the initial energy of the ions, in the direction of the wall, at the plasma-sheath boundary ($\sim kT_e$). This is the directed energy gained in the presheath region (see appendix 3). Therefore, we have

$$eV_w' = eV_w + kT_e \equiv eV_w + e/c.$$

eV_i is the recombination energy of the electrons and ions. eV_e is the average energy of the electrons reaching the wall ($\sim 2kT_e$). (Killian 1930).

For a tube with insulating walls, assuming a uniform axial electric field, we find,

$$I_a|X_w|L = 2\pi R(j_+|V_w'| + j_+|V_i| + j_e|V_e|)L, \qquad (2.4.1)$$

where I_a is the (axial) discharge current, and L is the length of the positive column. This becomes,

$$I_a|X_w| = 2\pi R j_+(|V_w'| + |V_i| + |V_e|), \qquad (2.4.2)$$

as the electron and ion currents to a floating insulator,(the walls) are equal, as discussed in section (2.2).

We obtain a similar expression to (2.4.2), for a metal tube, which takes into account the fact that the potential difference across the sheath increases as we move from the cathode end to the anode end of the metal segment. We write the energy balance equation, for a metal segment of length L, as,

$$I_a|X_m|L = 2\pi R(j_+(L/c) + \int_0^L j_+|V(x)|dx + j_+|Vi|L + \int_0^L j_e|V_e|dx), \qquad (2.4.3)$$

but, as the total electron current to the wall is equal to the total ion current, we have

$$\int_0^L j_- dx = \int_0^L j_+ dx = j_+ L,$$

as j_+ is a constant.

Equation (2.4.3) becomes,

$$I_- |X_-| L = 2\pi R(j_+ L\{|V_i| + |V_-| + 1/c\} + j_+ \int_0^L |V(x)| dx). \qquad (2.4.4)$$

Using equation (2.3.6), (2.4.4) becomes,

$$I_- |X_-| = 2\pi R j_+ (|V_i| + |V_-| + |V(0)| + 1/c - L|X_-|/2). \qquad (2.4.5)$$

Note: We can assume that the electron density n, is the same in insulating and conducting tubes. This is because it is only dependent on the axial current density, the pressure and the tube diameter. According to Chester (1968), we have, $n \approx KJp_-D(300/T_-)^{1/2}$, where K is a constant of the order of $2x10^{11}$ (Dunn (1974)) with J(amps/cm^2) the axial current density, p_-(torr) the gas pressure, D(mm) the tube diameter, and T_-(K) the gas temperature, giving n(cm^{-3}).

We may write equation (2.4.5), for the case of Argon, with j_+ given by equation (2.3.2), in the form

$$I_- |X_-| = \pi R e n (kT_-/m_+)^{1/2}\{15.7 + 3kT_-/e + |V(0)| - L|X_-|/2\}, \qquad (2.4.6)$$

as $V_- = 2kT_-/e$, and $1/c = kT_-/e$.

An expression for V(0) may be obtained from equation (2.3.7), such that

$$|V(0)| = |V_w| + (1/c)\ln[(\exp(Y_m)-1)/Y_m], \qquad (2.4.7)$$

where V_w is given by (2.3.4) and $Y_m=c|X_m|L$.

Thus, we find for a metal tube containing an Argon discharge,

$$I_m|X_m| \approx 7.2\times10^{-10} RnT_m^{1/2} \times(15.7+10^{-4}T_m(7.2+0.9\ln\{[\exp(Y_m)-1]/Y_m\})-L|X_m|/2). \qquad (2.4.8)$$

For a ceramic tube containing an Argon discharge, we obtain from (2.4.2)

$$I_m|X_c| \approx 7.2\times10^{-10}\ RnT_m^{1/2}(15.7+7.2\times10^{-4}T_m). \qquad (2.4.9)$$

2.5) The axial electric field in insulating and conducting tubes.

Equations (2.4.8) and (2.4.9) may be used to compare the axial electric field in ceramic and metal tubes. We have, for DC discharges at the same pressure and axial current,

$$I_m|X_m| = I_m|X_c| + S, \qquad (2.5.1)$$

where S is given by

$$S=7.2\times10^{-16}RnT_m^{1/2}(8.6\times10^{-5}T_m\ln\{[\exp(Y_m)-1]/Y_m\}-L|X_m|/2).$$

[To show that the following inequality is satisfied, $I_m|X_m| \geq I_m|X_c|$, we proceed as shown below. We start by assuming,

$$(kT_m/e)\ln\{[\exp(Y)-1]/Y\} \geq |X|L/2$$

which implies that S is greater than or equal to zero. We then obtain, successively,

$$\ln\{[\exp(Y)-1]/Y\} \geq e|X|1/2kT_m = Y/2$$

$$[\exp(Y)-1]/Y \geq \exp(Y/2)$$

$$(\exp(Y/2)-\exp(-Y/2))/Y \geq 1$$

$$(2\sinh(Y/2))/Y \geq 1.$$

We see that as $Y \to \infty$, we have $(2\sinh(Y/2))/Y \to \infty$,

and as $Y \to 0$, we get,

$$(2\sinh(Y/2))/Y \to 2((1+Y/2+Y^2/8+\ldots)-(1-Y/2+Y^2/8-\ldots))/2Y = Y/Y=1].$$

Therefore, $I_a|X_m|$ is always greater than or equal to $I_a|X_c|$. That is, we have shown that the axial electric field in a metal tube X_m, is always greater than or equal to that in a ceramic tube X_c. In the above derivation we showed that as Y (where Y=cXL) went to zero (which is the case as the segment length becomes small), X_m became equal to X_c. This implies that for small segment lengths (Y small), metal tubes have the same operating characteristics as insulating tubes.

We can calculate $S/(I_aX_c)$ using the values in table (2.1). The ratio turns out to be of the order of 0.03. Thus we find that for an argon ion laser discharge, with short metal segments, the axial electric field is only a few percent higher than the field characteristic of a ceramic tube.

(See Appendix 8 for form of equation (2.5.1) when the electron temperature of a discharge confined by metal walls is greater than the electron temperature of a discharge confined by ceramic walls.)

2.6) Calculation of the electron number density.

Equation (2.4.8) may be used to make a rough estimate of the electron number density. The following data is taken from a paper by Cornish and Maitland (1973).

Table 2.1 Calculation of electron density in a segmented metal tube.

L(cm)	R(cm)	(L/R)	X_m(V/m)	I_m(amps)	T_e(K)	$n_e(cm^{-3})$ (calculated)
1.6	0.15	10.1	650	25	31×10^3	2.1×10^{14} (1)
2.5	0.2	12.5	456	53	39×10^3	1.9×10^{14} (2)
2.5	0.3	8.3	288	65	26×10^3	1.5×10^{14} (3)
7.5	0.35	21.4	250	45	69×10^3	2.5×10^{13} (4)

The values of the electron number density obtained, are of the correct order of magnitude.

To verify the theory we may calculate the electron number density, ($n_e(1)$ and $n_e(2)$), in an argon ion discharge in a ceramic tube, using equation (2.4.9) and the experimental data of Kitaeva et al. (1974), and compare these values with those obtained by Kitaeva, ($N_e(k)$). Figure (2.4) is a plot of $n_e(1)$ and $n_e(2)$ versus $N_e(k)$. It can be seen that the calculated values of the electron density agree with those found by Kitaeva et al. within a factor of two.

As we have ignored the fact that some of the input energy goes into radiation and gas heating, the values

obtained, both for the metallic and the ceramic cases, are higher than the true values by a factor of 1/f, where f(I,X) is the fractional power input lost to the walls. Note also that the value of n_e calculated is that at the sheath edge which is less than the average values given by Kitaeva.

2.7) The variation in electron temperature.

In the previous sections we have made the assumption that the electron temperature in the two discharges (metal walled and ceramic walled) is the same. However, Von Engel (1965) has shown that $X/T_e \propto p$, where p is the gas pressure. Thus, for discharges of equal pressures we find that X/T_e is approximately constant. That is to say, T_e increases as X increases. This implies that the electron temperatures in ceramic and metallic tubes of equal length, are unlikely to be the same. Experiment shows (see section (3.3.2)) that the electric field in a segmented metal tube is greater than that in a quartz (insulating) tube when the radius and the pressure are the same. Consequently, we would expect the electron temperatures to be correspondingly higher (see Appendix 8).

If we look at the right hand sides of equations (2.4.8) and (2.4.9), we see that they are functions of the electron temperature. This dependence on the electron temperature implies that the power per unit length lost to the walls of a metal tube is always greater than that lost to the walls of a ceramic tube. The equations previously derived are more correctly written with the electron temperatures of the

plasma in a metal tube and a ceramic tube denoted by T_{em} and T_{ec}, respectively.

2.8) Variations in the positive ion sheath thickness in a metal tube.

The Child - Langmuir equation (Child 1911, Langmuir 1913), for plane parallel geometry, has been derived in appendix A4. It may be used to estimate the sheath thickness in a metal tube. We rewrite equation (A4.19) as,

$$y^2 = 3.7\times10^{-8}|V(y)|^{3/2}/nT_e^{1/2}, \qquad (2.8.1)$$

where y is measured from the plasma-sheath boundary to the wall. The equation has been derived for the case where there is no axial variation in the potential difference across the sheath. Consequently, we may use this equation only as a first approximation, when we consider metal walls. At any point along the axis of the segment, we may measure a "radial" potential across the positive ion sheath, between the plasma and the wall. According to equation (2.3.6) the axial potential, relative to the anode end of the segment, (x=0), varies as,

$$|V(x)| = |V(0)| - x|X|. \qquad (2.3.6)$$

We would expect the sheath thickness, y=s, (from equation (2.8.1)), to vary as,

$$s(x) \propto V(x)^{3/4}. \qquad (2.8.2)$$

Observations of glow discharges within conducting walls, (see section 3.2), show an increase in sheath thickness towards the anode end of the metal segment, which is consistant with the above theory. The sheath thickness in this case is an appreciable fraction of the tube radius, and it is more appropriate to use the Child-Langmuir equation for cylindrical geometry (equation (2.9.8)).

The axial current I, in a gas discharge is given by,

$$I = ne\mu_- |X| A, \qquad (2.8.3)$$

where A is the discharge tube cross-sectional area and μ_- is the electron mobility, assumed to be a constant. In high current density discharges, the sheath thickness is small; for a typical argon ion laser discharge, it is a fraction of a millimetre. In a low current glow discharge where the number density is much less, the sheath thickness is of the order of millimetres, and at the anode end of a segment can become an appreciable fraction of the tube radius. According to equation (2.8.3), for a constant current discharge, (assuming a constant electron density n) the axial electric field is inversely proportional to the cross-sectional area. An increase in sheath thickness leads to a reduction in the area available for current conduction, therefore the field in this region must necessarily increase to maintain the current. Observations of a striated discharge by Zeleny (1938) showed a bunching together of the striations at the anode end of a wire gauze segment. This

bunching together is indicative of an increase in the average axial field (Francis 1956).

2.9) The dependence of the maximum segment length on the radial electric field in the sheath.

In section (2.3.2) an expression is derived which shows that the maximum length of a metal segment is governed by the ratio of the electron temperature T_e, to the axial electric field, X. The criterion basic to this dependence is that no part of the segment should become positive.

We may establish a further dependence of the maximum segment length on X, by considering the potential difference across the positive ion sheath at the tube wall. The criterion in this case is that the radial field E_r, across the sheath at any point, must not exceed the critical field for "breakdown" (for example, secondary emission electrons from the segment ionise the gas in the sheath) of the gas. The following assumptions have been used:

1) In the discharges under consideration, the wall potential only penetrates to the sheath edge, the plasma remains unaffected. This is essentially Debye shielding (Appendix 2).

2) The higher the electron number density, the smaller the sheath thickness.

3) The sheath thickness is a function of the potential difference across the sheath.

4) Figure (2.1b) shows the variation in the potential difference between the plasma and the wall for a conducting

walled tube. We consider a metal tube to be made of very small circular sections. Each section of the wall is at a different potential, relative to the plasma. The anode end of the segment is defined as x=0 and the cathode end as x=L. The potential of the section at x_2 relative to that at x_1 is given by

$$|V(x_2)| = |V(x_1)| - |X|(x_2 - x_1),$$

where $x_2 > x_1$.

5) The electron/ion number density used in the calculations is that at the plasma-sheath boundary (this ignores the pre-sheath region (Appendix 3)).

6) The symbols V and X represent $|V|$ and $|X|$ (always positive).

The potential across the sheath at any point along the segment, is given by,

$$cV(x) = \ln[M.(\exp(cXL) - 1)/cXL] - cxX, \qquad (2.9.1)$$

where we have $M = (2m_+/\pi m_e)^{1/2}$, and $c = e/kT_e$.

In most cases we find $\exp(cXL) >> 1$, thus we may approximate equation (2.9.1) as follows. If we take two segments (S_1 and S_2, say) of lengths L_1 and L_2, such that $L_1 > L_2$, experiment shows that $X_1 > X_2$ (and therefore $T_{e1} > T_{e2}$; Von Engel(1965)). At the anode end of the segment (x=0) we find,

$$V_{A1}/V_{A2} = T_{e1}(\ln M + Y_1 - \ln Y_1)/T_{e2}(\ln M + Y_2 - \ln Y_2), \qquad (2.9.2)$$

where Y is given by Y=cXL. It can be shown that if we have Y_1 greater than Y_2, then $Y_1-\ln Y_1$ is always greater than $Y_2-\ln Y_2$, therefore the potential difference across the sheath at the anode end of segment S_1 is greater than the potential difference at the anode end of S_2; $\underline{V_{A1}>V_{A2}}$.

At the cathode end of the segment (x=L), we have

$$V_{C1}/V_{C2} = T_{e1}(\ln M-\ln Y_1)/T_{e2}(\ln M-\ln Y_2). \qquad (2.9.3)$$

If Y is greater than unity and less than M ($L_1>L_2$), then the potential difference across the sheath at the cathode end of S_1 can be less than, greater than, or equal to the potential difference at the cathode end of S_2. This inequality depends on the value of T_{e1}/T_{e2} (>1) relative to the value of $(\ln M-\ln Y_1)/(\ln M-\ln Y_2)$ (<1); $\underline{V_{C1}<,=,>V_{C2}}$. (Note: For argon M=216, so the limits for Y will hold. In previous theory (section (2.3.2)) M=Y effectively gives the limit for the maximum segment length.)

To summarise, if L_1 is greater than L_2, which implies that X_1 is greater than X_2, we have $L_1X_1>L_2X_2$. As the field X, and length L, increase, we see from equations (2.9.2) and (2.9.3) that the voltage across the sheath increases at the anode end of the segment and may increase or decrease at the cathode end. Any changes in external parameters which also increase the electric field will have the same effect, for example if the tube radius, R, is decreased or the pressure, p, increased.

For a planar electrode geometry we may write the Child-Langmuir law (Child 1911, Langmuir 1913) as,

$$j_+ = (2\epsilon_o/9)(2e/m_+)^{1/2}(V^{3/2}/s^2), \qquad (2.9.4)$$

for electrodes of separation s and j_+ given by equation (2.3.2). Equation (2.9.4) may be used for the case of an argon ion laser discharge, as a thin sheath may be approximated to a plane parallel geometry. For a constant j_+, it can be seen from equation (2.9.4) that

$$s \propto V^{3/4}. \qquad (2.9.5)$$

As a first approximation to the "radial" field E_r, we may write,

$$E_r \approx V/s \approx V^{1/4} \qquad (2.9.6)$$

which implies that the "radial" field E_r increases slowly as V increases. For example, doubling the potential difference across the sheath (2V) leads to an increased field of only 1.2 times the field at the original potential difference (V). As the potential difference across the sheath increases, as we move from the cathode-end to the anode-end of a segment, the radial field also increases. It is possible that the radial field at the anode-end of the segment may exceed the "breakdown" field strength in the sheath. We can define the maximum length of a metal segment, as the length at which the radial electric field in the sheath at the anode-end of a metal segment is equal to the "breakdown" field.

It has been shown (equation (2.9.2)) that an increase of X or L, can lead to an increase in the potential

difference across the sheath at the anode-end of a metal segment, and breakdown may then occur to the wall if the breakdown field is exceeded. We thus expect the maximum segment length L_{max} to be inversely proportional to the axial electric field. As the axial field is proportional to the gas pressure and inversely proportional to the tube radius, we have

$$L_{max} \propto R/p \qquad (2.9.7)$$

The constant of proportionality depends on the gas and the discharge current.

Experimental observations show that reducing the radius of the metal tube confining the discharge, or increasing the pressure, reduces the maximum usable length of tube (segment). The discharge then no longer penetrates the tube, the current instead passes through the tube walls. In some of the rare gases, the axial electric field starts to increase again as the pressure is reduced below about 2 torr (Francis 1956), which explains the observation that in some cases the discharge only penetrates the segments over a narrow pressure regime.

The Langmuir equation for cylindrical geometry (Langmuir 1913) is

$$(j_+)_a = (2\epsilon_o/9)(2e/m_+)^{1/2}(V^{3/2}/RQ\beta^2), \qquad (2.9.8)$$

for an inner emitter of radius Q and an outer collector of radius R, where $\beta = \beta(R/Q)$ has been tabulated (Langmuir

1913), and $(j_+)_a$ (equation (2.3.2)) is the ion current density at the emitter.

In glow discharges, we have observed a sheath whose thickness may be some large fraction of the tube radius R (Chapter 3). Where R/Q varies between 1 and 2, β^2 has an approximately linear variation given by,

$$\beta^2 \approx K(R/Q - 1), \qquad (2.9.9)$$

where K=0.275, and is the value of β^2 at R/Q = 2. Taking Q as the radius of the plasma-sheath boundary, then R-Q=s, the sheath thickness. We may rewrite equation (2.9.9) as,

$$\beta^2 \approx K(R-Q)/Q \approx Ks/Q. \qquad (2.9.10)$$

From equations (2.9.8) and(2.9.10) we obtain,

$$V^{3/2} \propto RQ\beta^2 \propto KRs \qquad (2.9.11)$$

Therefore, we have

$$E_r \approx V/s \propto V^{-1/2}. \qquad (2.9.12)$$

A decrease in the potential difference V, across the sheath, and subsequent decrease in sheath thickness, will lead to an increase in the "radial" field E_r, in the sheath.

From equation (2.9.3) we deduce that an increase in segment length and/or axial field may lead to a reduction in the potential difference across the sheath at the cathode

end of the segment. A smaller potential difference would result in a higher radial field (equation (2.9.12)), at the cathode-end, which may exceed the "breakdown" field. If this is the case, "breakdown" may occur at the cathode end of the segment. We can then define the maximum length of a metal segment as the length at which the radial electric field in the sheath at the cathode-end of the segment is equal to the "breakdown" field.

2.10) Relationship between the maximum length of a metal segment, in an established discharge, and the tube radius and pressure.

The maximum length of a metal segment for the case of an argon ion laser discharge is found in section (2.3.2) to be,

$$L_{max} = (kT_e/eX)(2m_+/\pi m_e)^{1/2} \qquad (2.10.1)$$

We use equation (A1.20) (Appendix 1) to find the electron temperature (long mean free path case). Substituting the expression for the electron temperature into equation (A1.16) gives the axial electric field in terms of the radius and pressure. These expressions for T_e and X may be substituted into equation (2.10.1). Also, we have (for $X/p > 1$ V/cm.torr) that the average fraction f (equation (A1.15)), of electron energy lost in a collision with a gas molecule (atom) is proportional to X/p. That is, we have

$$f \approx \delta(X/p), \qquad (2.10.2)$$

where δ is a constant of the order of 3×10^{-8} pascal m/V for argon (Von Engel 1965). (As (X/p) increases, more inelastic collisions occur which result in the electrons losing a large fraction,f of their energy.) We finally get an expression of the form,

$$L_{max} \approx (C_1/p)\ln(C_2pR), \qquad (2.10.3)$$

where $C_1 = (r_1^2/\delta V_i)(2m_+/\pi m_e)^{1/2}$ and $C_2 = aeV_i(4M/\pi m_e)^{1/2}$, r_1 is the electron mean free path at 1 pascal, V_i is the ionisation potential of the gas, while a is a constant. The form of equation (2.10.3) agrees with experimental observation. The maximum segment length is seen to increase as the pressure decreases and as the radius increases.

2.11) Conclusions.

We have derived an expression for the maximum length of a metal segment in an established, DC discharge, of the type used for argon ion lasers. To determine the maximum length, one criterion chosen is that the cathode end of a metal segment should never become positive with respect to the plasma. The maximum length is a function of the axial electric field, and decreases as the field increases. The relationship between segment length and axial electric field, leads to a dependence of the maximum length on segment radius and gas pressure. The maximum length is proportional to the radius and inversely proportional to the pressure.

An approximate expression for the radial electric field in the positive ion sheath, which forms between the plasma and the metal wall, has been derived. This radial field depends on the segment length. In an argon ion laser DC discharge (thin positive ion sheath at the walls) the radial field increases at the anode end of the segment as the segment length increases. In a discharge of low current density (thick positive ion sheath) the radial electric field in the sheath at the cathode-end of the segment may increase, as the segment length increases. The increase in radial field with segment length limits the maximum length of a metal segment. The maximum length may be defined as the length at which the radial electric field in the positive ion sheath, at one end of the segment is equal to the "breakdown" field.

We have found that the power lost to the wall is greater in a metal tube. Thus, for ceramic and metallic tubes (of equal length, radii, ambient pressures and currents), the longer the metal segment, the larger the ratio of the axial electric fields X_m/X_c becomes. In the limit, as the segment length becomes small, the electric field along the axis of the segmented metal tube approaches the electric field along the axis of a ceramic tube.

The thickness of the positive ion sheath, at the walls, is a function of the potential difference across the sheath. We deduce that the thickness of the positive ion sheath at the anode end of a "long" segment is greater than the thickness of the sheath at the cathode end. This variation

of thickness has been observed in discharges at low current densities.

References.

A.E.Sheindlin, E.I.Asinovskii, Proc. 6th IPIG, Vol.2., 1963, p 379

J.D. Rigden. " A metallic plasma tube for ion lasers." IEEE J. Quant. Elec., Vol. QE-1, 1965, p 221.

F.F.Chen. "Electric probes in plasma diagnostic techniques.", Eds. R.H. Huddlestone and S.L. Leonard (New York : Academic Press.),1965, p 113.

V.F.Kitaeva,A.N.Odintsov,N.N.Sobolev,"Continuously operating Argon ion lasers." Sov.Phys. Usp.,Vol. 12, 1970, p 699.

A. Maitland. "Theory of segmented metal discharge tubes for argon lasers." J. Phys D, Appl. Phys., Vol 4, 1971, p 907.

J.C.L. Cornish, A. Maitland. "High current discharges in segmented metal tubes." J. Phys. D, Appl. Phys., Vol 6, 1973, p 1899.

K.G. Hernqvist, J.R. Fendley Jr. "Construction of long life argon lasers." IEEE J. Quant. Elec., Vol. QE-3, No. 2, 1967, p 66.

T.J.Killian. "The uniform positive column of an electric discharge in mercury vapour." Phys. Rev. Vol. 35, 1930, p 1238.

A.N.Chester "Experimental measurement of gas pumping in an argon discharge." Phys. Rev. Vol 169, No. 1,1968, p 184.

M.H.Dunn. "Perturbation spectroscopy of the argon ion laser" PhD thesis, 1974.

V.F.Kitaeva,Yu.I.Osipov,N.N.Sobolev,A.L.Shelekhov,V.P.Agheev "Probe measurements of Ar^+ laser plasma parameters." IEEE J.Quant.Elec, Vol QE-10, 1974, p 803.

A.Von Engel. "Ionized gases." 2nd edn.,(Oxford: Clarendon Press.) 1965, p 244.

C.D. Child, Phys. Rev.I, 32, 1911, p 492.

I.Langmuir, Phys. Rev.II,2, 1913, p 450.

J.Zeleny "On the role of tube walls, and surface and space charges in electrical discharges through rarefied gases." Journal of the Franklin Institute. Vol. 226, 1938, p 35.

G.Francis. "The glow discharge at low pressure." Handbuch der Physik, Gas discharges 2, Vol.22, 1956, p 53.

Figure 2.1 Discharge tube potentials.

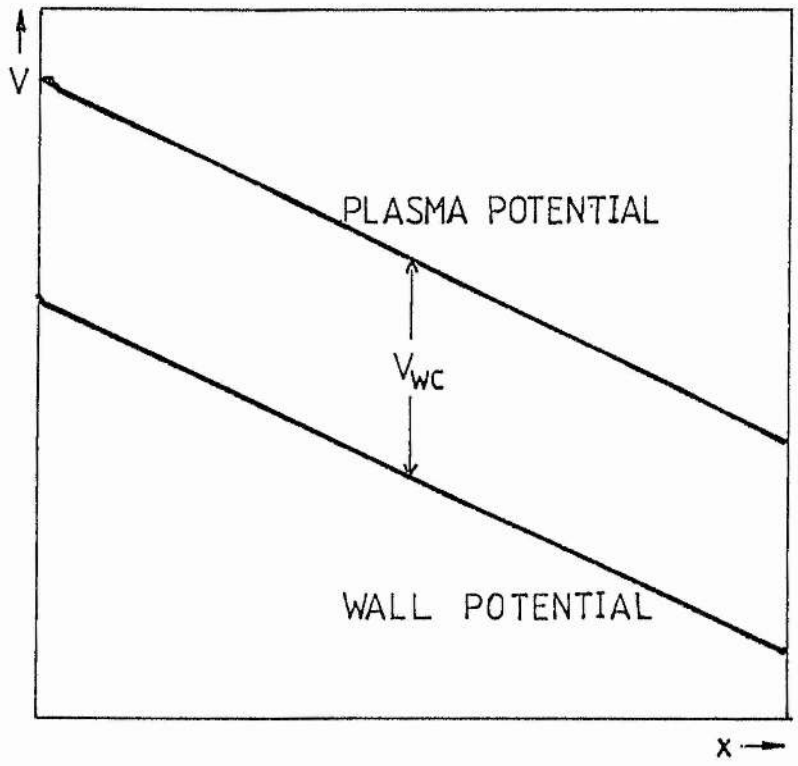

a) Insulating (ceramic) tube.

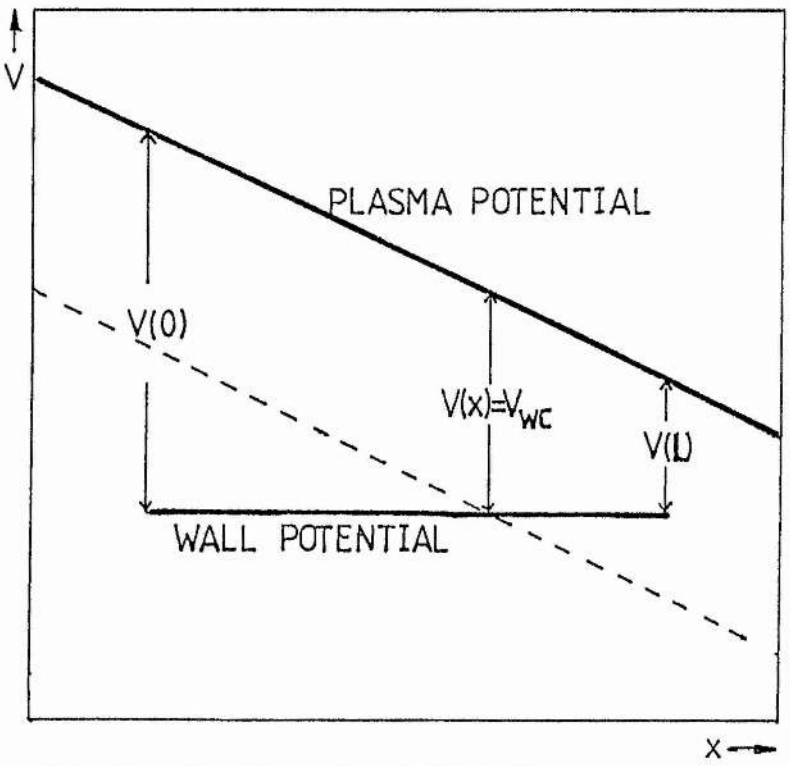

b) Conducting (metal) tube.

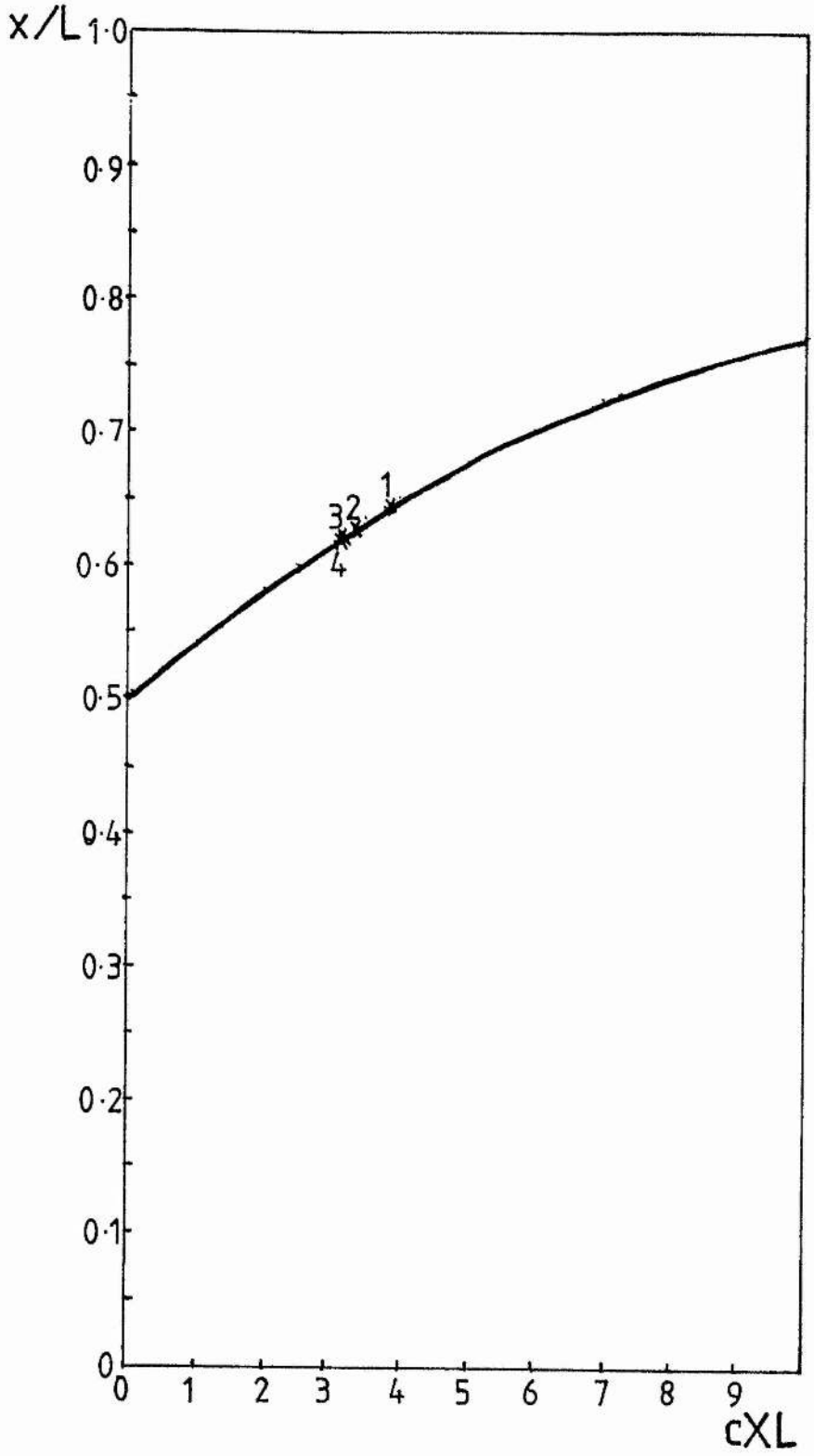

Figure 2.2 Plot of cXL versus x/L for a metal segment.

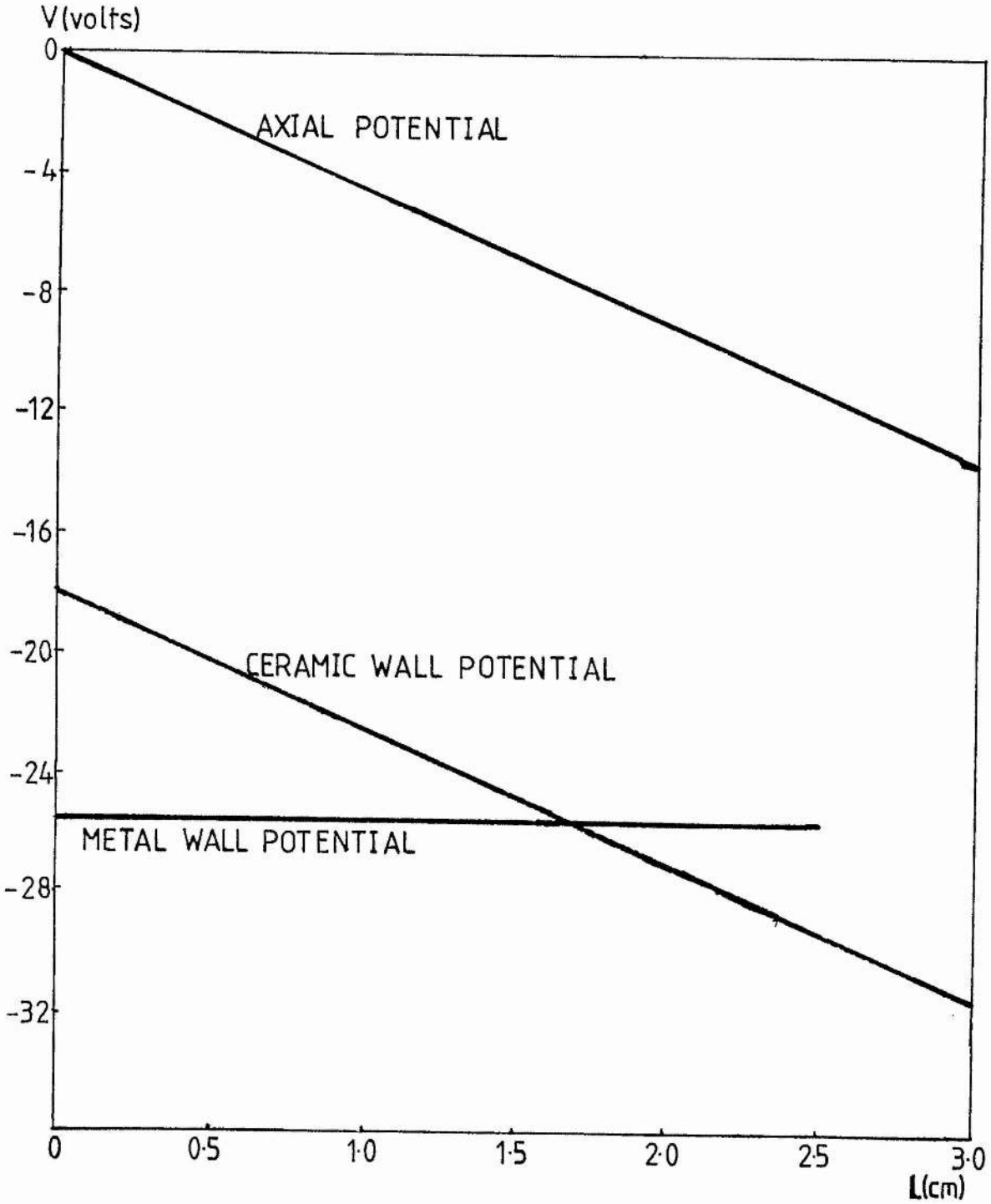

Figure 2.3 Discharge tube potentials for $T_e = 39 \times 10^3$ K and X=456 V/m.

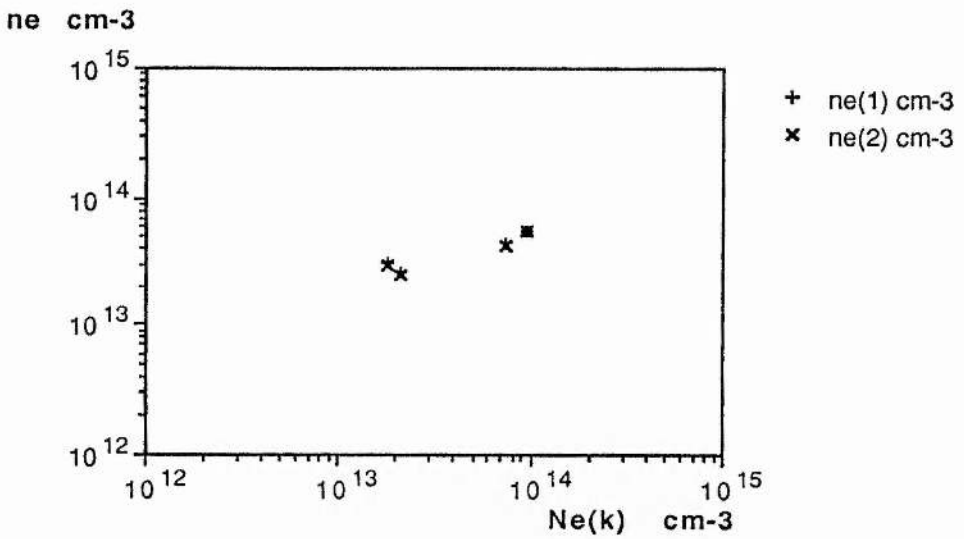

Figure 2.4 Electron number densities in argon-ion laser discharge (ceramic tube).
Ne(k) - electron density found by Kitaeva.
ne(1) - electron density calculated using the electric field due to Ebert.
ne(2) - electron density calculated using the measured electric field.

CHAPTER 3

LOW CURRENT (DENSITY) DISCHARGES.

3.1) Introduction.

The following experiments examine the properties of low current wall stabilised, gas discharges with metallic boundaries of the order of a few centimetres diameter. The boundaries are generally in the form of cylindrical metal segments, contained within a quartz or pyrex tube which acts as the vacuum envelope.

The combination of low current and wide bore gives low current densities ($\approx 10^{-3}$ amps/cm^2). Low current density discharges can have thick (of the order of millimetres) positive ion sheaths adjacent to the tube walls, which may reduce the diameter of the conduction path. In tubes with conducting walls, the sheath can be seen to increase, on moving from the cathode end to the anode end of the metal tube.

The axial electric fields in the positive column of a gas discharge are measured for the respective cases of insulating and conducting boundaries. The results show that the axial fields are higher when the boundaries (walls) are conducting.

Estimates of the current in the wall of a metal segment can be made by measuring the current between (interconnected) adjacent metal segments. The current between the segments is found to depend on the gas pressure and the discharge current between the anode and the cathode.

3.2) Variations in the positive ion sheath thickness.

The circuit shown in figure (3.1) is used in the experiments. The circuit produces a low ripple DC voltage across the tube. A Hartley Measurements model 411 capacitor charging unit is used as the power supply. A copper segment of length 21 cm and internal diameter 29 mm is placed in a 40 cm long, 30 mm diameter quartz tube. The electrodes consist of two 15 cm pieces of 5 mm brass pipe. The tube is sealed with rubber bungs, and is evacuated to approximately 1 millibar. Glow discharges are produced in atmospheric air.

Observation of the discharge reveals that the diameter of the discharge at the anode end of the segment, is smaller than the diameter at the cathode end of the segment. If the copper cylinder is replaced by one of wire mesh, the whole of the discharge enclosed by conducting boundaries can be seen. The discharge gradually contracts towards the anode end of the segment. This decrease in discharge diameter appears to be nonlinear. Similar observations were made in a pyrex tube coated with a thin (low resistance), semi-transparent layer of silver. Discharges have been observed to pass down a silvered tube 1 metre long.

The contraction of the discharge is explained by the argument given in section (2.8). We apply the Child-Langmuir equation for cylindrical geometry (1913) to the positive ion sheath which forms between the plasma and the walls. From equation (2.9.11) we find,

$$s \propto V^{3/2}, \qquad (3.1)$$

where s is the sheath thickness, and V is the potential difference across the sheath. The potential difference between the wall and the plasma is greater at the anode end of a segment than at the cathode end. We would, therefore, expect the sheath at the anode end of the segment to be larger than at the cathode end. As there are few collisions in the sheath, little light is emitted, and the volume appears darker than the adjacent plasma. Thus, when the sheath is large we have a constricted discharge at the anode end of the segment.

3.3) Variations in the axial electric field.

3.3.1) Quartz tube.

The following experiments determine the effect of metallic walls on the axial electric field X, in the positive column. The circuit used is shown in figure (3.2). The discharge tube is a quartz tube of dimensions 110 cm by 3 cm diameter. The tube anode is a nickel wire and an aluminium cylinder is the cathode. Six nickel wire probes are situated at intervals of about 16.5 cm along the tube. The discharge current is maintained constant at 11.7 milliamps. The pressure is varied between 0.4 and 0.8 millibar.

Voltage and current measurements are made between the probes, at various pressures. Graphs of potential (of each probe relative to probe 1) versus position allow the axial electric field to be estimated. The results are shown in

figure (3.3), which is a plot of axial electric field versus pressure.

3.3.2) Quartz tube containing metal segments.

In order to observe the effects of metal segments on the electric field, a quartz tube, with the same dimensions as that described in the previous section, containing metal segments was constructed. Six 15 cm by 2.9 cm diameter copper cylinders are situated along its length. The segment separation is 1.5 ± 0.2 cm. Each segment has a probe directly attached to it. On the opposite side of the cylinder, a probe passes through a hole and makes contact with the plasma. These probes, which are insulated from the segments, are separated by 16.5 ± 0.2 cm. The pressure is varied between 0.4 and 0.8 millibar in 0.1 millibar steps. The discharge current is held constant at 11.7 mA. At these pressures the discharge always forms in the gas along the axis of the segments. The calculated values of the electric field are also shown in figure (3.3). It can be seen that the electric field in the tube containing the metal segments is about 20% higher than that in the empty quartz tube.

Energy balance considerations (section 2.4) predict a higher axial electric field in a tube with conducting walls, as the energy losses at the walls are greater than when the walls are insulating.

3.4) Observations of a discharge with conducting walls.

The quartz tube containing the metal segments, described in section (3.3.2) is used to make observations of the discharge. The metal segments are labled A to F from cathode to anode. The length of the segments may be effectively increased by joining adjacent segments. When the pressure is varied between 0.2 and 1.0 mbar, the following can be observed.

1) A striated pink glow fills most of the tube, except at the highest pressures. Although the striations indicate non-uniformities in potential, the estimates of the average electric field in section (3.3.2) are believed to be still valid. (Plots of probe potential, relative to probe 1, versus probe separation, give a linear variation.)

2) The following sequence occurs, for six independent segments, as the pressure is increased. The variation in sheath thickness within the segments is initially small and the discharge column almost fills the cylinders. The column then starts to constrict, and the variations in sheath thickness become more pronounced. The discharge then becomes fainter, and more purple, and moves to the tube walls where glows appear. These glows are pink on the cathode facing end of a segment and purple on the anode facing end of a segment.

3) When A and B are connected a narrow pink discharge appears in the gap between them. (The discharge passes into both the segments).

4) When E and F are connected, a purple glow appears in

between them, which is extinguished as the pressure increases.

5) When all the segments are connected no glows are seen in the gaps between the segments, except in the gap between E and F, where a purple glow, which starts in F, elongates and passes into E as the pressure falls.

In air, pink glows are characteristic of the positive column, and purple of the negative glow. As the pressure increases, the axial electric field in the positive column increases. Referring to figure (3.4), we find the potential difference between adjacent segments of the same length, V_{12}, to be given by,

$$|V_{12}| = |V(0)| - |V(L)| + d|X_o|, \qquad (3.4.1)$$

where V(0) is the potential difference across the sheath at the anode end of the segment, V(L) that at the cathode end, d the distance between segments, and X_o the longitudinal field in the region between the segments. But we also have,

$$|V(0)| - |V(L)| = L|X_m|, \qquad (3.4.2)$$

where L is the length of a segment and X_m the axial field inside the metal segment. We have assumed in figure (3.4), for simplicity, that the fields are equal, whereas, in reality, X_m, is greater than X_o. From equations (3.4.1) and (3.4.2), we find that the potential difference between adjacent segments is,

$$|V_{12}| = L|X_m| + d|X_o|. \qquad (3.4.3)$$

Equation (3.4.3) shows that the inter-segment potential difference depends on the electric fields (and therefore the pressure and radius), the segment length and the segment separation. This dependence implies that the field between adjacent segments may also increase as the segment length increases. If the critical breakdown field is exceeded, breakdown may occur between adjacent segments. Each end of the segment then acts as either a cathode or an anode, as shown in figure (3.5). Most of the current then flows through the segment walls; thus the discharge within the segment becomes fainter. The formation of "electrodes" at both ends of the segment, may explain the observations described in (2) on page 44, as the pressure (and hence the axial electric field) increases.

Figure (3.6 a) shows the appearance of a discharge between two segments. Figure (3.6 b) shows the effect of connecting two segments together. Since the sheath thickness is a function of the potential difference across the sheath, the appearance of the discharge may be explained by figure (3.6 c) which shows the floating potentials in the tube.

3.5) Measurement of the current between connected segments.

The circuit shown in figure (3.2) is used to produce a glow discharge in the quartz tube containing the copper segments. The two inner segments, labled C and D in

figure (3.5), are connected through an ammeter. In effect, this connection produces a metal segment of twice the length of the other copper segments in a way which enables the inter-segment current to be measured. The discharge voltage, and current between the segments (I_m), is measured at different pressures at four values of the anode-cathode discharge current (I_a).

Figure (3.7) is a plot of the ratio of the inter-segment current I_m, to the discharge current I_a, against pressure, at each value of the discharge current. It can be seen that, as the pressure increases, the ratio of the inter-segment current to the discharge current (I_m/I_a), also increases. This is due to the increase in the axial electric field which accompanies increasing pressure.

If we consider the axial electric fields in the discharge tube at two different pressures p_1, p_2 (Right hand side of the Paschen curve) where

$$p_2 > p_1, \qquad (3.5.1)$$

then we find that the axial electric fields are such that,

$$X_2 > X_1. \qquad (3.5.2)$$

The points Y and Z are situated at either end of the connected segments, as shown in figure (3.6b). If V_1 and V_2 are the potential differences in the plasma between Y and Z, at the two pressures then, from (3.5.2) we get,

$$V_2 > V_1. \qquad (3.5.3)$$

Maitland and Cornish (1972) have found that the current between inter-connected metal segments is proportional to the potential difference in the plasma (between Y and Z), along the axis of the segments. With this dependence of the current on the potential difference, we find that the two inter-segment currents, I_{m1} and I_{m2} are such that,

$$I_{m2} > I_{m1}. \qquad (3.5.4)$$

Dividing both sides of equation (3.5.4) by I_d (the anode-cathode current), we then have,

$$(I_{m2}/I_d) > (I_{m1}/I_d). \qquad (3.5.5)$$

The increase in the ratio of the inter-segment current to the discharge current (I_m/I_d), as the pressure increases can be seen in figure (3.7)

The current ratio (I_m/I_d), at a particular pressure, increases as the discharge current decreases. If we assume that the drift velocity remains approximately constant, a smaller current implies a reduction in the free charges available in the gas. As the number of free charges decreases, the conductivity of the gas decreases, implying an effective increase of the impedance of the discharge within the segment. The metal wall provides a conduction path in parallel with the discharge. Therefore, as the impedance of the metal segments remains constant, (I_m/I_d)

increases as the discharge impedance increases. At 5 milliamps, measurements show that inter-segment current I_m, is equal to the anode-cathode discharge current I_a.

At constant pressure, the axial electric field (and hence the potential-fall in the plasma along the segment axis) decreases as the discharge current increases. For the two discharge currents, I_{a1} less than I_{a2}, we have

$$X_2 < X_1. \qquad (3.5.6)$$

From (3.5.6) and the dependence of the inter-segment currents on the axial electric field, we conclude,

$$(I_{m2}/I_{a2}) < (I_{m1}/I_{a1}). \qquad (3.5.7)$$

The data plotted in figure (3.7) show an increase in (I_m/I_a) as the discharge current decreases, at constant pressure.

3.6) The longitudinal wall current.

In section (2.3.1) we discussed the electron and ion currents to the wall of a metal segment. The electron current, from the plasma to the wall, is seen to depend (equation (2.3.3)) on the potential difference across the positive ion sheath, and hence decreases on moving from the cathode end to the anode end of a metal segment (see figure (2.1b)). From current continuity considerations (Kirchoff's first law), the longitudinal electron current in

the segment I_w, decreases on moving towards the anode end of the segment, whereas the axial current in the plasma I_p increases. At any axial position x within the segment we have,

$$I_D = I_p(x) + I_w(x), \qquad (3.6.1)$$

where I_D is the discharge current in the external circuit. This effect has been investigated by Stephens and Allen (1976). Hence the inter-segment current measurements described in the previous section are equivalent to the current in the wall at the central section of a metal segment (tube) of twice the length of the segments used in the experiments.

3.7) Conclusions.

Direct observation and theory shows that the thickness of the positive ion sheath between the plasma and the wall decreases on moving from the anode end to the cathode end of a floating metal segment. The sheath thickness at a particular circumference is a function of the potential difference across the sheath, and hence the sheath thickness decreases as the potential difference decreases. The potential difference at the anode end of the segment (and hence the sheath thickness) increases as the axial electric field in the plasma increases (as the pressure increases and/or the discharge current decreases).

The axial electric field in a discharge inside a metal

segment has been found, in our experiments, to be greater than one in a tube with insulating walls. This is predicted in section (2.5), from consideration of the energy balance (section (2.4)) between input energy and that lost at the tube walls.

Measurements have been made of the current between adjacent metal segments. The ratio of the inter-segment current to the anode-cathode discharge current (I_m/I_a), increases as the pressure increases (constant discharge current), and as the discharge current decreases (constant pressure).

References.

C.D.Child. Phys.Rev.I, 32. 1911, p 492.

I.Langmuir. Phys. Rev.II, 2. 1913, p 450.

A.Maitland and J.C.L.Cornish. "Electron temperatures in a segmented-metal argon-ion laser." J. Phys. D, 5, 1972, p 1807.

F.D.Stephens and J.E.Allen. "Axial wall currents in cylindrical metal discharge vessels." Gas Discharges IEE Conference Publication 143. 1976, p 331.

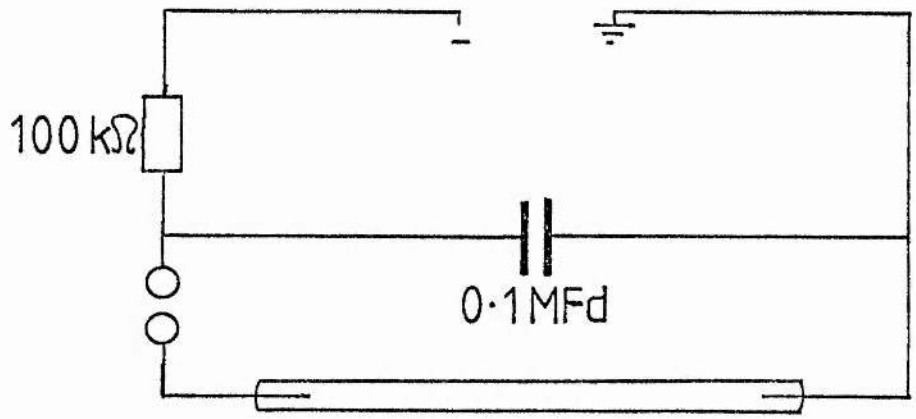

Figure 3.1 Circuit used to observe the variation of the positive ion sheath thickness at a conducting surface.

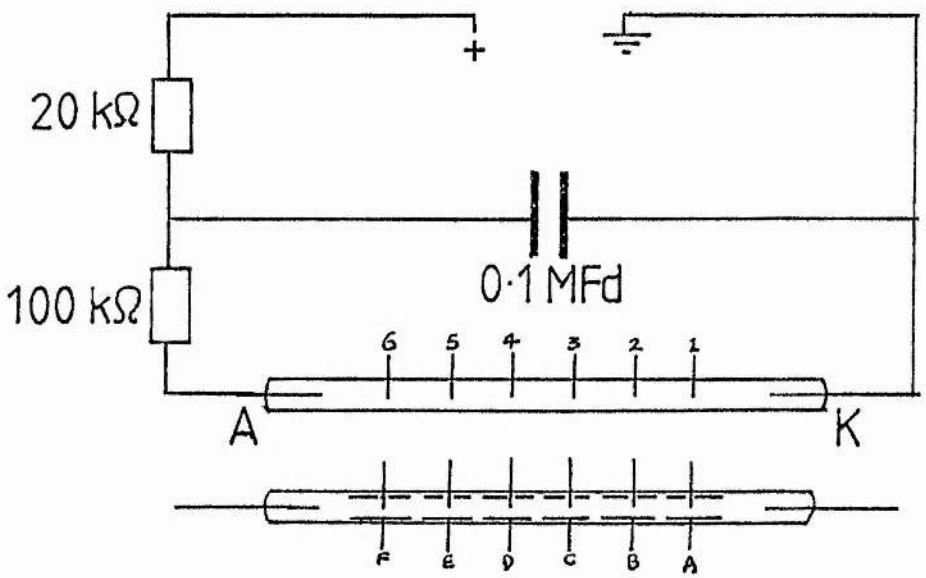

Figure 3.2 Circuit used to determine the axial electric field (X).

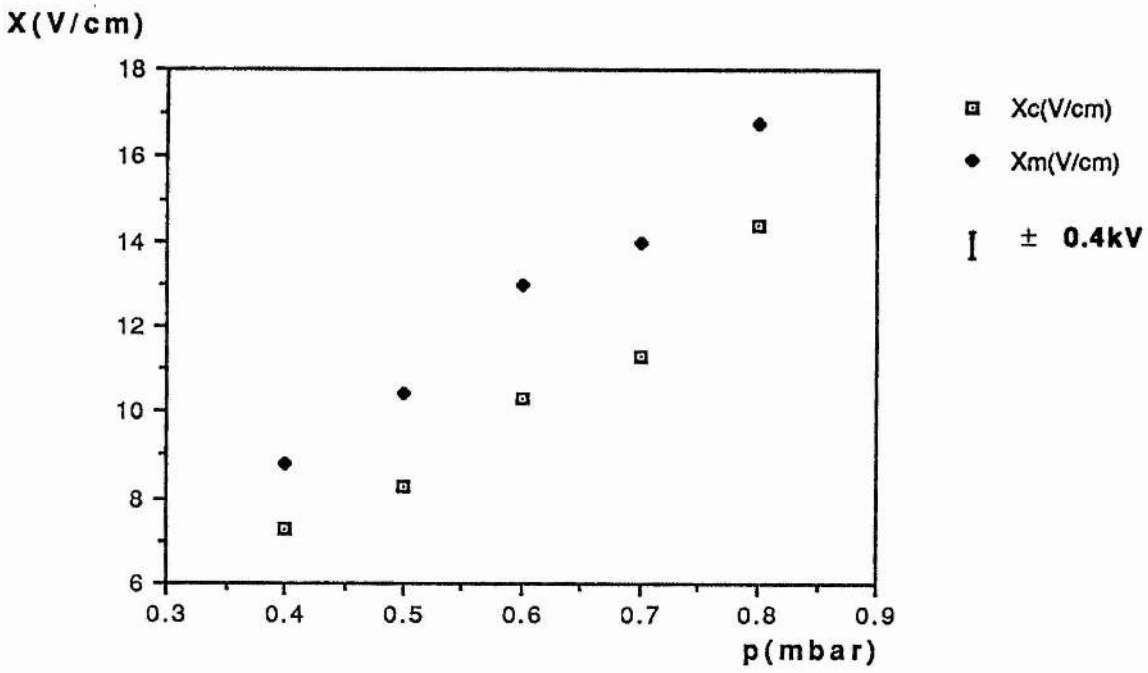

Figure 3.3 Plot of axial electric field X, (Xc - quartz tube, Xm - metal cylinders) versus pressure p.

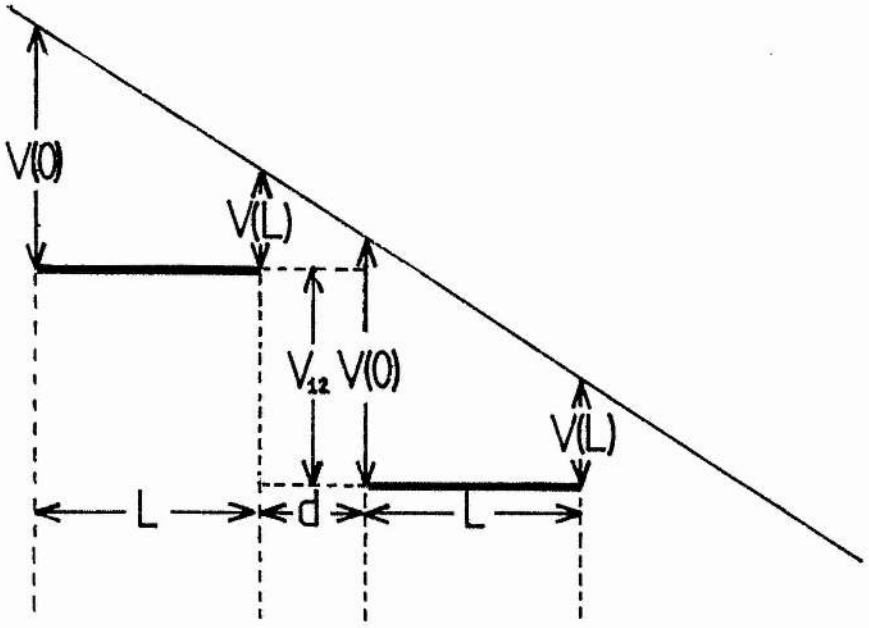

Figure 3.4 Floating potentials of metal segments in an established discharge.

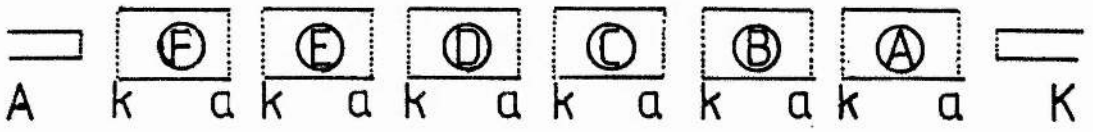

Figure 3.5 Formation of anodes and cathodes at the ends of floating metal segments.

Figure 3.6 The appearance of the glow discharge in the regions between the metal segments.

a) No interconnections.

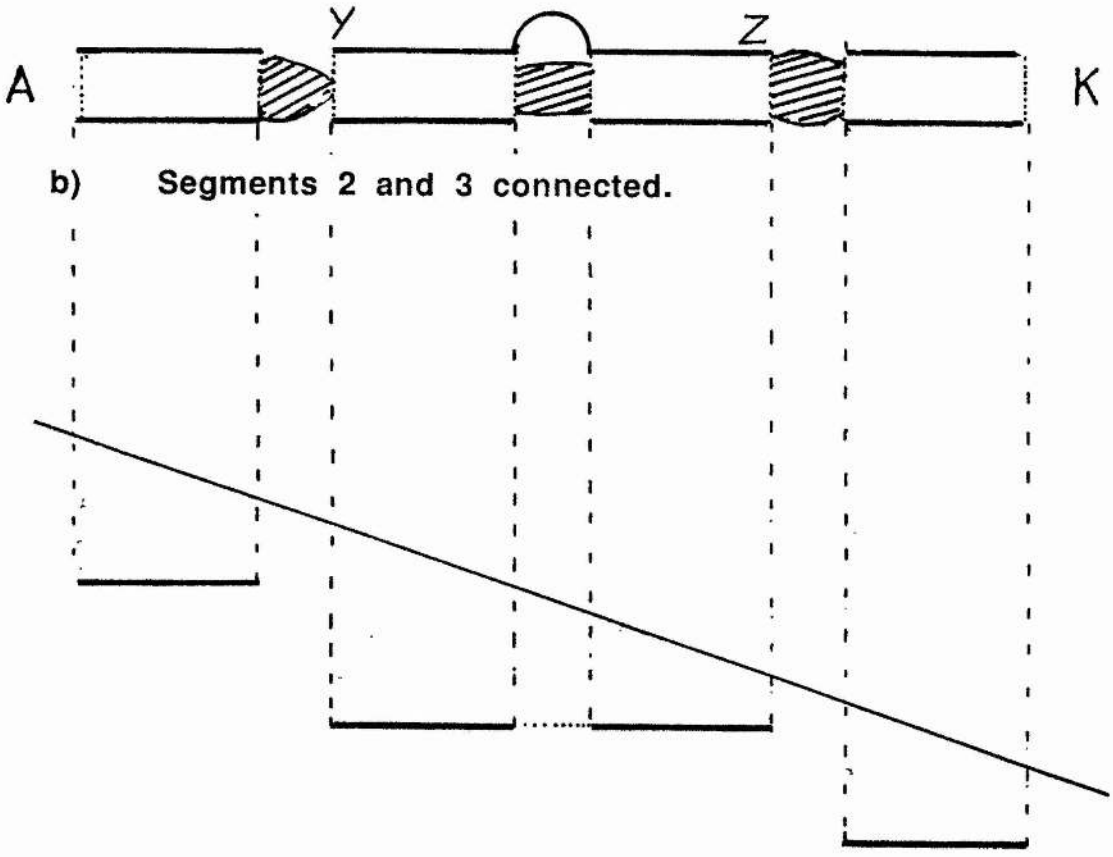

b) Segments 2 and 3 connected.

c) Wall potentials for case b. The sheath thickness is a function of the potential difference between the plasma and the wall.

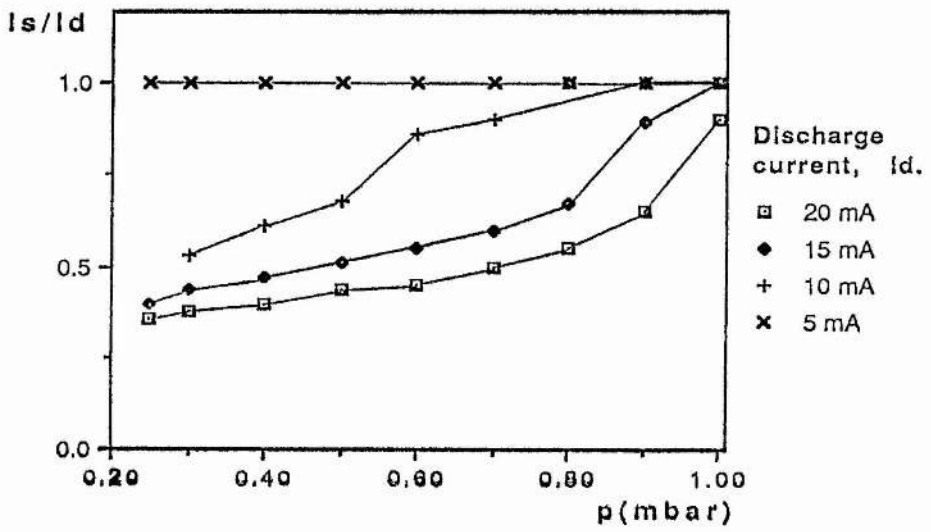

Figure 3.7 Plot of the ratio of inter-segment current to discharge current (I_s/I_d) versus pressure (p).

CHAPTER 4.

EQUIPMENT.

4.1) Introduction.

This chapter describes the apparatus used to produce a high current density DC discharge in an argon-metal vapour mixture. A basic schematic of the system is shown in figure (4.1). The three main parts of the system are;

(i) The plasma jet and vacuum system.

(ii) The discharge tube.

(iii) The power supplies.

Particular emphasis is placed on the design and construction of the discharge tube. This tube is in three parts; an outer, water-cooled, segmented aluminium "support" tube, a quartz tube, and the molybdenum segments that confine the discharge and hold the metal that is to be vaporised.

4.2) The vacuum system and plasma jet cathode.

The plasma jet is a modified standard B.O.C. unit. The construction of the jet has been described by Maitland (1969), along with its uses and its advantages over other thermionically emitting cathodes. The plasma jet produces many ionised species which help with discharge initiation.

The basic features of the jet are as follows. The cathode is a narrow, thoriated-tungsten rod which is ground to a point at one end. The tip of the rod is at the centre

of an annular, water cooled, copper anode. Gas enters through a pipe at the side of the cathode and is pumped away through the anode orifice. There is a pressure difference maintained between the cathode chamber and the plume chamber (figure (4.1)). When a high voltage (approximately 400 V) is applied between the electrodes, an arc is struck. The arc is forced out into the plume chamber, because of the pressure differential, as a plume of ionised gas. This acts as the cathode for the laser system.

Two vacuum pumps are used. A Genevac GHS 12, single stage, rotary pump of pumping speed 340 litres/min evacuates the system to about 1 torr. A G.E.C. AGMB 130 mechanical booster pump with a pumping speed of 3960 litres/min maintains the system at a pressure below 0.01 torr. The normal operating pressure in the plume chamber, required to maintain a steady jet, is in the region 0.1 to 0.5 torr.

4.3) The discharge tube.

In essence, we have three coaxial tubes, each with a separate function.

a) The outer tube (vacuum envelope) is a water-cooled, segmented aluminium tube.

b) A quartz tube is used to "line" the inside of the vacuum envelope, and to hold the molybdenum segments.

c) The molybdenum segments are aligned along the axis of the quartz tube and form a tube along which the discharge passes.

4.3.1) The aluminium support tube.

The disassembled aluminium tube, henceforth known as the support tube, may be seen in plate (4.1). Figure (4.2) shows the tube in detail. It is based on the design for an argon ion laser (Cornish and Maitland 1973). In the present case the bore has been enlarged.

The aluminium cathode flange bolts directly onto the plume chamber. The flange is water-cooled. The first aluminium segment (figure (4.3)) is bolted onto this flange. The twelve water cooling holes in the first segment coincide with a circular groove in the flange. This groove allows access to the water outlets.

There are a futher eleven aluminium segments, each with a 40 mm internal diameter. These interlock as shown in figure (4.2). Each segment is separated from its neighbour by two O-rings, a nylon spacer and a nylon ring. The nylon spacers, which prevent compression of the O-rings, and nylon rings provide a fixed clearance of about 3 mm between the segments. The O-rings provide the water and vacuum seals. The tenth segment (nearest the anode) has an internal diameter of 36 mm, to retain the quartz tube.

The tube is assembled by stacking all the segments on top of the cathode segment, using locating rods to ensure alignment of the water channels. When the segments are positioned correctly, the compression tube may be slipped directly over them and bolted to the cathode flange. The compression tube is basically a brass cylinder, used to ensure that all the O-rings between the aluminium segments

are compressed. It is designed such that, when the segments are compressed together leaving only the 3 mm clearance between them, they just fit inside the tube. The nylon rings which separate the aluminium segments also prevent contact between the compression tube and the segments. The tube is maintained at approximately earth potential by being in electrical contact with the cathode flange.

The final aluminium segment (figure(4.4)), is situated at the anode end of the compression tube. This segment is connected to the water inlet pipes. The internal diameter differs from that of the other segments in that the diameter increases to form a truncated cone with an angle of 25° towards the anode. This shape reduces the amount of sputtered material entering the discharge. If the segment had been made with a constant bore, sputtering would have tended to produce a similar cone-shaped geometry. (The cone shape prevents the formation of a double sheath (Bridges and Halsted 1967) which normally occurs at abrupt changes in the discharge tube diameter.)

The air-cooled anode jacket bolts onto the "cone" segment, but is insulated both from it and the anode by nylon rings and bushings in the bolt holes. The anode consists of a brass flange into which a split hollow brass pipe (figure (4.5)) has been brazed. The anode has its own water-cooling.

The anode end-piece bolts onto the anode. The end-piece supports the aluminium Brewster angled mount. The mount is designed to ensure that minimum losses occur at the windows. The mounts retain 30mm x 3mm (laser grade) quartz windows. A

side-arm on the end-piece has a connection for an electrophoresis tube. This tube leads back to the plume chamber, and reduces the build-up of pressure gradients in the discharge tube. A needle valve is connected into the system via a T-piece in the electrophoresis tube. This valve allows the system to be brought up to atmospheric pressure slowly, to prevent the molybdenum segments from being dislodged.

4.3.2) The quartz tube.

A quartz tube, of 35 mm internal diameter, slides down the centre of the support tube. This tube contains the molybdenum segments, shown in figure (4.7). A quartz spacer is sealed into the anode end of the tube to retain the molybdenum segments. The quartz tube prevents metallic deposits being formed on and between the aluminium segments. The quartz has the advantage of having a high devitrification temperature. As it is transparent the molybdenum segments may be loaded with ease.

4.3.3) Molybdenum segments.

The bobbins, shown in figure (4.6), consist of cylinders of molybdenum (O.D. 10 mm, I.D. 6 mm), with thin 24 mm diameter molybdenum discs at each end held in place by a retaining plug. The bobbins have a total length of 25 mm. The retaining plugs each have a 2 mm diameter axial hole. These bobbins are held inside thin walled molybdenum

cylinders which are spot welded to the end discs. Molybdenum is used because of its high melting point and its low vapour pressures at the expected operating temperatures of about 1600°C.

A high current density discharge can be maintained along the axis of the molybdenum segments (cylinders plus bobbins). The axial gas temperature is high enough to produce a suitable vapour pressure (≈ 0.01 torr) of the enclosed metal. The cylinder surrounding the bobbin allows the bobbins to be held by alumina rings (figure (4.7)). The cylinder also acts as a radiation shield. The alumina rings have a 25 mm internal diameter, a 32 mm outer diameter and an approximate length of 10 mm. The molybdenum segments are wedged tightly within the rings by thin pieces of molybdenum.

Zirconia felt (a good insulator) is wrapped around the alumina rings to allow the segments to fit snuggly inside the tube. This prevents the discharge from establishing itself anywhere other than the central bore. Quartz spacers give a 10 mm separation between segments, and a 25 mm separation between alumina rings. Supporting the segments in such a fashion allows two problems to be solved:

i) The temperature of the quartz tube in contact with the zirconia felt will remain below the devitrification temperature of quartz (1100°C), although high temperatures (1600°C +) may be obtained in the central bore.

ii) The metal vapour condenses onto the cooler parts of the tube (the quartz spacers) leaving metallic deposits. The spacers do not become completely coated because of

shadowing by the molybdenum cylinders which prevents metal being sputtered onto a small area of quartz adjacent to the alumina rings. This prevents the formation of a continuous metal track, which would allow the current to run through it, instead of the gas. The quartz tube containing the molybdenum segments is shown in figure (4.7).

The segments may be aligned using a piece of wire threaded along the centre. After alignment, a suitable length of quartz spacer is inserted at the cathode end of the quartz tube to hold the segments in position. This spacer also has a wrapping of zirconia felt to hold it in position.

A zirconia washer is placed in the cathode flange and covers the end of the quartz tube. The washer prevents a discharge being initiated in the gap between the quartz tube and the aluminium segments. A brass washer prevents the quartz spacer from sliding into the plume chamber. The two washers are held in place by an aluminium retaining ring which screws into the cathode flange. The whole assembly bolts onto the side of the plume chamber.

4.4) The power supplies.

A schematic diagram showing the power supply connections is given in figure (4.8). The maximum output voltage from the plasma jet supply is about 40 volts. This is not enough to ignite the discharge so it is necessary to use the jet starter supply. The plasma jet usually ignites when the voltage across the electrodes is about 400 volts

(Argon, 0.3 torr). The starter supply is then switched off to leave the plasma jet operating at 30 amps and 15 volts. A blocking diode protects the power supply which drives the jet.

The cathode of the plasma jet is not connected to earth (through the discharge tube supply) until after jet ignition. If the cathode is connected directly to earth, the jet anode would "see" two earths, one at the cathode and one at the plume chamber. The discharge path between the anode and the plume chamber is the more favourable, because of the lower pressure. Consequently there is a tendancy for an arc to be struck between them. Connecting the jet cathode to earth after ignition solves this problem. (Connection c, figure (4.8)).

The main discharge power supply (Brentford Supply, BS) is controlled by a Brentford on-load voltage regulator (50 kVA, single phase, at 415 volts). Figure (4.9) shows the rectification and smoothing components connected to the regulator. An L-section filter produces smoothing. High wattage resistors are connected in series with the discharge tube. These resistors limit the current at breakdown and ensure that the total resistance of the load always remains positive (Appendix 7). Firebars are ideal for current-limiting resistors, as they can dissipate powers of up to 1 kW. The Brentford supply is connected across the system between the support tube anode and the plasma jet cathode.

Under typical discharge conditions (for example, three molybdenum segments, 0.5 torr argon) the maximum output of the Brentford supply is about 9 amps at 2.5 kV (limited by

power dissipation in the load resistors). In order to obtain higher current densities, a Motor Generator supply (Newport Instruments Magnetic Power Supply (C904)) is used. The Motor Generator can provide a current of 100 amps at 250 volts. The maximum current available is, however, limited to about 20 amps by the impedance of the discharge.

The Brentford supply is used to initiate the discharge, as the maximum output voltage of the Motor Generator is less than the anode-cathode breakdown voltage. When the discharge becomes stable (no current or voltage fluctuations), at a current of about 5 amps, the Motor Generator is energised. (The discharge has a positive dynamic impedance at currents greater than about 5 amps, hence load resistors are unnecessary in the Motor Generator circuit.(Appendix 7)) The Motor Generator current is increased until the total current is about 10 amps. The power may then be removed from the Brentford supply, leaving the Motor Generator supplying a current of 5 amps.

References.

A.Maitland. "A plasma jet as cathode for an argon laser." J.Phys.D, Vol 2. 1969. p 535.

J.C.L.Cornish and A.Maitland "A demountable argon ion laser of "all-metal" construction." J.Phys.E,Vol.6, 1973. p 880.

W.B.Bridges and A.S.Halsted "Gaseous ion laser research." AFAL TR6789, Hughes Research Labs. Malibu, California. 1967.

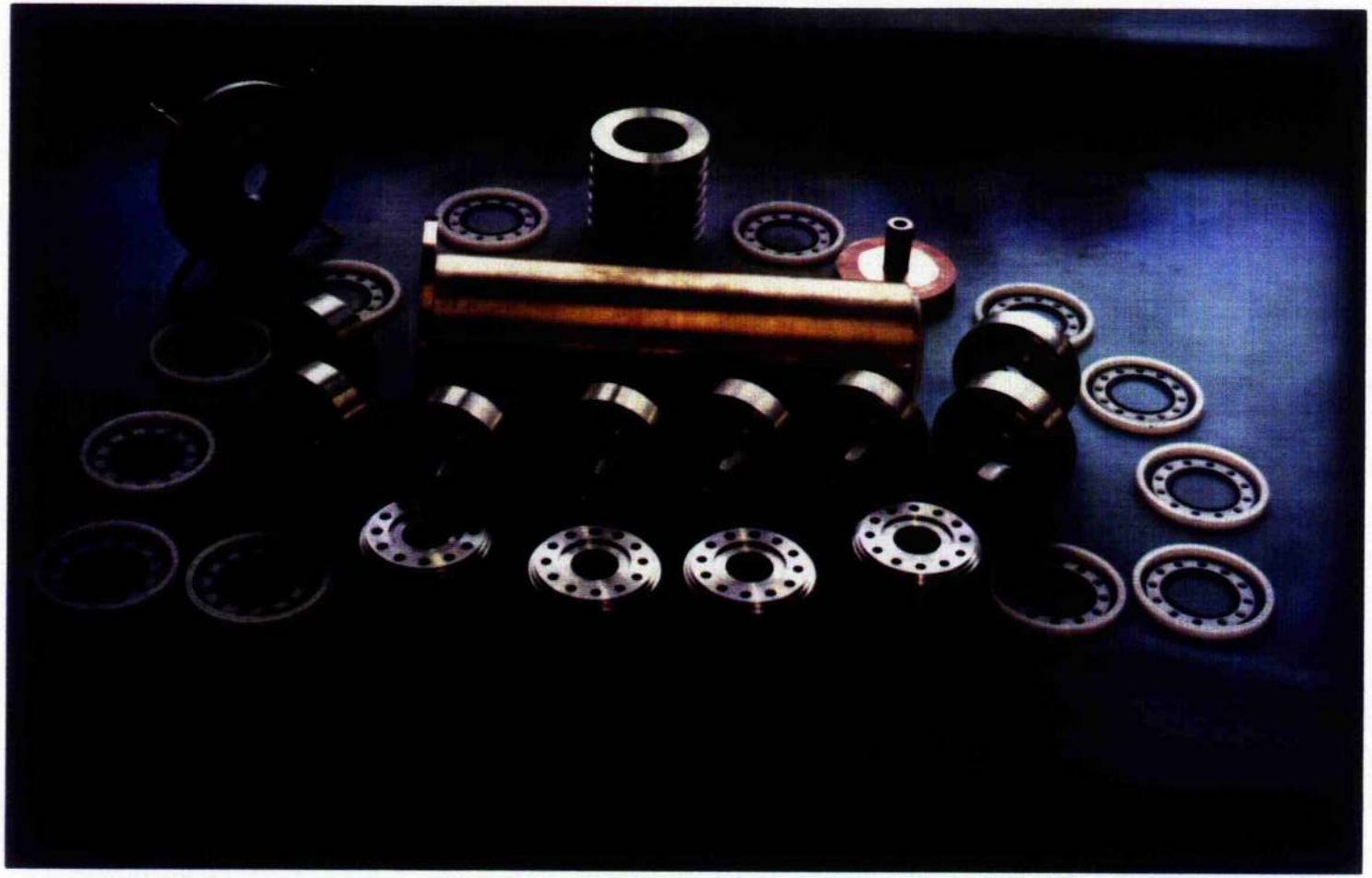

Plate 4.1 The disassembled aluminium support tube.

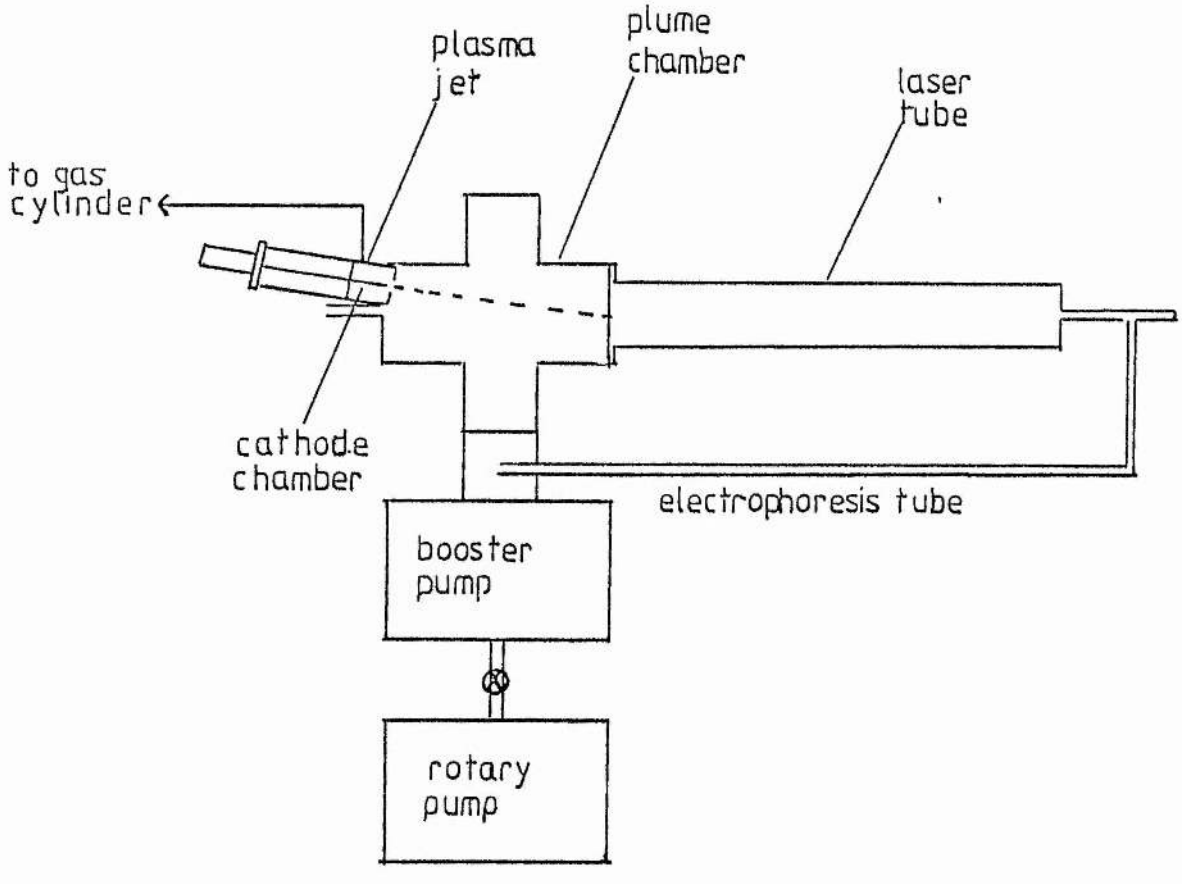

Figure 4.1 Schematic diagram of the "laser" system.

ALUMINIUM TUBE.

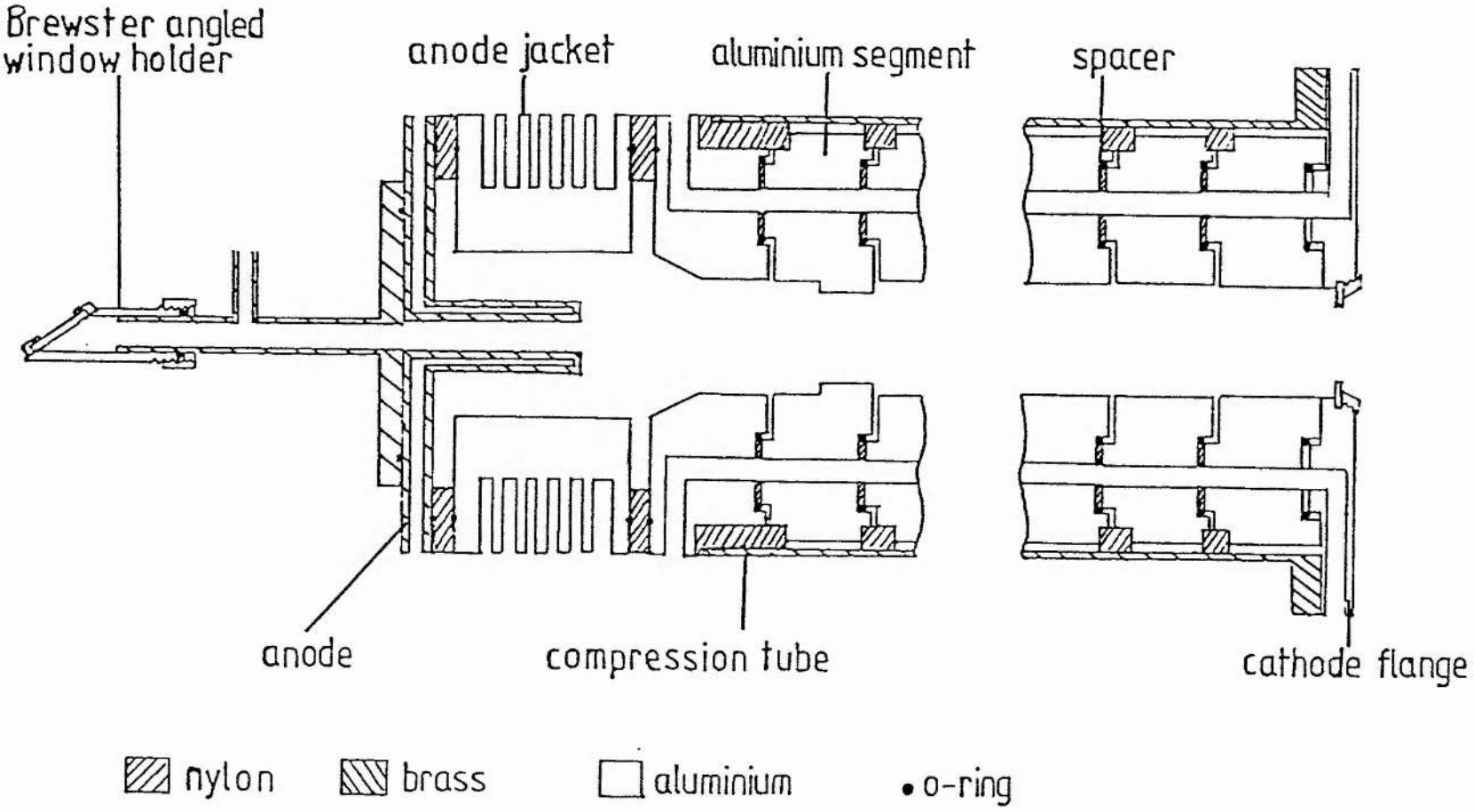

Figure 4.2 Support tube - Longitudinal cross-section.

Figure 4.3 Aluminium segments.

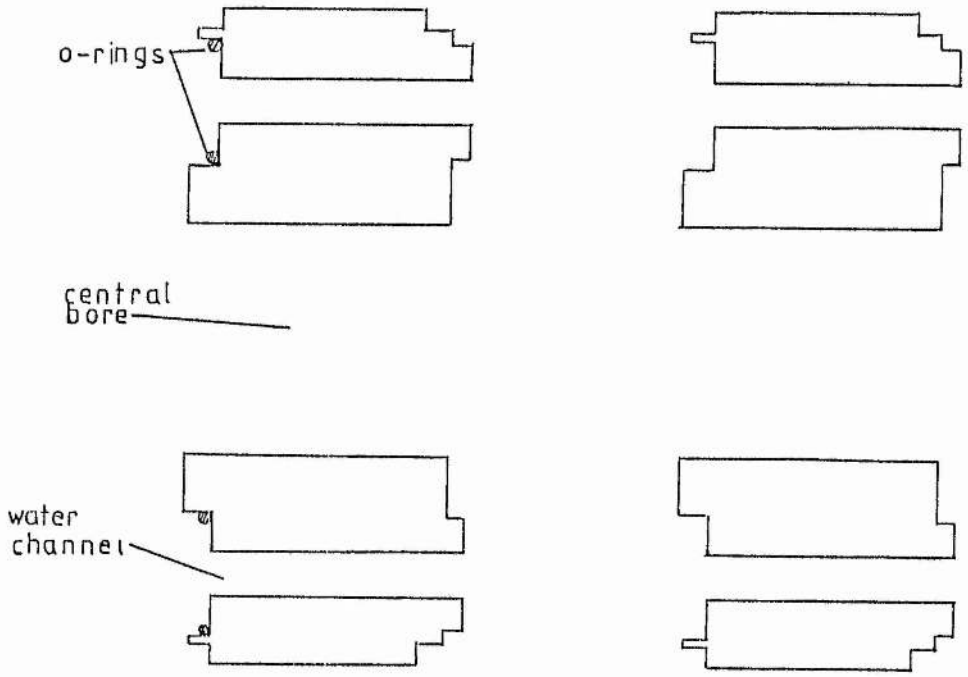

a) Longitudinal cross-section.

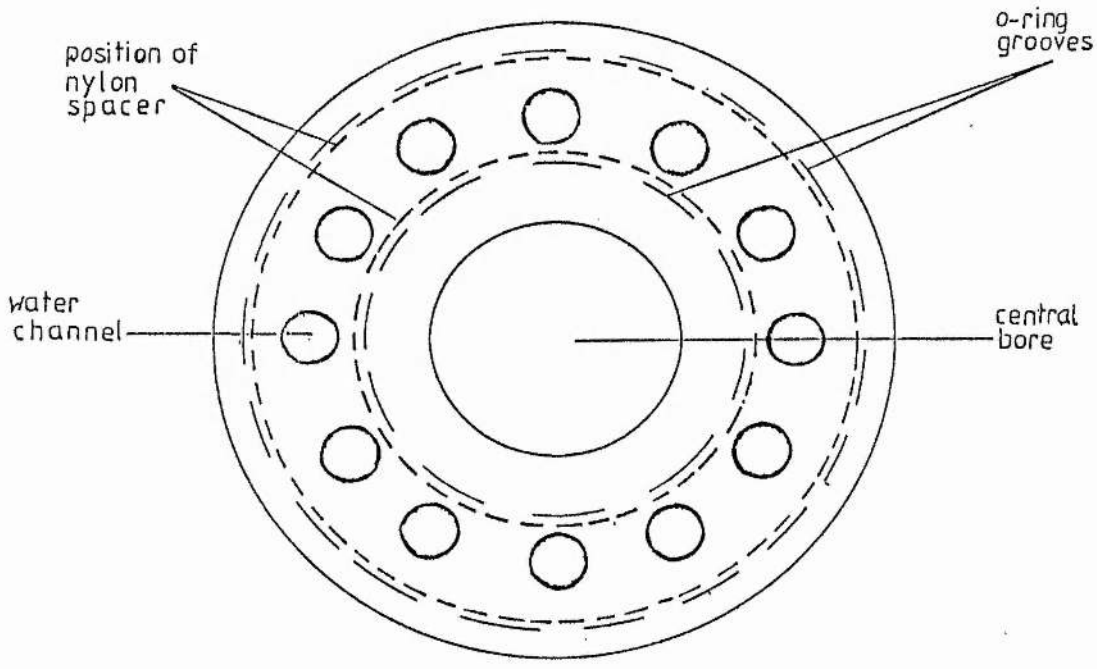

b) Transverse cross-section.

Figure 4.4 Aluminium "cone" segment.

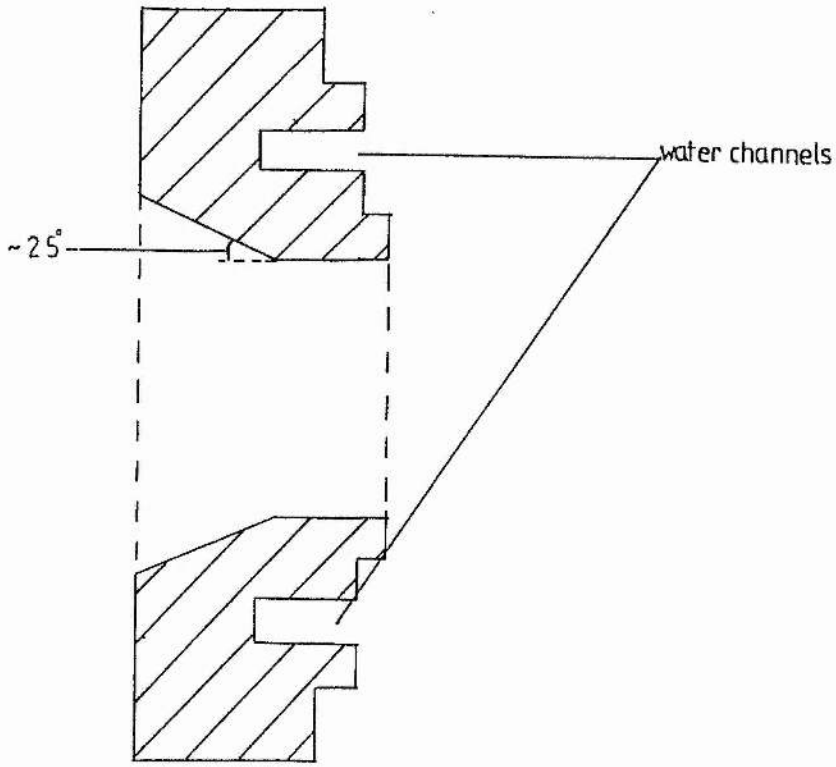

Figure 4.5 Brass anode.

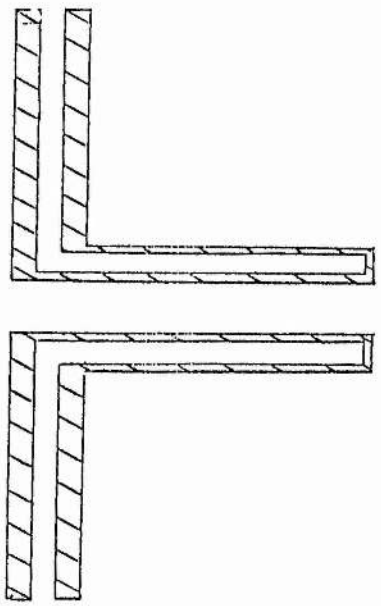

a) Longitudinal cross-section.

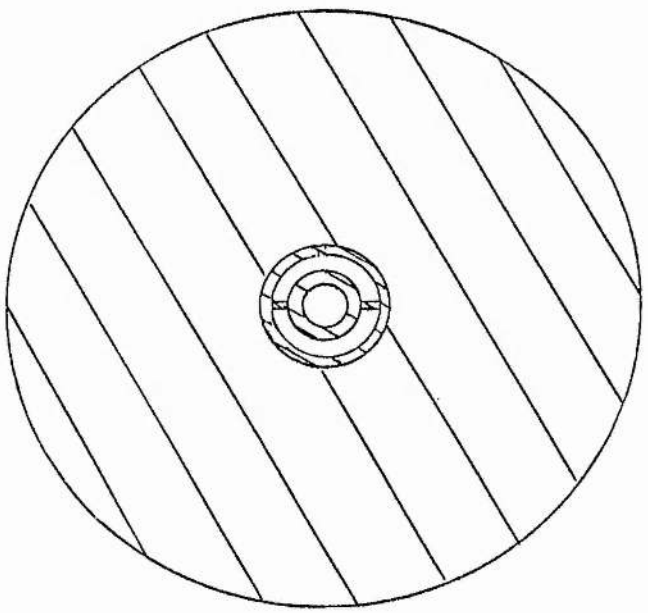

b) Transverse cross-section.

Figure 4.6 Molybdenum bobbin.

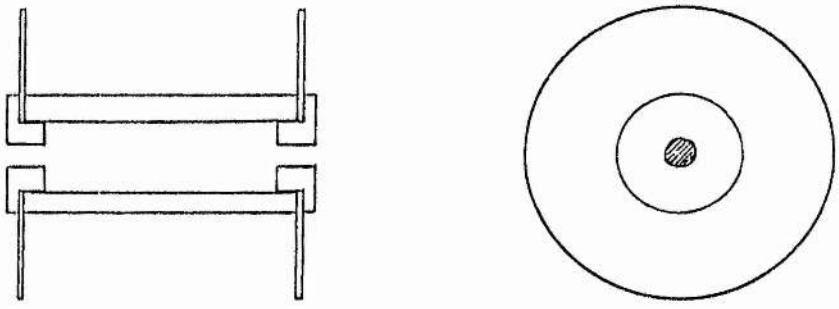

a) longitudinal cross-section.

b) side view.

Figure 4.7 Quartz tube containing molybdenum bobbins.

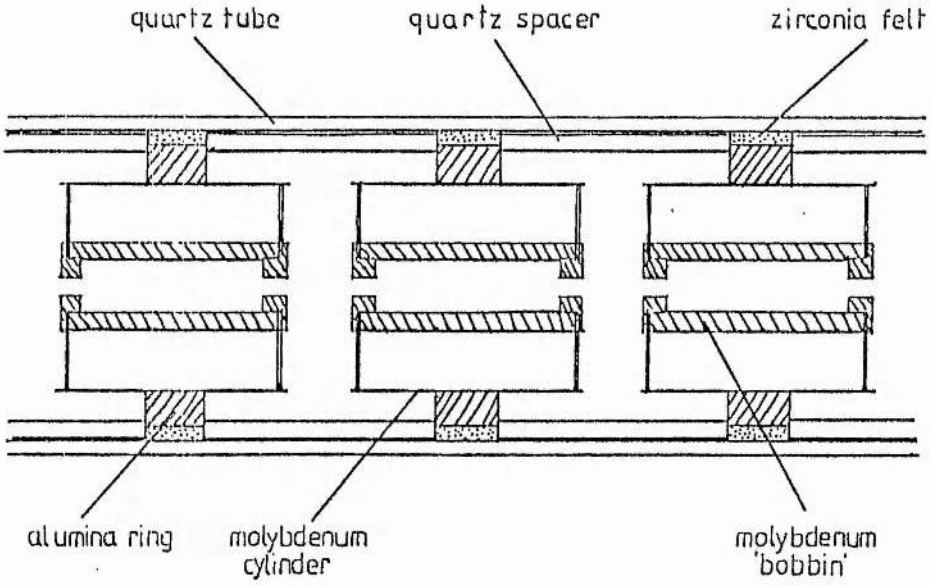

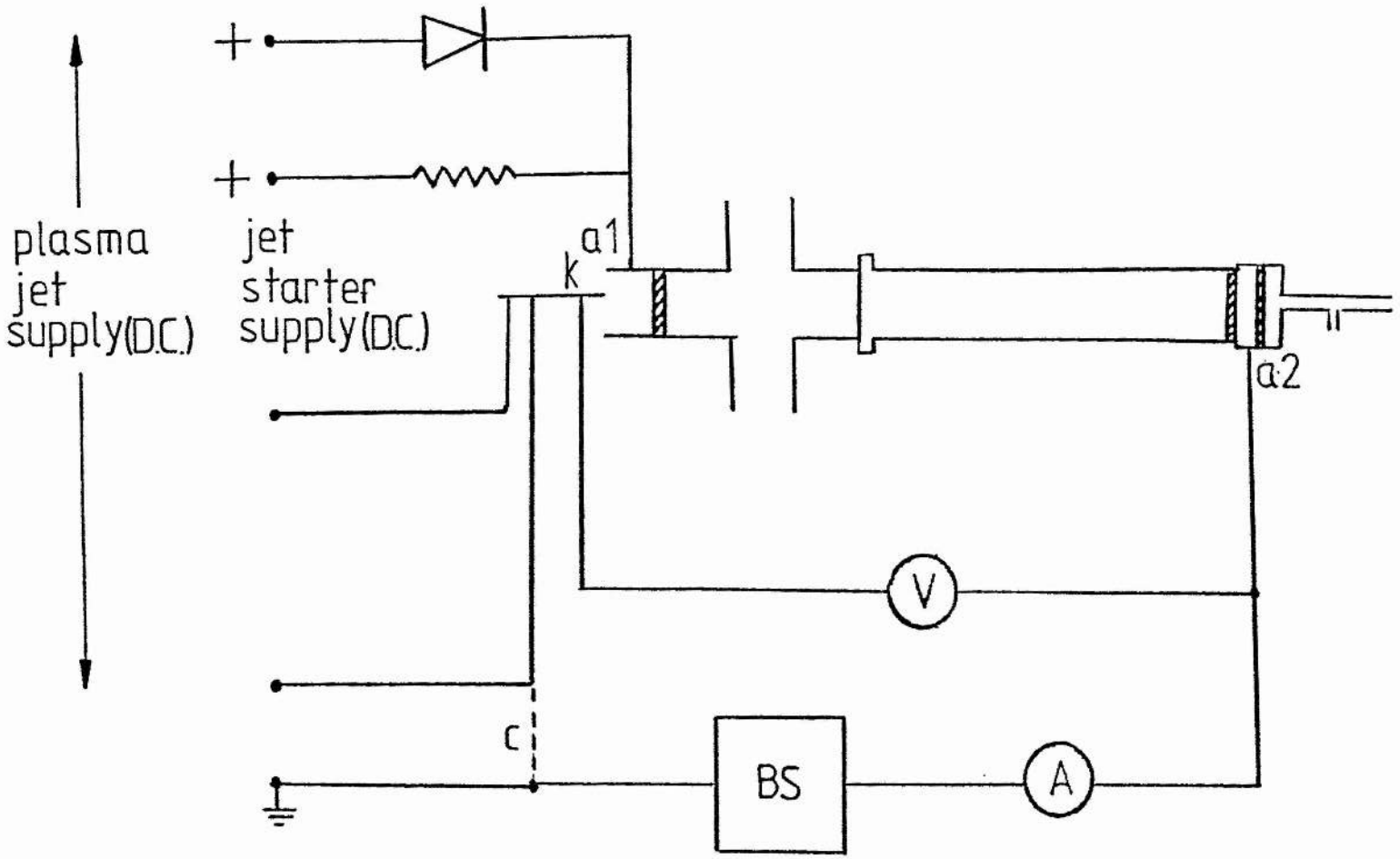

Figure 4.8 Power supply connections.

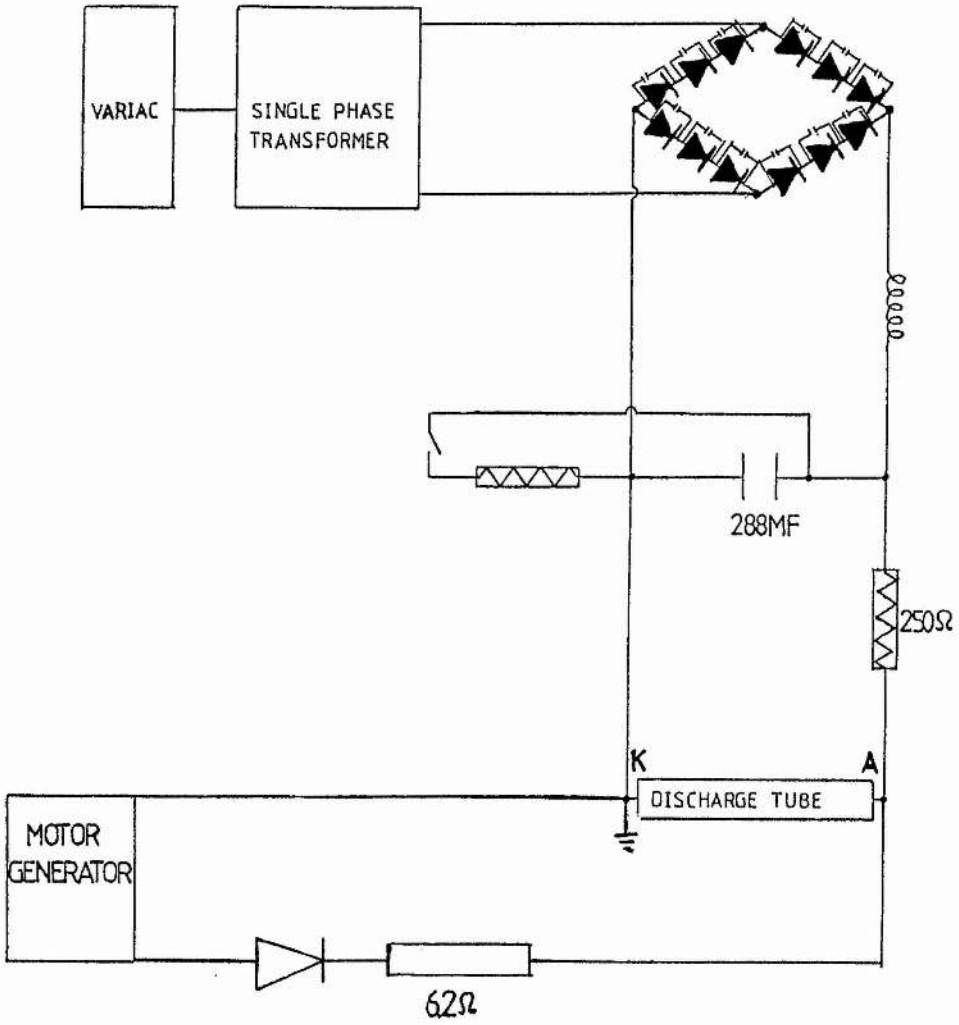

Figure 4.9 Brentford Regulator and Motor Generator supply circuit.

CHAPTER 5

EXPERIMENTAL WORK ON THE MOLYBDENUM SEGMENT DISCHARGE TUBE.

5.1) Introduction.

A high current density discharge in a noble gas/metal vapour mixture is discussed. The use of molybdenum segments to confine the discharge allows high current densities, along with high wall temperatures to be obtained. Metal, usually in the form of pieces of wire, is contained within the molybdenum segments. The wire supplies metal vapour through discharge heating. The high current densities produced in the system should lead to ionisation of the vapour, followed by excitation of the ions by direct electron impact. This mechanism may produce lasing transitions in the blue to ultraviolet regions of the spectrum, such as occur in the continuous wave argon ion laser. As the metals have much lower ionisation potentials (Silver; V_i = 7.6 V), than the noble gases (Argon; V_i = 15.8 V), such a laser has the possibility of being inherently more efficient.

A plasma jet is used as the cathode of the system. The jet allows large currents to be drawn without damage and provides a source of preionisation for starting the high current density discharge. Argon is used because it is atomic and thus enables a stable plasma jet to be obtained. It is also a suitable buffer gas for metal vapour lasers

Current limiting (or load) resistors are used to stabilise the discharge (appendix 7). Two sets, of nine fire

bars connected in series, connected in parallel, provide a total resistance of 250 Ω. The maximum power dissipation is 1 kW (V_{max} = 240 volts.) per bar, which limits the maximum discharge current (from the Brentford regulator power supply section(4.4)) to about 9 amps.

The discharge tube consists of three components. The outer support tube is of segmented design and is shown in figure (4.2). The aluminium segments are insulated from each other by nylon spacers and sealed with neoprene O-rings. The tube is water-cooled. A quartz tube sits within the support tube. The quartz tube contains the molybdenum segments, figure (4.7).

Measurements of discharge sustaining voltage, as a function of current and pressure are made. The sustaining voltage is seen to depend on the number of metal segments and whether metal vapour is present in the discharge.

The axial gas temperature of an argon ion laser may be estimated from the formula given by Chester (1968). The gas temperature is proportional to the current density and the tube diameter. A gas temperature of 1000°C is obtained from the formula, at current densities of 120 amps/cm^2 in a 2 mm bore tube.

In order to obtain suitable metal vapour densities (≈ 0.1 torr) silver was chosen for the initial experiments. Silver has a vapour pressure of ≈ 0.1 torr at 1150°C (Nesmeyanov 1963), and ultra-violet laser radiation has been obtained from the neon-silver hollow-cathode laser (Gerstenberger et al. 1980).

5.2) Argon discharge.

After the plasma jet is established it is generally allowed to run for ten minutes, until it appears to stabilise, and fluctuations in voltage and the associated fluctuations in intensity cease to occur. The pressure in the plasma jet plume chamber is set at about 0.3 torr.

The main discharge is initiated by applying a voltage of between 1.4 and 1.8 kV from the Brentford regulator supply (section (4.4)). (The breakdown voltage increases as the number of segments increases.) The sustaining voltage of the discharge then settles at several hundred volts. The final voltage depends on the value of the current. Crude choice of current is made by selection of the value of the current limiting resistors which is much greater than that of the dynamic impedance of the discharge. The voltage (and therefore the current) may be continuously varied by the Brentford regulator. Suitable currents may be obtained between the discharge extinction value (≈ 0.5 amps) and the power supply limit set by power dissipation in the load resistors (≈ 9 amps). Voltage and current measurements are taken using a model 8 II and an 8 IV AVO meter. The 8 IV AVO meter is fitted with an AVO DC current shunt, allowing currents up to 45 amps to be measured. Pressure values, at the plume chamber, are measured using an AEI VH8 thermocouple (6.4 mA current).

The light emitted by the discharge has a high ultra-violet content. The ultra-violet light is detected by observing the fluorescence it produces on a sheet of white

paper.

The power dissipated per segment at a current of 7 amps is approximately 360 watts over an internal area of 4.71 cm^2. The power density is then 76 W/cm^2 at the segment wall. When the discharge is extinguished after running for some time at currents greater than 7 amps, the metal segments are seen to glow red.

5.2.1) Discharge paths.

In the design and construction of discharge tubes with metallic boundaries, care must be taken to prevent paths other than the axial path being available to the discharge. The external diameter of the alumina rings (figure (4.7)), which surround the molybdenum segments, is slightly less than the internal diameter of the quartz tube. This difference produces a small gap between the ring and the top of the tube. The discharge may then form in this gap rather than along the axis of the metal segment. The gap is filled with a strip of zirconia felt to prevent a discharge forming along the path on the outside of the segments.

If the zirconia felt does not completely surround the alumina rings and a narrow gap is left between two ends of the felt, a discharge may still form in this gap. The high current density in the gap, between the ends of the felt, would cause the wall temperature to rise above the softening point of quartz, and could produce a hole in the quartz tube. This would allow ionised gas to come into contact with the adjacent aluminium segment. A conduction path would then

be established between this segment and the earthed segment at the exit of the plume chamber (figure (5.1)).

There is a tendency for a discharge to form along a path with insulating boundaries (alumina ring and quartz tube), in preference to one with conducting boundaries (axis of metal segments). A discharge forms along the path with the lowest maintenance (sustaining) potential difference between the anode and the cathode (section (7.10.2)). The energy losses at the walls (and hence the discharge sustaining voltage) are less in tubes with insulating walls than in tubes with conducting walls (section (2.4)).

After several hours of operation, a silvery deposit of molybdenum could be seen on the quartz spacers. The resistance of the coating on the spacers was measured with a digital volt meter and found to be between 4 and 15 kΩ. As these values are very much greater than the dynamic impedance of the discharge it is unlikely that the spacers would represent a preferred path as opposed to the gas.

If a low resistance coating of metal is formed on the quartz spacers between the molybdenum segments, the two segments become electrically connected. The connection of adjacent segments produces a metal segment of over twice the length of the molybdenum segments (two segments plus the coated spacer (figure (4.7))). The increased length of metal may exceed the maximum length of a metal segment for axial discharge formation (section (2.3.2)). If the maximum length is exceeded, the current will flow through the molybdenum segments and the metal coating, rather than along the axis of the segments.

5.2.2) Operation using five segments.

With five segments contained in the tube, the breakdown voltage is approximately 1.8 kV, at a pressure of 0.28 torr. At currents of the order of 5 amps (350 V) a bright spot can be observed on a piece of paper placed next to the anode-end window. The spot implies that the discharge is running along the central bore. At currents below 1 amp, the region of high current density may be observed directly by eye. At the cathode side of the discharge the ultra-violet glow on a piece of paper is surrounded by a pink annulus, due to the plasma jet discharge in the plume chamber; the bright central spot cannot be seen.

Current fluctuations ($\approx \pm$ 0.5 amps) can occur when the discharge current is about 7 amps, although the voltage remains approximately constant at 260 volts. These fluctuations may be due to out-gassing of materials, as the segment temperature increases.

The voltage-current characteristic curve at a pressure of 0.35 torr is shown in figure (5.2). Below 6 amps the discharge exhibits a negative dynamic impedance (see appendix 6). Above 6 amps the characteristic is typical of a normal glow discharge (appendix 1), where the discharge voltage remains constant (270 $\pm$ 5 volts) as the current increases.

5.2.3) Operation using four segments.

With an initial pressure of about 0.4 torr (thermocouple gauge) the breakdown voltage of the gas, in the molybdenum segment discharge tube, is approximately 1.5 kV. The voltage-current characteristic curve for 4 segments, at a pressure of 0.42 ± 0.02 torr, is shown in figure (5.2). Comparing this curve with that for five segments (figure (5.2)), it can be seen that the sustaining voltage is of the order of 60 volts less than for the five segment case. Experiments show that there is a slight increase in the sustaining voltage with pressure (≈ 10 volts per 0.1 torr). Therefore, although the characteristics were measured at slightly different pressures, the increase in sustaining voltage with increasing pressure does not account for the voltage differences recorded when the number of segments is changed. The difference in the sustaining voltage between the four and five segment discharges shows the trend of a decrease in discharge voltage as the number of metal segments decreases.

In low pressure gas discharges, approximately 50 % of the input energy is lost through charged particles delivering their kinetic and potential energies to surfaces in contact with the discharge (Francis 1956). If the internal surface area decreases, then the energy loss decreases. The reduced energy loss means that less power (ie a lower voltage, at constant current) is required to maintain the discharge. The sustaining voltage of the discharge is found to decrease when a segment is removed

because a large surface area of tube, the molybdenum segment and alumina ring, is effectively "replaced" by a much smaller surface area, the length of quartz tubing which surrounds the alumina ring (see figure (4.7)).

5.2.4) Operation using three segments.

Figure (5.2) shows a V-I characteristic curve for a three-segment discharge at a pressure of 0.33 torr. It can be seen that the sustaining voltages of the three-segment discharge lies below the voltages obtained when four or five segments are used. The reduction in sustaining voltage as the number of metal segments decreases is mentioned in the previous section, with reference to the relationship between the area of the surface in contact with the discharge and the energy losses. The energy losses decrease as the surface area decreases.

At the lower operating voltages encountered when three segments are used, it is possible to use the Motor Generator power supply (after discharge initiation, as described in section 4.4). This supply has a maximum output voltage of 250 volts, and currents of up to 20 amps may be obtained with the discharges under consideration (The maximum available current from the Brentford supply is 9 amps).

To determine whether laser action occurs at currents greater than 10 amps, argon ion laser mirrors (488 nm) were placed at each end of the system. A 2 metre, 100% reflector was placed at one end of the system and a 2 metre, 98% reflector was placed at the other end. No lasing was

observed. The absence of laser action is probably due to the use of only 7.5 cm of active length in a total discharge length of approximately 1 metre. Absorption regions (argon II) may be present near the plasma jet cathode. Absorption, window and mirror losses would outweigh the gain for argon II (0.01 dB/cm (300 amps/cm^2 at 488 nm) Sayers 1969).

In order to assess tube damage at current densities in excess of 300 amps/cm^2, the molybdenum segments, alumina rings, and zirconia felt were examined. The zirconia felt had deteriorated, becoming grey and disintegrating around the edges. The felt had stuck to the alumina rings in some places. It also appeared to have shrunk so that the rings were no longer held tightly in place within the quartz tube. "Silvery" deposits were present on the sides of the alumina rings. The middle molybdenum segment appeared to have some material build-up at the entrance and exit holes. This build-up is probably due to sputtering, by ion bombardment, within the segment.

The next stage of experimentation involved placing a suitable metal, as a lasing medium, within the segments.

5.3) Experiments with silver as the discharge medium.

Laser action has been observed in the silver ion at 318 nm and 462 nm, in the neon-silver hollow-cathode laser (Gerstenberger et al. 1980.) In the hollow-cathode laser, silver densities of the order of 10^{14} cm^{-3} are produced through sputtering. In order to obtain this vapour density

through discharge heating, temperatures in excess of 1000°C must be produced. This temperature is within the estimated operating temperature range of the system. (The segments are assumed to be in thermal equilibrium with the gas, and the gas temperature may be estimated from the formula given by Chester (1968)) At 1000°C the vapour pressure of silver is approximately 0.01 torr (Nesmeyanov 1963).

5.3.1) Optics.

The optical cavity consists of two 1 inch diameter, 2 metre radius of curvature, concave mirrors (BK7, Technical Optics). The mirrors are coated to give approximately 100% reflectivity between 320 nm and 450 nm at 0° angle of incidence (see figure (5.3)). The mirrors are placed about 10 cm from the Brewster windows in order to produce a stable optical cavity, of length 1.80 metres.

To align the mirrors, a helium-neon laser is directed down the tube and reflected by the far laser mirror back onto a pinhole card on the front of the laser. The mirror is adjusted until the incident and reflected beams coincide. The reflected beam is initially detected by its reflection from a flat piece of glass, used as a beam splitter, situated between the discharge tube and the laser (figure (5.4)). The beam splitter may then be removed and the near laser mirror placed in the beam. The near mirror is then adjusted so that both reflected spots are coincident with the pinhole, ensuring that both mirror surfaces are normal to the beam.

As 100% reflectors are used, any laser emission may be detected by the reflections from the Brewster angled windows. The positions of the reflected beams on the laboratory wall next to the system, are found using the alignment laser. Pieces of white card are placed at these positions in order to see any fluorescence produced by the discharge radiation.

5.3.2) Argon-Silver Discharge.

Five molybdenum segments are each loaded with silver wire (2 X 1.5 cm lengths of 0.5 mm diameter, Johnson Mathey Puratronic). Five segments give approximately 12.5 cm of active length.

The discharge is allowed to settle over a period of about one hour, with a constant power supply voltage maintained. The voltage across the tube and the current, over this period, are shown in figure (5.5). The decrease in the discharge voltage with time is believed to be mainly due to the removal of outgassed contaminants from the system.

After ascertaining the current where the discharge characteristic becomes positive ($\approx$ 5 amps), it is possible to use the Motor Generator. The discharge sustaining voltage at currents up to 20 amps, at a pressure of 0.3 torr, is shown in figure (5.6). Although laser emission has not been observed, strong fluorescence of a white card indicates a high intensity of ultra-violet radiation to be present.

Above 20 amps the discharge goes into a mode characterised by bright blue flashes in the plume chamber,

and accompanied by an increase in the discharge current. These flashes are probably due to arcing between the molybdenum segments, across the quartz spacers. The increased current activates the protection facility of the Motor Generator, thus extinguishing the discharge.

5.3.3) Tube Damage.

Many of the quartz spacers have a silvery grey coating on them and show signs of devitrification (see plate (5.1)) implying that they have reached a temperature greater than 1100°C. The outer quartz tube is undamaged. The resistance of the coating in this case can be about 0.2 - 0.4 Ω (as opposed to the 4 - 15 kΩ coating described in section (5.2.1)), which is of the order of the dynamic impedance of the discharge. The total current may therefore pass through the metal coating rather than the gas. The devitrification of the spacers could have been caused by surface flashover of the coated quartz between the segments. The effects of the discharge on the segments and tube can be seen in plates (5.2) and (5.3).

In order to prevent metallic coats forming along the whole length of the spacers, quartz spacers are used which have a reduction in diameter halfway along their length (see plate (5.4)). The narrow bore region of these spacers extends into the discharge path and should be heated to such a degree that metallic coat formation will be impaired. The prevention of metalisation reduces the chance of arcing between the segments.

5.3.4) Argon-Silver discharge characteristics.

A V-I characteristic for an argon-silver discharge (five molybdenum segments) taken at low currents, is shown in figure (5.7). Comparing the discharge characteristic curves, with and without silver present (figure (5.7)) shows that the discharge containing silver has a lower sustaining voltage than that without. This reduction in voltage is not due solely to silver being present. At low currents the input power to the discharge is insufficient to produce significant amounts of silver vapour to reduce the sustaining voltage. The low voltages recorded are probably partially due the removal of contaminants from the system through discharge heating.

The discharge voltage gradually increases with time, due to the migration of silver to the cooler parts of the tube and out of the high current density region. The maximum output voltage of the Motor Generator power supply is reached at currents of about 20 amps. Hence, these relatively high sustaining voltages limit the maximum current density attainable.

The problems of high sustaining voltage, and metallic coating, made it nescessary to redesign the metal segments and use copper vapour as the discharge medium. Copper is chosen as it has a vapour pressure between 0.1 and 1.0 torr from 1400°C to 1600°C (Nesmeyanov 1963), and lasing transitions are produced in the neon-copper hollow-cathode discharge (Gerstenberger et al. 1980). The design of the segments, using experimental work on low current density

glow discharges, is discussed in the following chapter. Further experimental work on an argon-copper vapour discharge is described in chapter 8.

5.4) Conclusions.

High current density discharges have been obtained in argon and argon/silver-vapour mixtures. The sustaining voltage depends on the number of metal segments used to form the discharge capillary, and increases with the number of segments. The increase in sustaining voltage with segment number is due to the increased surface area (and hence increased energy loss) of the discharge tube as segments are added.

The argon/silver-vapour discharge has a lower sustaining voltage than an argon discharge, under similar conditions of pressure, current and tube geometry. Silver has a lower ionisation potential than argon, hence the lower sustaining voltage.

At currents in excess of 10 amps, most of the silver is lost from the segments after about one hour's operation. Such rapid loss could be due to the silver boiling. (The silver vapour pressure is of the order of the argon pressure (0.1 torr) at 1150°C.) The high silver vapour pressure produced when the silver boils leads to a low resistance coating forming on the quartz spacers. The current may then pass through this coating, re-vapourising it. Arcs can then form in the metal vapour between the molybdenum segments. These arcs lead to the formation of unstable discharges, and

can result in devitrification of the quartz tube and spacers.

References.

A.N.Chester. "Experimental measurements of gas pumping in an argon discharge." Phys. Rev. 169(1), 1968, p 184.

M.D. Sayers. "Single pass gain as a function of discharge current for the 4880 A argon ion laser." Phys. Lett. 29A, 1969, p 591.

D.G. Gerstenberger, R.Solanki, G.J. Collins. "Hollow cathode metal ion lasers." IEEE J.Quant.El., QE-16, 1980, p 820.

G. Francis. "The glow discharge at low pressure." Handbuch der Physik, Vol. 22, 1956, p 53.

An.N. Nesmeyanov. "Vapour pressure of the elements." Translated and edited by J.I. Carasso, Infosearch Ltd.,1963.

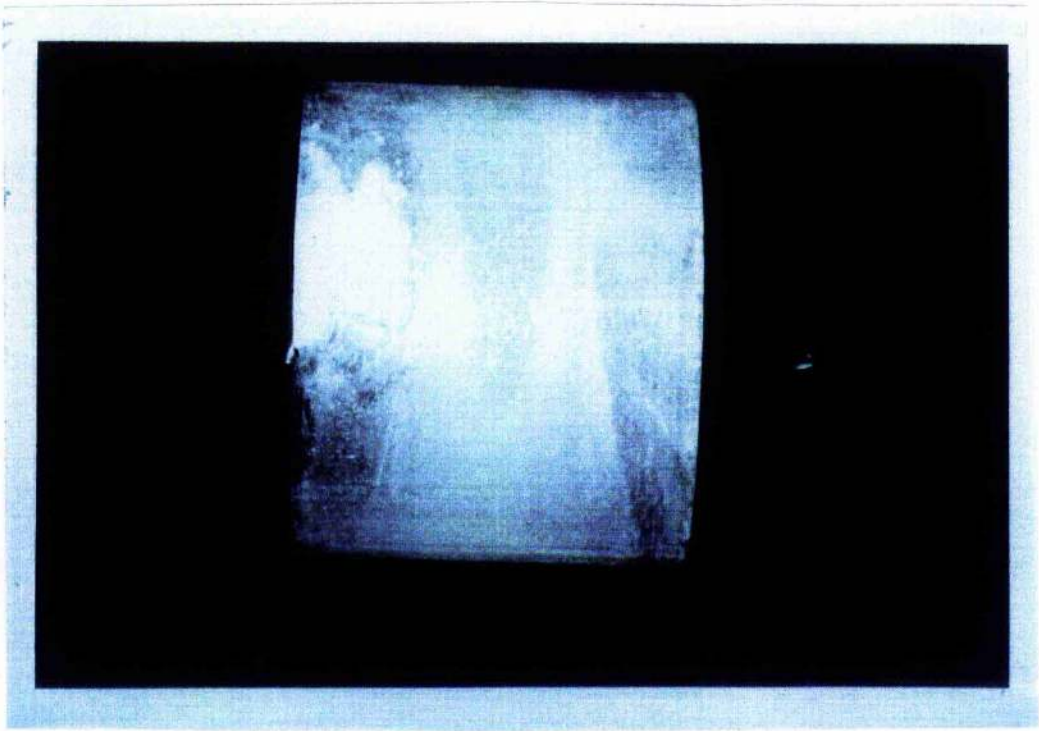

Plate 5.1 Devitrified quartz spacer.

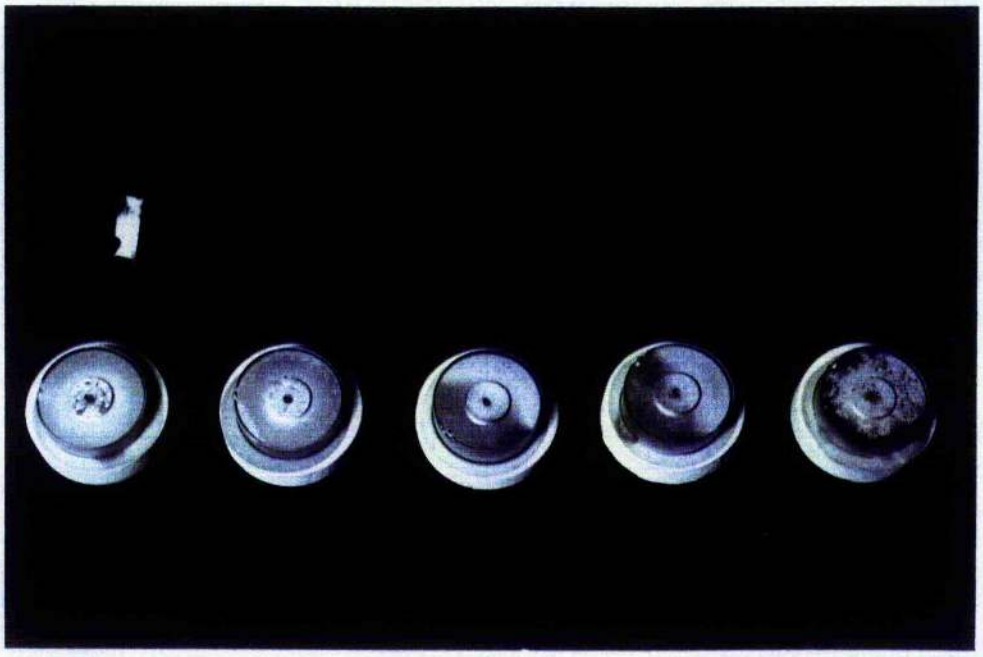

Plate 5.2 Molybdenum segments used to confine an argon-silver discharge. Cathode-facing side up.
The arrow is placed at the segment nearest to the anode.

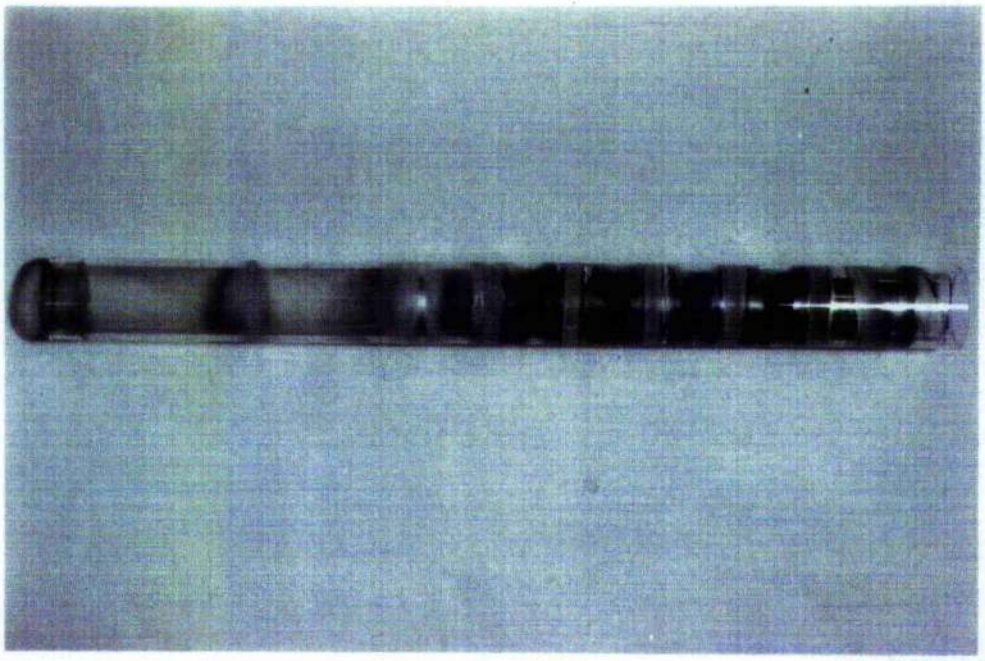

Plate 5.3 Quartz tube showing signs of metallic coating.

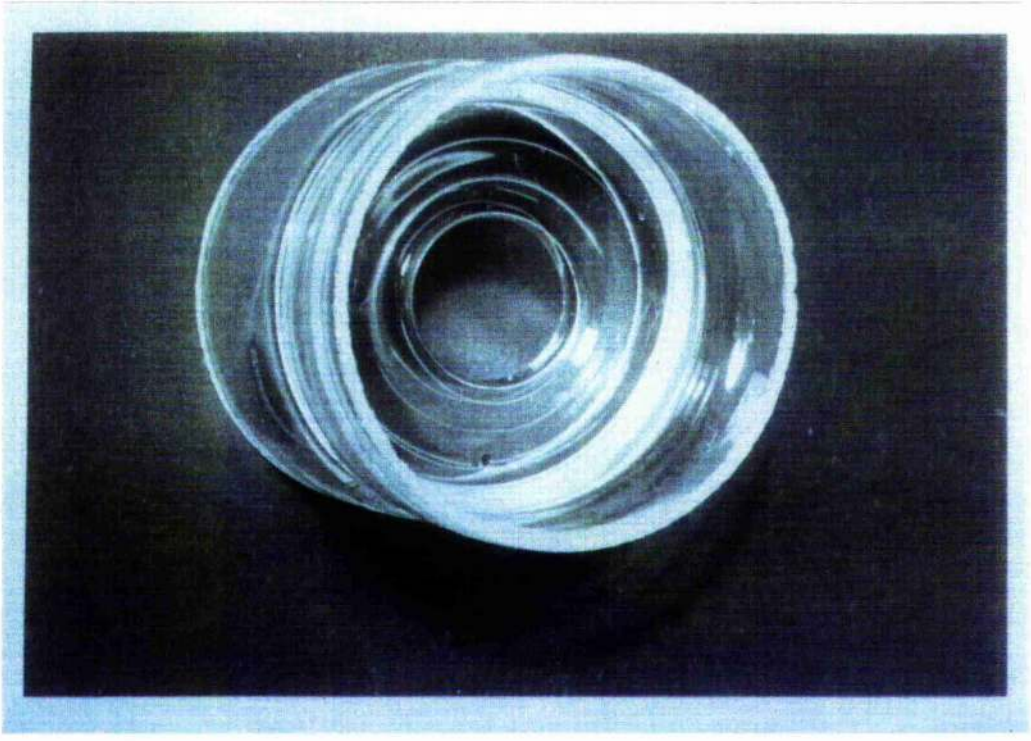

Plate 5.4 Quartz spacer with reduced diameter.

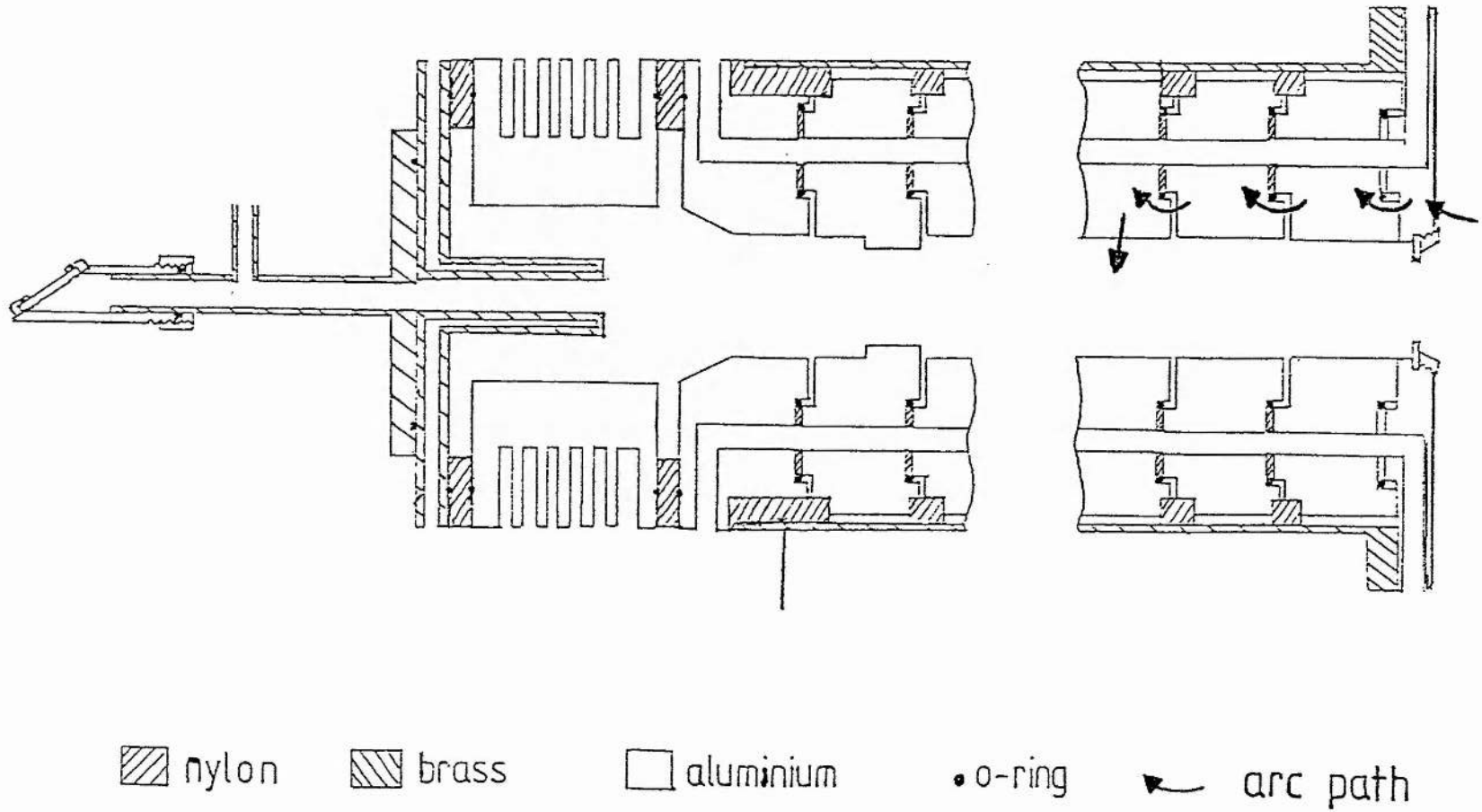

Figure 5.1 Arc path which caused damage to the support tube.

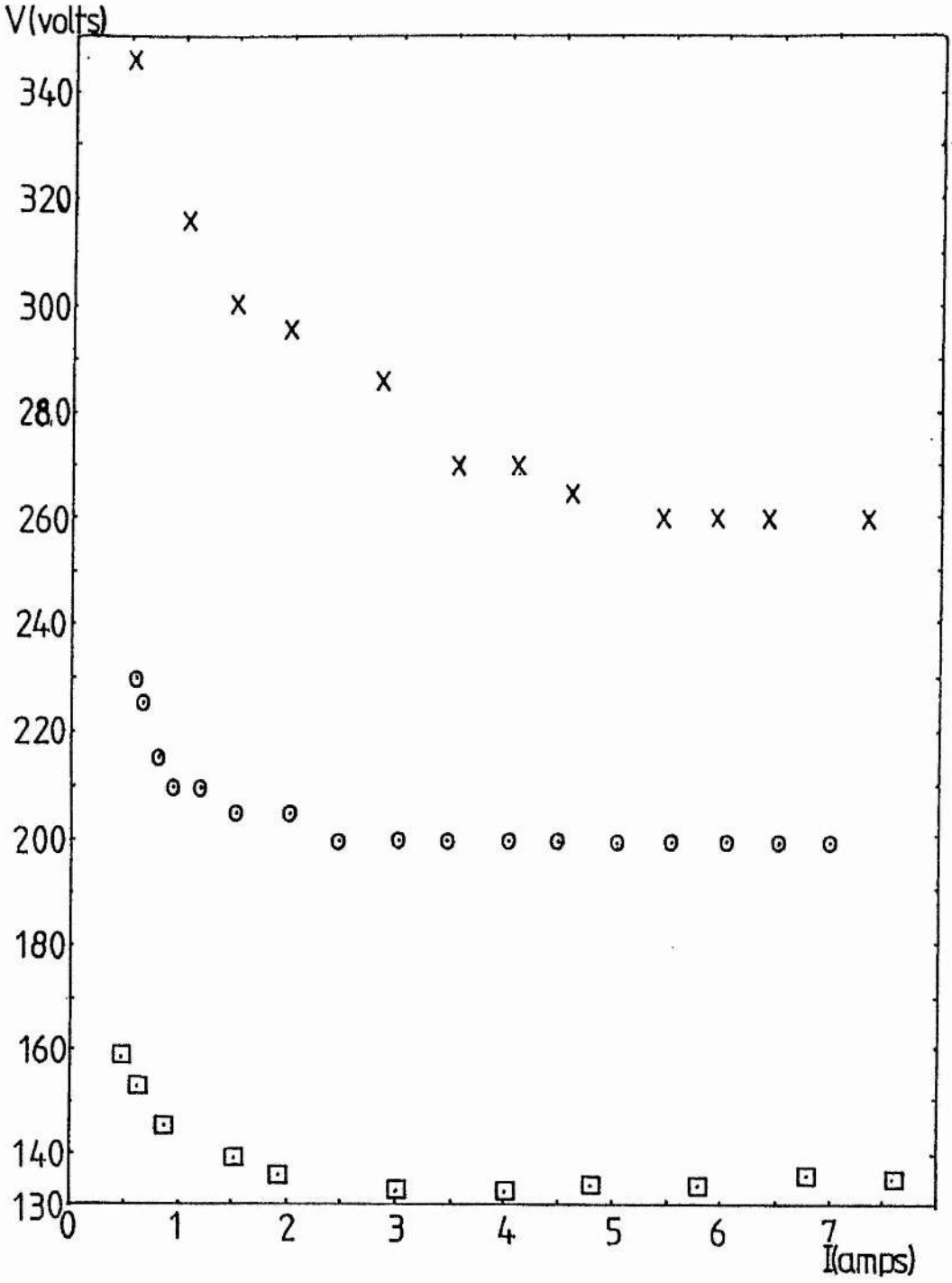

Figure 5.2

Voltage-Current characteristics - Argon discharge.

X 5 segments; 0.35 + 0.01 torr.

⊙ 4 segments; 0.42 + 0.02 torr.

⊡ 3 segments; 0.33 + 0.01 torr.

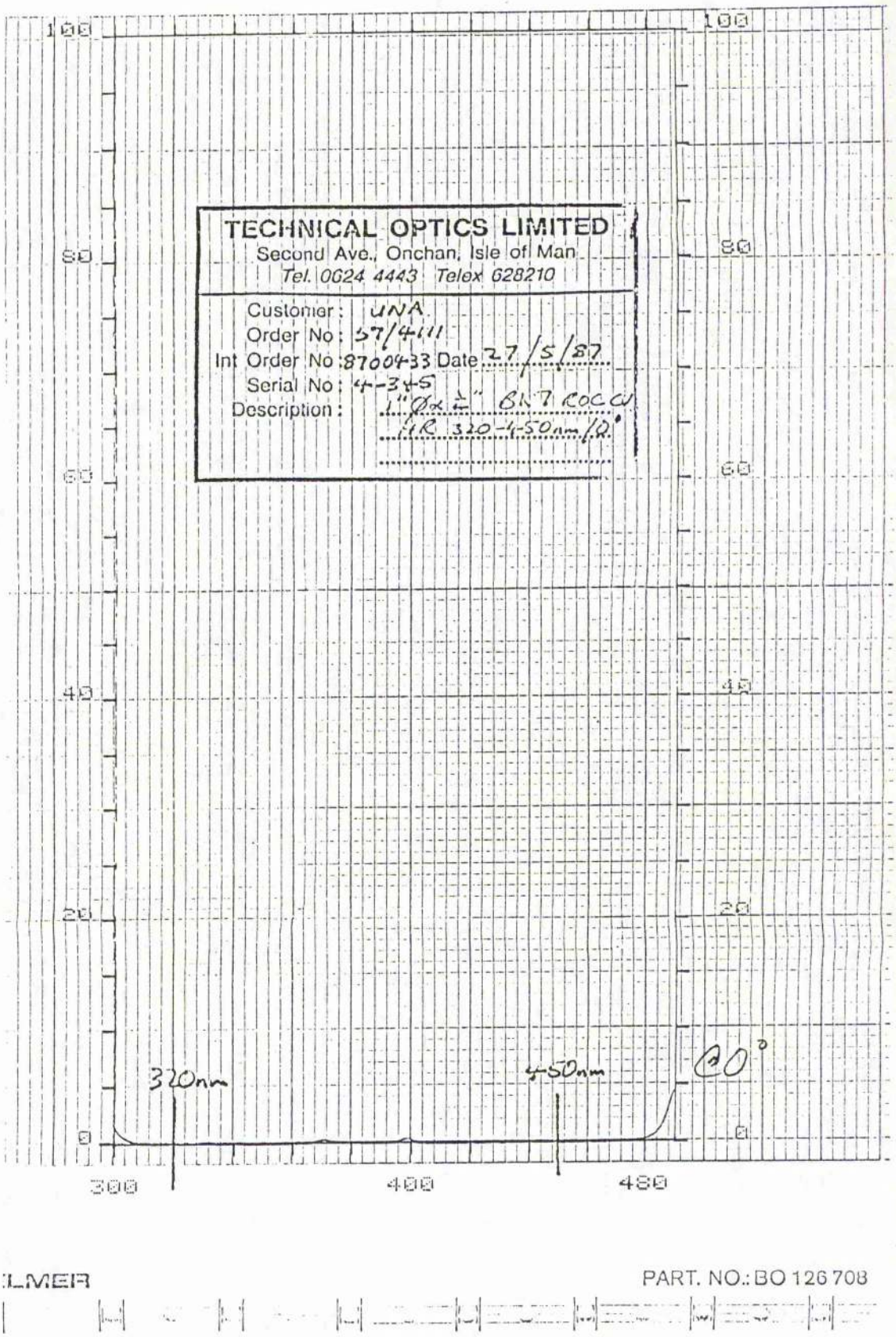

PERKIN ELMER PART. NO.: BO 126 708

Figure 5.3 Mirror transmission

Figure 5.4 Optical system for cavity alignment.

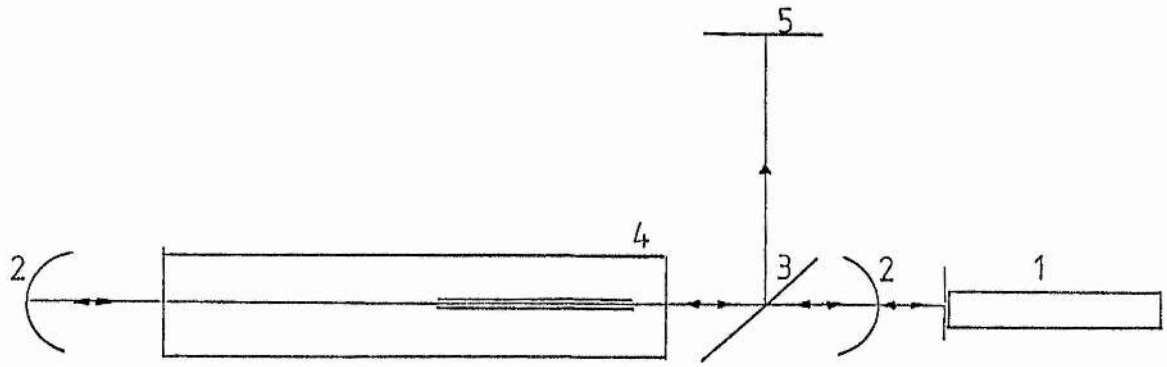

1. Helium - Neon alignment laser.
2. Mirrors.
3. Beam splitter.
4. Discharge tube.
5. White card.

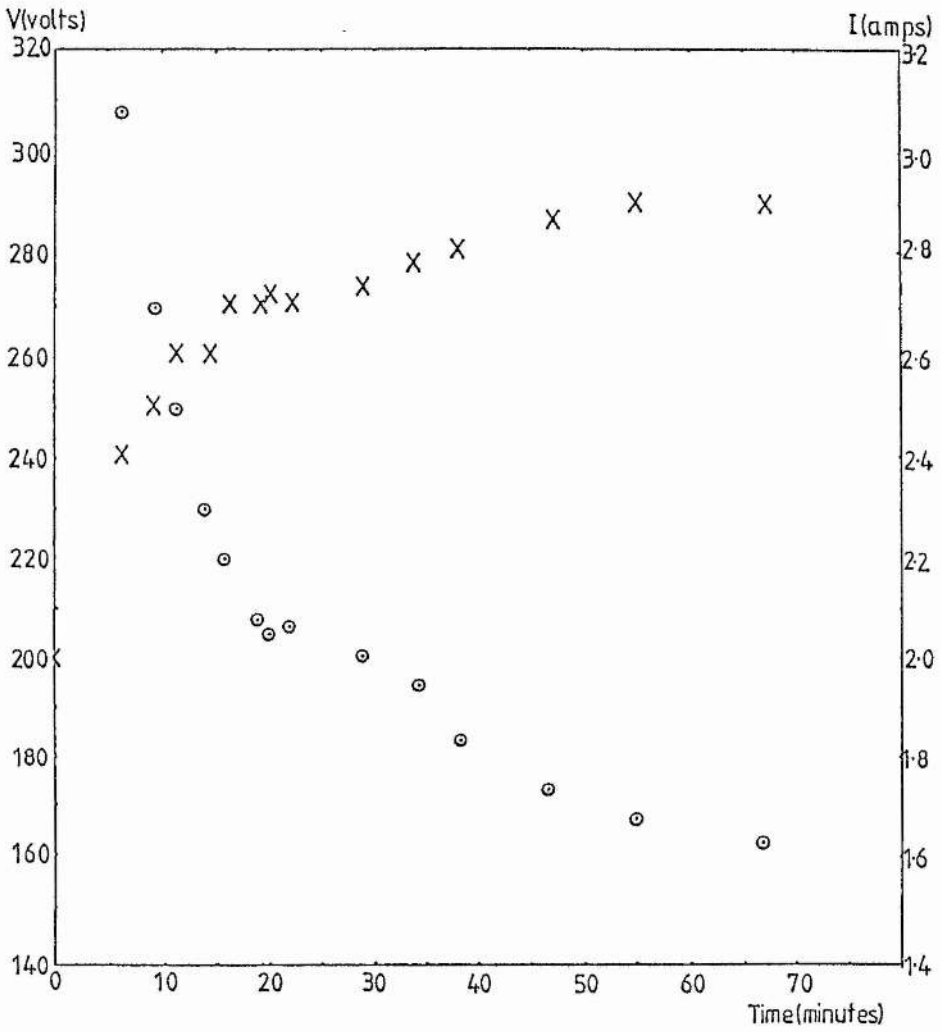

Figure 5.5 Discharge voltage (⊙) and current (X) as a function of time after discharge initiation. Argon-Silver discharge-5 segments. Pressure 0.46 torr. At t=0, V=412 volts, I=2 amps.

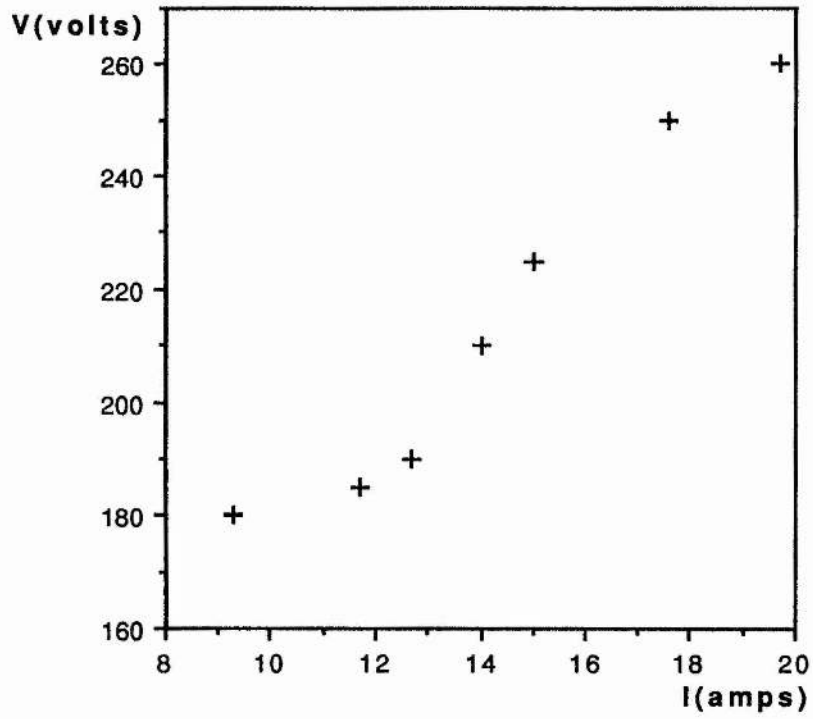

Figure 5.6 Voltage - current characteristics. Argon-Silver discharge, 5 segments.

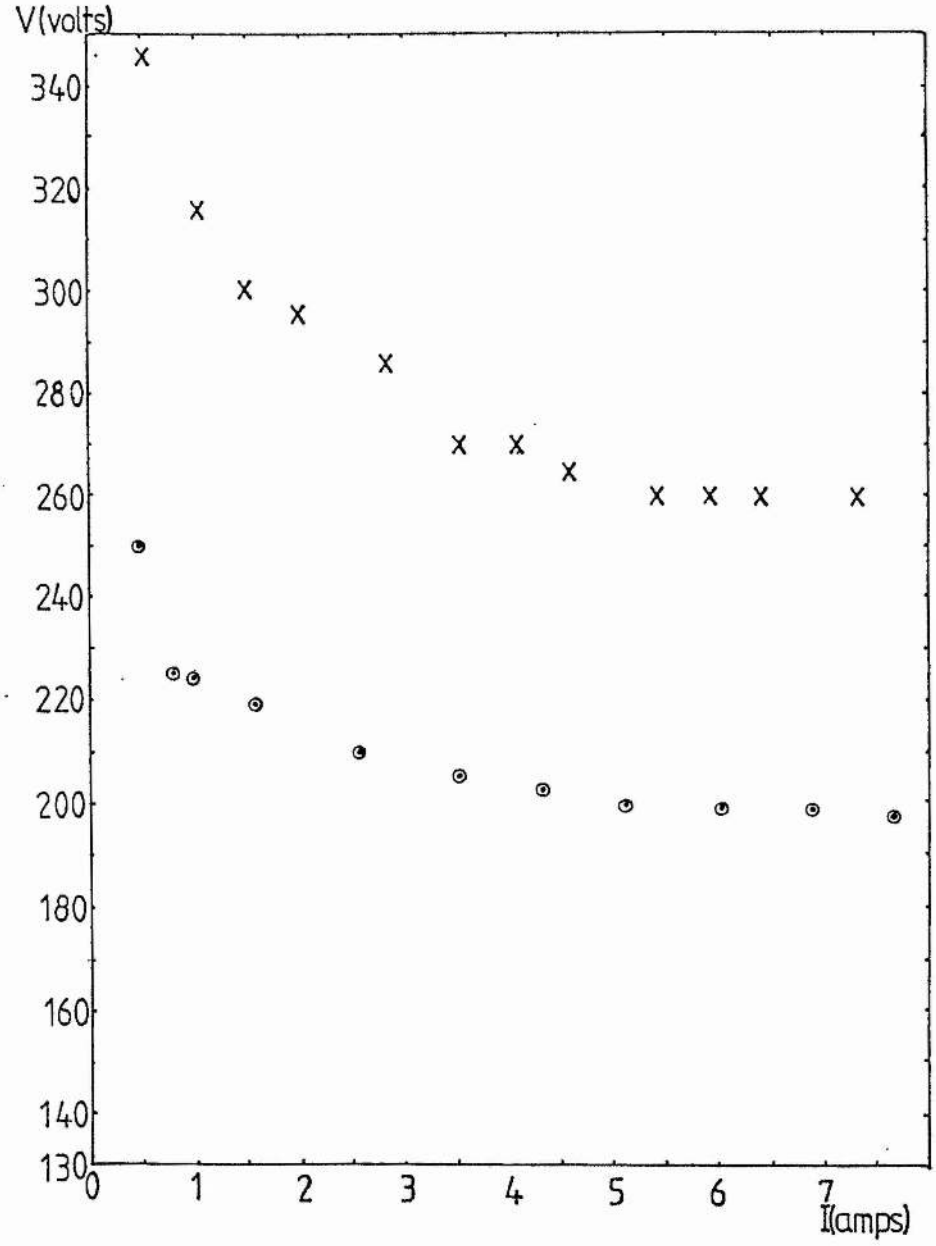

Figure 5.7 Voltage-Current characteristics.
X - Five segments, argon discharge.
⊙ - Five segments, argon-silver discharge.

CHAPTER 6.

DUAL-BORE METAL TUBES.

6.1) Introduction.

In their early work on noble gas ion lasers, Halstead et al. (1968) used thin metal discs, with axial holes, separated by insulators, to confine the discharge. This discharge tube was a dual-bore tube, (alternate narrow and wide bore sections), as shown in figure (6.1). (It should be noted that alternating metal and insulator boundaries greatly complicates considerations of discharge processes.) They found that provided that the inter-disc spacing was less than the calculated electron mean free path, the discharge remained confined between the discs and the current density was maintained.

In this chapter we describe metal "cups" (figure (6.2)), which interlock to form continuous metal tubes with dual-bores (figure(6.3)). A discharge can be maintained along the axis of such a tube under certain pressure and current conditions. The maximum length of these dual-bore tubes may be determined by the total length of the narrow bore sections.

The effects of tube length and location, on breakdown voltage and sustaining voltage, are investigated in low current ($\approx$ 10 mA) glow discharges (Appendix 1). Low current discharges may be produced using simple apparatus, which allows greater flexibilty to alter tube geometries. Contaminants which can affect measurements, are present in

the discharges under consideration. However, results appear to be reproducable, and trends in breakdown voltage and sustaining voltage can be deduced, as discharge parameters are varied. The results obtained in the low current density case give insight into the design of a high current density discharge tube. (Breakdown mechanisms are the same in both types of discharge, as are the loss mechanisms which determine the sustaining voltages.)

6.2) Dual-bore metal tubes.

The maximum length (axial discharge) of a metal segment in an established DC discharge is inversly proportional to the axial electric field (section (2.3.2)). The field is inversly proportional to discharge tube diameter (Francis, 1956). Hence, the maximum length of a segment is proportional to the tube diameter. Metal segments therefore have a maximum "length-to-bore" ratio. Thus, the maximum length of a narrow bore segment (2.5 cm for a 1 mm bore segment) is shorter than the maximum length of a wide bore segment (Greater than 1 m for a 4 cm bore tube).

Figure (6.1) shows a metal tube whose diameter varies along its length (dual-bore). The wide bore regions are several times the diameter of the narrow bore. We have argued that the axial electric field is higher in the narrow bore regions than the wide bore regions. (For example in a glow discharge in air at 0.1 torr, 10 mA discharge current; D=8 mm, X=4.1 V/cm and D=2.5 cm, X=2.8 V/cm (Francis 1956)). In effect the maximum segment length decreases as the

voltage drop along the segment axis increases (with higher axial electric fields). The total voltage drop, V_t, along the axis of a dual bore tube may be written as,

$$V_t = N(X_n L_n + X_w L_w),$$

where X_n and X_w are the axial electric fields in the narrow and wide bore sections, L_n and L_w are the lengths of the narrow and wide bore sections and N is the total number of sections. Provided we have,

$$X_n L_n > X_w L_w,$$

then as the number of sections increases, we have

$$V_t \approx N X_n L_n,$$

that is, the voltage drop along the tube is determined mainly by the total voltage drop in the narrow bore sections. Therefore, it is largely the total length of the narrow bore sections which produces the voltage drop that determines the maximum length of a dual-bore metal tube.

6.2.1) Double sheath formation.

In order to maintain current continuity at a tube constriction, the electron current density must be greater inside the constriction than outside. Also, the rate of loss of charge is greater inside the constriction. Therefore, the

electrons must gain energy in order to increase the ionisation rate within the constriction, to increase the electron number density and compensate for the increased loss. This energy is provided by the accelerating field of the double sheath which forms at the cathode-end of a constriction. A plasma sac also develops, which protrudes into the lower current density region (towards the cathode). This sac provides a larger surface area for electron collection (and constrains the sheath field to a lower value.). These plasma sacs are observed as glowing "balls", as the enclosed plasma has the same electron density as the plasma inside the constriction (see cover plate). The double sheath which forms at the constriction of a discharge tube has been discussed by Andrews and Allen (1971).

It is thought that double sheaths are unlikely to form in high current density discharges in dual-bore tubes, provided that the current density is maintained between the narrow bore sections. That is, that the length of the wide bore sections is less than a value which depends upon the electron mean free path (Halsted et al (1968)).

6.2.2) High current density discharge tube design.

A high current density (metal-vapour/noble-gas) discharge tube may be devised, based on argon-ion laser tubes (Halsted et al.(1968)). The tube is of the form shown in figure (6.3). A continuous, dual-bore metal tube is formed by replacing the insulated spacers (wide bore) in an argon-ion laser by metal spacers. The maximum length of this

tube may be limited only by the total length of narrow bore sections. Experiment suggests (Halsted et al (1968)) that the length of the wide bore sections must be less than the electron mean free path (calculated), to ensure that a high current density is maintained in these sections. The electron mean free path may be calculated from the total collision cross-section (Delcroix 1968) and is of the order of 2 cm at 1000°C and 0.1 torr in argon. (Simplified calculation shows that at a current of 10 amps (narrow bore diameter 4 mm, wide bore length 1 cm), the maximum spread of the discharge in the wide bore section is only about 1% of the narrow bore diameter.)

Pieces of wire may be placed in the wide bore sections of the dual-bore tube. Metal vapour is produced by discharge heating of the wire. The metal vapour may then be ionised in the high current density discharge.

The use of long dual-bore tubes (as opposed to short segments) reduces the number of insulating spacers, which are possible arc sites (section (5.3.3)), in the system. The absence of these arc sites results in stable gas discharges.

6.2.3) Metal cups.

To investigate gas discharges in dual-bore tubes, metal segments, or cups, were designed, which interlock to form variable lengths of tube. These brass cups, figure (6.2), have an outer diameter of 35 mm, so that the cups fit snuggly in the available quartz tubing. The inner diameter of the wide bore section of the cups is 31 mm, while that of

the narrow bore section is 3 mm. The narrow bore region is 3 mm or 2 mm long. This allows tubes of the same length, but with different total lengths of narrow bore section, to be investigated. The overall length of the cup is 1 cm. A groove is machined around the edge of the flat face of the cup which allows the segments to fit together. A push-fit is used to produce a good electrical contact. Viewing holes (1 mm diameter) are drilled in the wall of each cup.

6.3) Experiment.

The brass cups, described in the previous section, are placed in a quartz tube of dimensions 40 cm x 35.5 mm diameter. The tube is sealed at both end with rubber bungs, through which 10 cm long brass pipes protrude. The quartz tube is evacuated through the brass tube used as the cathode (high negative potential), and gas enters through the pipe used as the anode (earth). The vacuum pump is an Edwards (12) two-stage rotary pump. Gas flow is controlled by a rough valve and a fine control needle valve. The input pipe is either left open to the atmosphere or connected to an argon cylinder (zero grade). Pressure measurements are made with a pirani gauge head, situated between the needle valve and the system, with an Inficon PG3 controller. The controller may be set for measurements using either nitrogen or argon. The circuit used in the experiments is given in figure (6.4).

The experimental procedure is as follows. A group of cups are placed within the quartz tube, to form a dual-bore

brass tube. The distances from anode tip to cathode tip, cathode tip to the cup nearest to the cathode, and anode tip to the cup nearest to the anode, along with the total length of the dual-bore tube, are recorded (See table 6.1). The breakdown voltage and initial sustaining voltage are measured at various pressures. The state of the discharge, that is to say whether the discharge penetrates along the axis of the metal tube or flows to the walls, is also recorded. The distance from the anode to the anode-end of the tube is maintained approximately constant during the experiments, as a reference position. (The effect of moving the tube can be seen by comparing the results of the 15 cup, 2 mm length bore case (15 x 2) with that denoted by 15 x 2_o in tables (6.2) and (6.3). The 15 x 2_o tube is closer to the anode than any of the other brass-cup tubes.)

The anode-tube separation (T-A), cathode-tube separation (C-T), and segment length (L), are given, with measurements for both the experiments in air and in argon (Table (6.1)). The total number of cups, N, is represented as a x b, where a is the number of cups and b either 2 or 3, defining the total length l, of the narrow bore region in millimetres. (eg N = 6 x 3 gives l equal to 18 mm)

The anode-cathode separation (A-C) is 28 ± 0.2 cm.

Table 6.1.

		Air		Argon	
N	L(cm)	C-T(cm)	T-A(cm)	C-T(cm)	T-A(cm)
6 x 3	5.5	14.0	8.5	13.3	8.9
9 x 3	8.3	11.3	8.5	10.8	8.7
12 x 3	11.0	8.6	8.5	8.0	8.7
15 x 3	13.9	6.9	7.5	5.4	8.8
6 x 2	5.3	14.4	8.6	13.6	9.1
9 x 2	7.7			11.4	8.8
15 x 2	12.7	7.0	8.3	6.3	9.0
15 x 2_o	12.7	12.0	3.3	11.6	3.8

The subscript $_o$ in table (6.1) refers to the case where T-A is smaller than in the other experiments. All measurements have an accuracy of ± 0.2 cm.

6.4) Results.

Figures (6.5) to (6.20) are plots of breakdown voltage, (V_b), or sustaining voltage, (V_s), versus pressure (p), cathode-tube separation (d_{cm}), total length (l) of narrow bore region or the total length (L) of the metal tube.

The measured breakdown voltages lie on the right hand side of the Paschen curve. In general, the breakdown voltage increases as d_{cm} increases (as L decreases). The increase in breakdown voltage as d_{cm} increases is due to a "Paschen law" (Von Engel 1965) dependence of the breakdown voltage on the "electrode" separation, for breakdown between the cathode and the dual-bore tube. This dependence is investigated further in chapter 7.

When the discharge lies along the axis of the tube the sustaining voltage of the discharge increases as L and l increase. The axial electric field (in the positive column) is found to be a function of segment length, and increases as the segment length increases (section(2.5)). A higher axial electric field and hence a larger potential difference along the positive column, leads to an increase in the discharge sustaining voltage. The axial electric field also increases as the tube diameter decreases. Hence, higher sustaining voltages are obtained, as the total length of narrow bore sections increases.

When the conduction path is through the metal walls of the dual-bore tube the sustaining voltage of the discharge decreases as L or l increase. In this case, two discharges in series are produced. One discharge is formed between the

cathode and the tube, and the other between the tube and the anode. The anode-tube separation d_{am}, is kept fixed. An increase in tube length therefore leads to a reduction in the cathode-tube separation d_{cm}. A decrease in d_{cm} leads to a reduction in the potential difference (assuming a constant axial field), between the cups and the cathode, and hence a reduction in the discharge sustaining voltage.

The discharge path dependence on pressure, gas and dual-bore tube length is investigated. In some cases the discharge forms on the axis (case A - gas path), and in others conduction occurs through the metal walls, (case W - metal path). In a few cases the discharge initially penetrates the axis of the tube and then moves to the walls (case B). Occasionally a stable state of either A or W is obtained (W+A). These results are given in tables (6.2) and (6.3) for air and argon. Where N again represents the number of cups.

Table 6.2. The discharge path, in air at various pressures and numbers of brass cups.

PRESSURE(torr)	3.1	1.7	0.95	0.53	0.4	0.33
N						
6 x 3	W+A	A	A	W	W	W
9 x 3	W+A	A	W	W	W	W
12 x 3	B	B	W	W	W	W
15 x 3	W	B	W	W	W	W
6 x 2	A	A	A	B	W	W
15 x 2	W	A	B	W	W	W
15 x 2$_o$	W	W	W	W	W	W

Table 6.3. The discharge path, in argon at various pressures and numbers of brass cups.

PRESSURE(torr)	3.1	1.7	0.95	0.53	0.4
N					
6 x 3	A	A	B	W	W
9 x 3	B	W	W	W	W
12 x 3	B	W	W	W	W
15 x 3	W	W	W	W	W
6 x 2	A	A	A	A	A
9 x 2	B	B	W	W	W
15 x 2	A	A	B	W	W
15 x 2$_o$	W	W	W	W	W

The following points should be noted:

a) The conduction path is always through the metal tube at the lowest pressures used in the experiments (except for the six cups with 2 mm length narrow bore sections, (6 x 2), with argon).

b) A discharge forms along the axis of the cups most readily at 3.1 and 1.7 torr.

c) The conduction path is always through the walls, when the 15 x 2 cups are offset ($15x2_o$ - the separation between the metal tube and the anode is smaller in this case.).

d) Discharge penetration, along the tube axis, occurs most readily for the 6 x 2 cups.

Zeleny (1938) suggested that, for an on-axis discharge, the fall in potential (Vg) in the gas (positive column) along the axis of the segment should be less than the sum of the anode fall (Va), and cathode fall (Vc) at the ends of the metal segment, that is to say,

$$Vg < Va + Vc \quad , \qquad \text{ON-AXIS DISCHARGE.} \qquad (6.4.1)$$

$$Vg > Va + Vc \quad , \qquad \text{WALL CONDUCTION.} \qquad (6.4.2)$$

We have assumed that the fall of potential in the metal is negligible. (The resistance of 15 cups is approximately 0.5 ohm.) Experimental results, given in the following chapter, show that the discharge is established along the path with the lowest sustaining voltage.

A few other observations should be drawn to the reader's attention. After breakdown occurs, the discharge

will tend to remain in the initial mode of operation. It will either remain on the axis, or the current will pass through the walls, as the pressure is changed. This suggests, that once penetration along the axis occurs, the ionisation produced allows the current to pass under conditions of pressure where normally, at discharge initiation, the current would pass through the metal. Thus, preionisation is an important factor in discharge penetration.

If small pressure pulses are applied to the discharge, for instance by tapping the inlet valve, a discharge which only partially penetrates the cups can be caused to penetrate them all. The pressure pulses probably force plasma into the cups where penetration has not occured. This acts as a preioniser and breakdown along the axis of all of the cups occurs. The condition when partial penetration occurs, is given by,

$$fVg + Va + Vc < Vg, \qquad (6.4.3)$$

where f is the fraction of the total segment length, where penetration occurs. We now look at factors which will influence the values of Vg, Va and Vc.

In molecular gases, for example Nitrogen (air), the axial electric field in the positive column (and hence the sustaining voltage) may be a factor of ten or more greater than the field in rare gases (Von Engel, 1965). The anode falls (which are of the order of the ionisation potentials) and cathode falls for argon and air (normal glow discharge)

are given as,

	Va (volts)	Vc (volts)	Va + Vc (volts)
Argon	15.7	130	145.7
Air	15.5	375	390.5

where we have used the value of Vc for copper electrodes, and have assumed that the ionisation potential of air is equal to that of nitrogen. The voltage drop Vg, in the positive column is much lower when argon, as opposed to air, is used; therefore the condition for an axial discharge given by equation (6.4.1) is more likely to be met for a discharge in argon than for a discharge in air.

We may rewrite equation (6.4.1) for the total sustaining voltage as,

$$Va + Vc + dX_q + LX_m < 2(Va + Vc) + dX_q. \qquad (6.4.4)$$

This reduces to

$$LX_m < Va + Vc, \qquad (6.4.5)$$

where X_q is the axial electric field in the discharge bounded by quartz of length d, and X_m is the axial electric field in the discharge bounded by the metal of length L. We see that for a discharge to form on the axis, the total segment length and the axial electric field should be as small as possible, and the cathode fall at the metal as large as possible. Hence discharges are more likely to form on the axis of short metal segments, with high cathode falls, and in rare gases than molecular gases.

6.5) Conclusions.

Dual-bore tubes formed from inter-locking brass cups have been described. It is suggested that a discharge will form on the axis of such a dual-bore tube, provided that the total length of the narrow bore sections does not exceed the maximum length of a single metal segment with the same diameter as the narrow bore sections.

Measurements of breakdown voltage and sustaining voltage have been made for discharges, in dual-bore tubes of various lengths, in argon and in air. The sustaining voltage (axial discharge) increases as the length L, of the dual-bore tube, and total length l, of narrow bore sections, increases. The discharge sustaining voltage decreases as the cahode-tube separation d_{cm} decreases (L and l increase) when the conduction path is through the metal wall.

The breakdown voltage decreases as L increases and as d_{cm} decreases. A decrease in d_{cm} is effectively a reduction in the electrode separation, for breakdown between the cathode and the metal cups. The breakdown voltage depends on the total length of metal tube and its position between the anode and the cathode.

The formation of discharges along the axis of a metal tube depends on the axial electric field. Axial discharge formation is more likely when low axial electric fields result. The potential fall in the gas along the tube axis may then be less than the sum of the anode fall and the cathode fall at the metal forming the tube. The axial field is a function of the pressure, the tube radius, and the tube

length. The gas type, and also to a lesser degree, the metal forming the tube are also important in determining whether an axial discharge will form. In order to obtain discharge penetration, the cathode fall of the tube should be as large as possible, and an atomic gas should be used as opposed to a molecular gas. This suggests that the use of long metal tubes in metal vapour lasers is a distinct possibility.

References.

A.S. Halsted, W.B. Bridges, G.N. Mercer. "Gaseous Ion Laser Research.", Technical report AF-5237, Hughes Research Laboratories, 1968.

A. Von Engel. "Ionized Gases." 2nd Ed., Clarendon Press, Oxford, 1965.

G. Francis. "The Glow Discharge at Low Pressure". Handbuch der Physik XXII, ed. S. Flugge, Springer-Verlag, 1956.

J. Zeleny. "On the role of tube walls, and surface and space charges in electrical discharges through rarefied gases." Journal of the Franklin Institute, 226, 1938, p 35.

J.G. Andrews and J.E. Allen. "Theory of a double sheath between two plasmas." Proc. Roy. Soc. Lond. A 320, 1971, p 459.

J.L. Delcroix. "Plasma Physics" Vol. 2 "Weakly ionized gases." John Wiley and Sons Ltd. 1968.

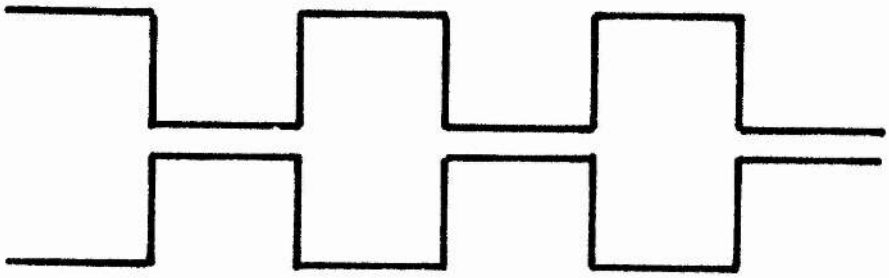

Figure 6.1 Discharge tube with varying diameter. (Dual-bore tube.)

Figure 6.2 Brass cup.

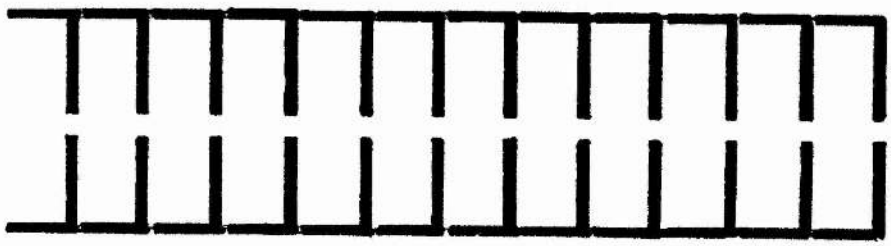

Figure 6.3 Brass cups positioned to form dual-bore tube.

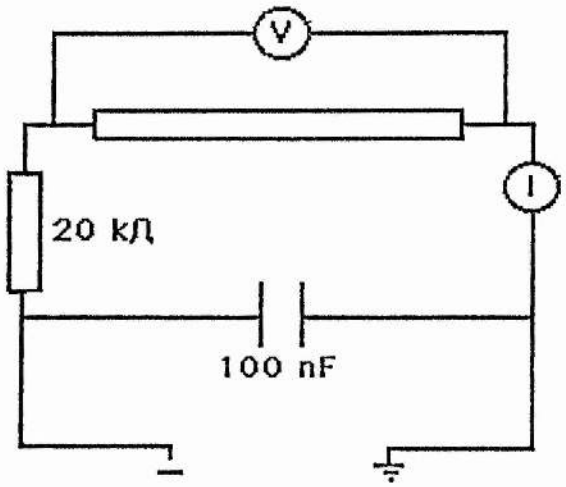

Figure 6.4 Circuit used for measurement of breakdown voltage and sustaining voltage.

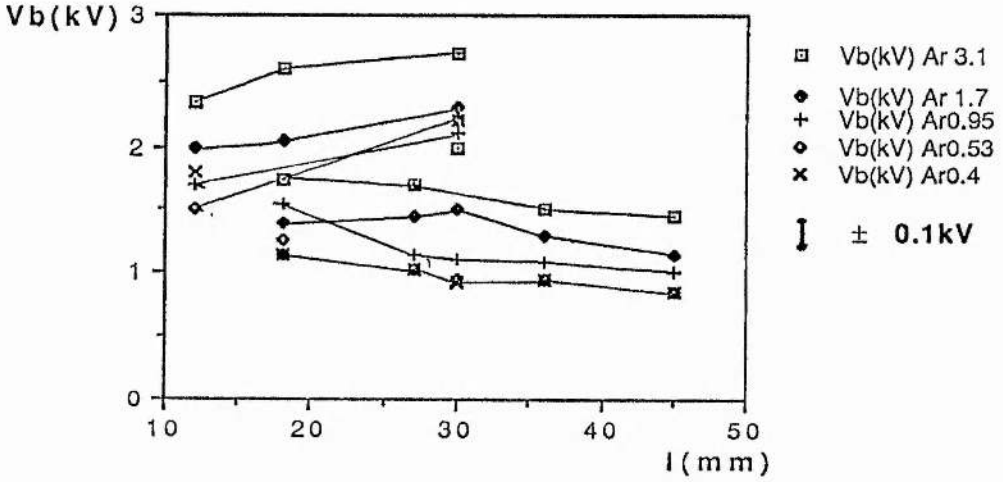

Figure 6.5 Breakdown voltage of argon versus total length of narrow section of dual-bore tube, at various pressures.

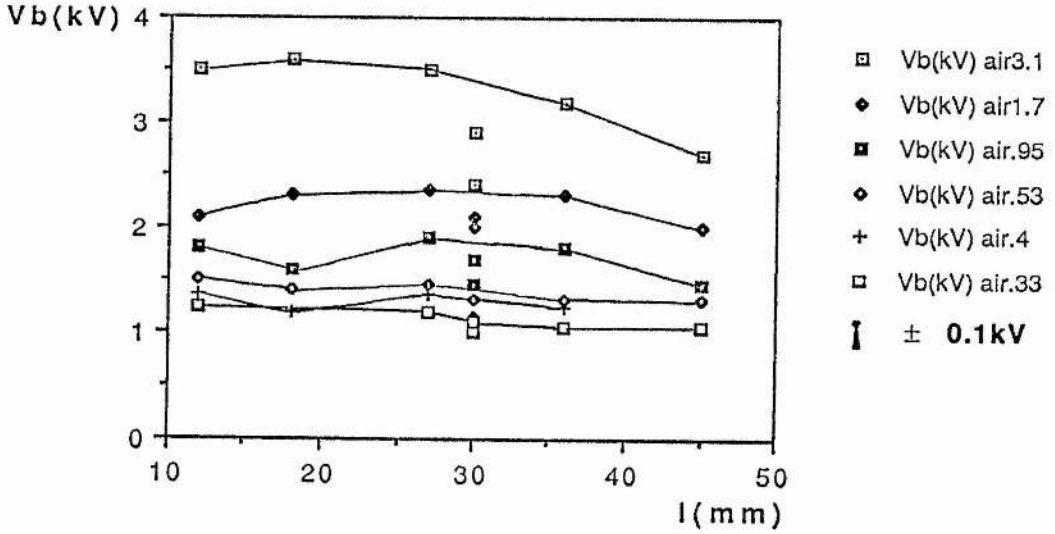

Figure 6.6 Breakdown voltage of air versus total length of narrow section of dual-bore tube, at various pressures.

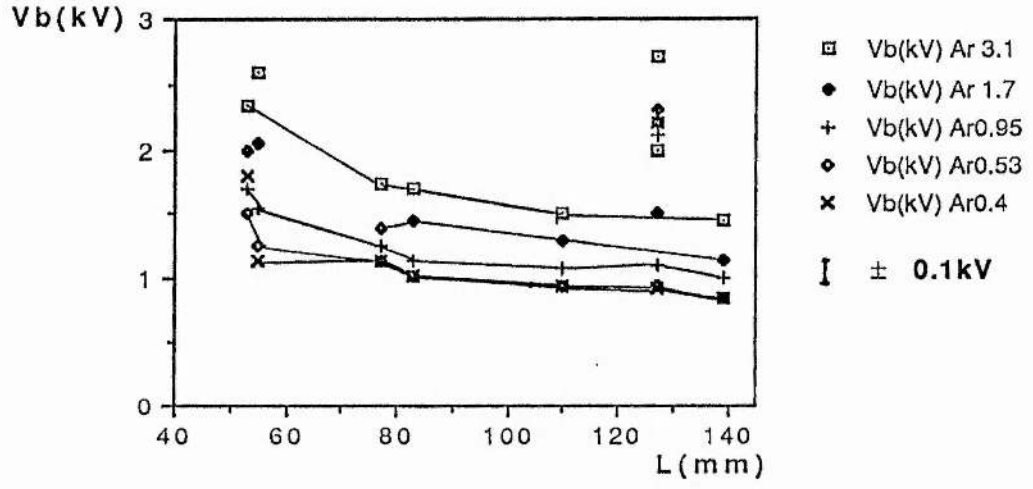

Figure 6.7 Breakdown voltage of argon versus total length of dual-bore tube, at various pressures.

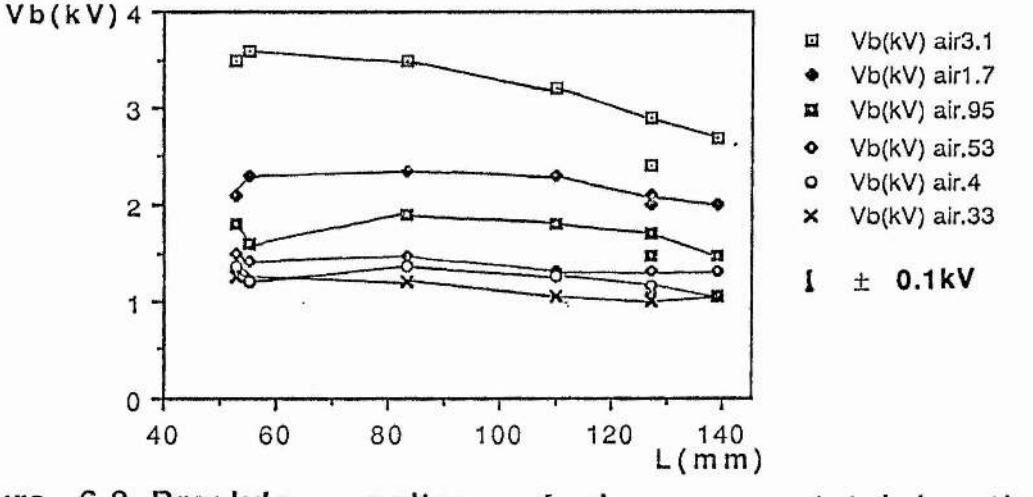

Figure 6.8 Breakdown voltage of air versus total length of dual-bore tube, at various pressures.

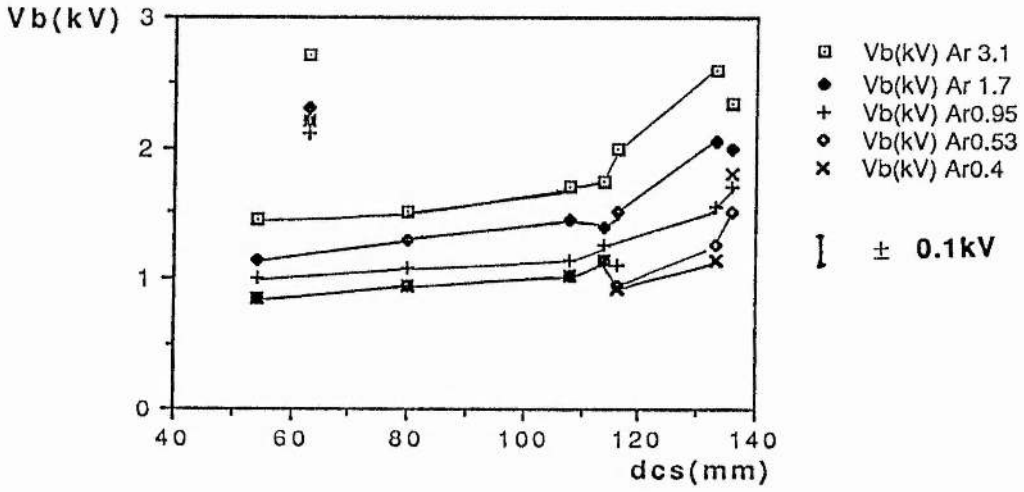

Figure 6.9 Breakdown voltage of argon versus distance from cathode to dual-bore tube, at various pressures.

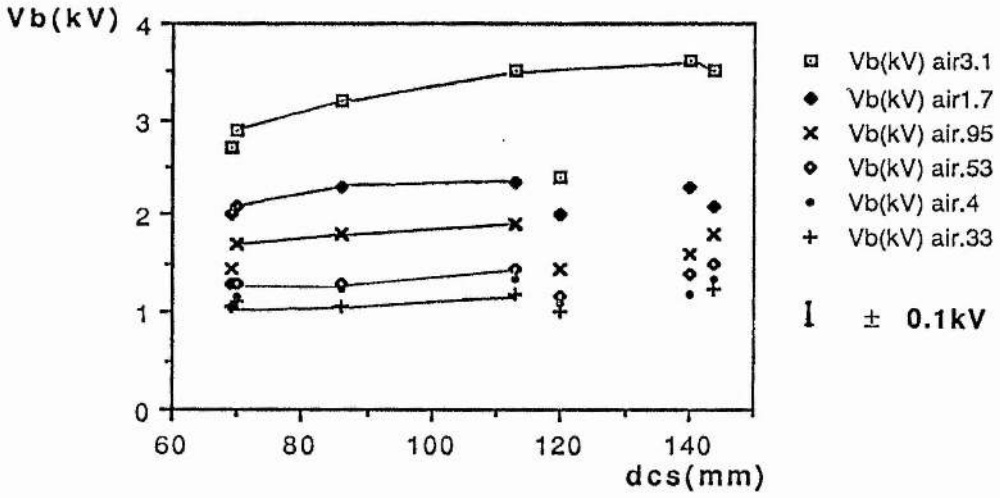

Figure 6.10 Breakdown voltage of air versus distance from cathode to dual-bore tube, at various pressures.

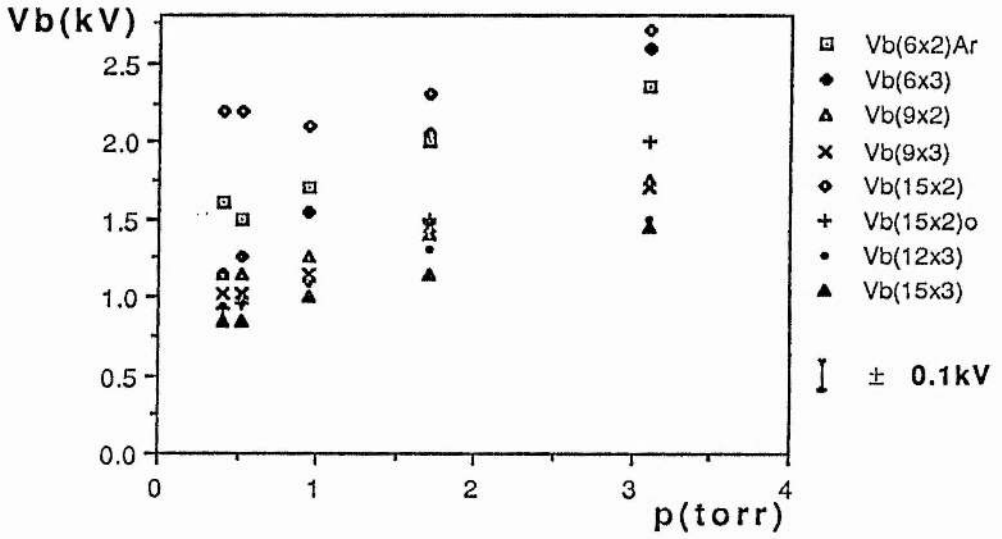

Figure 6.11 Breakdown voltage of argon versus pressure, for dual-bore tubes of different lengths.

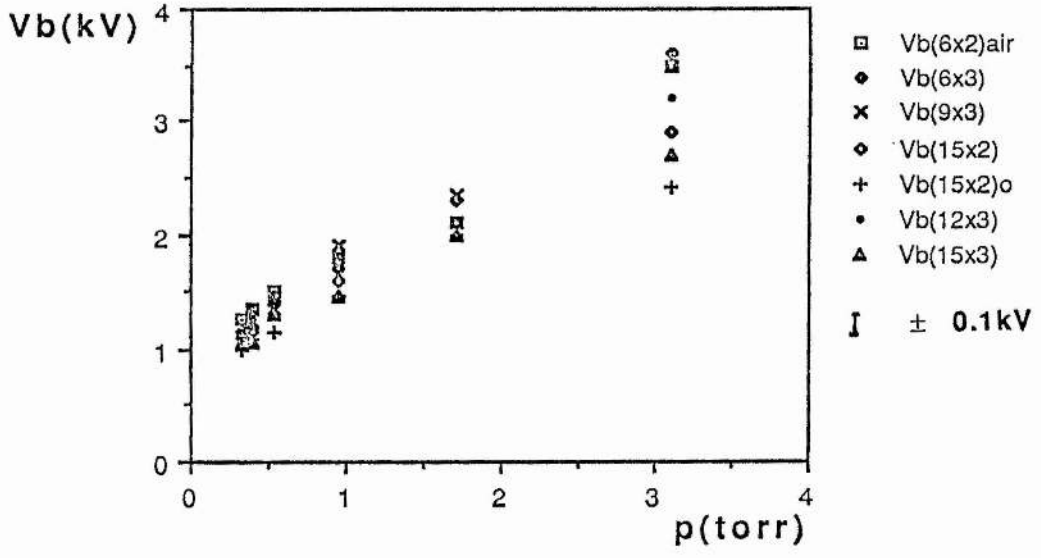

Figure 6.12 Breakdown voltage of air versus pressure, for dual-bore tubes of different lengths.

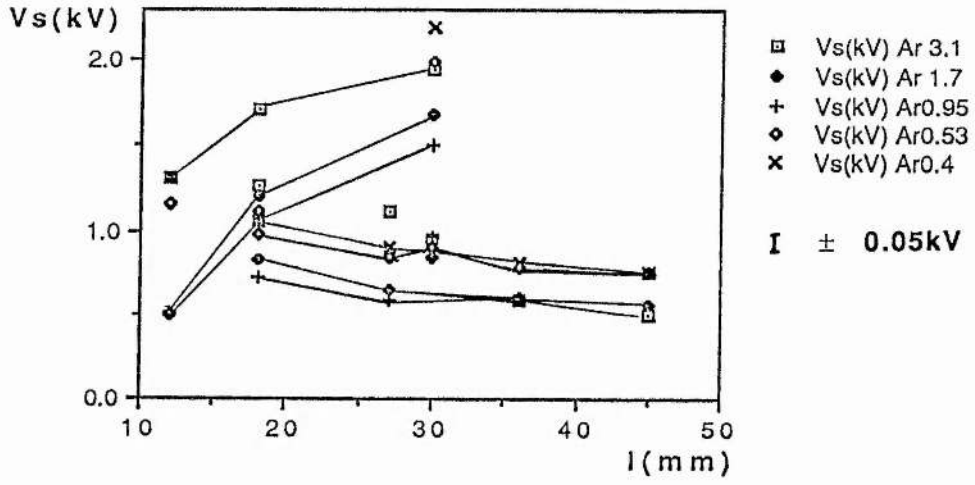

Figure 6.13 Sustaining voltage of argon versus total length of narrow section of dual-bore tube, at various pressures.

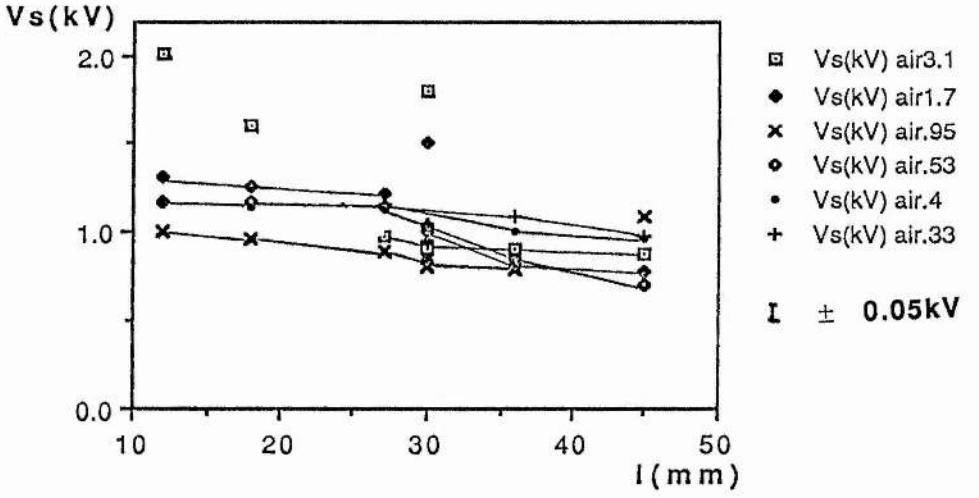

Figure 6.14 Sustaining voltage of air versus total length of narrow section of dual-bore tube, at various pressures.

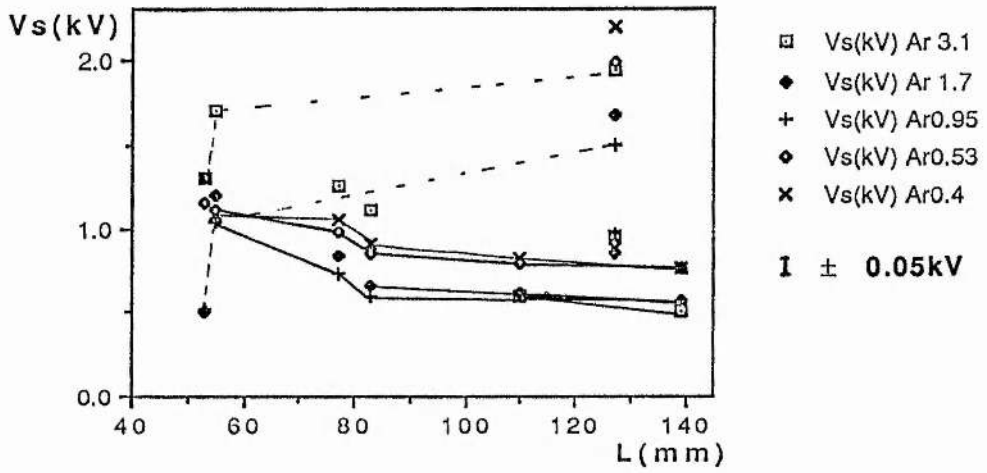

Figure 6.15 Sustaining voltage of argon versus total length of dual-bore tube, at various pressures.

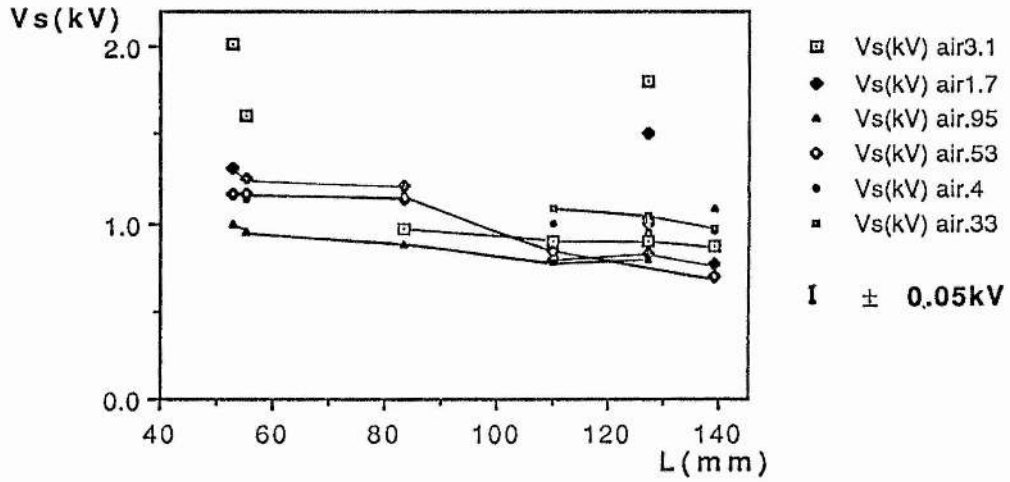

Figure 6.16 Sustaining voltage of air versus total length of dual-bore tube, at various pressures.

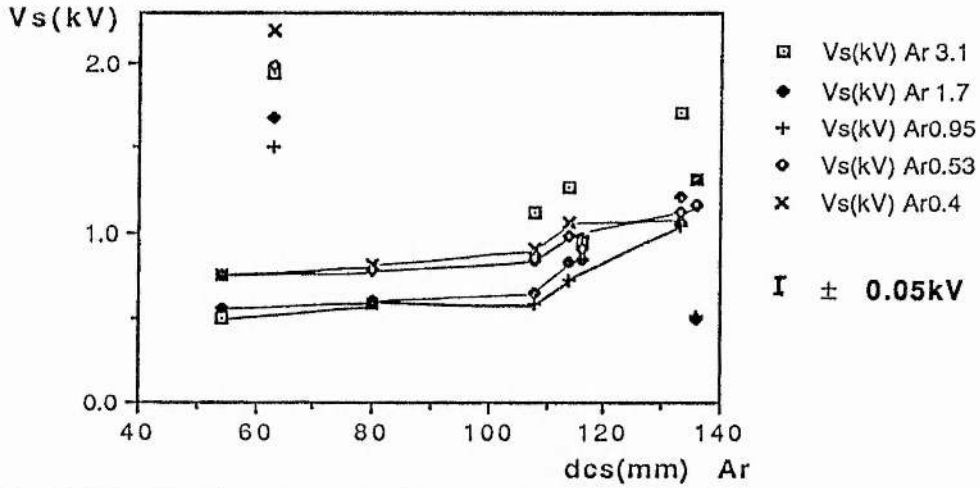

Figure 6.17 Sustaining voltage of argon versus distance from cathode to dual-bore tube, at various pressures.

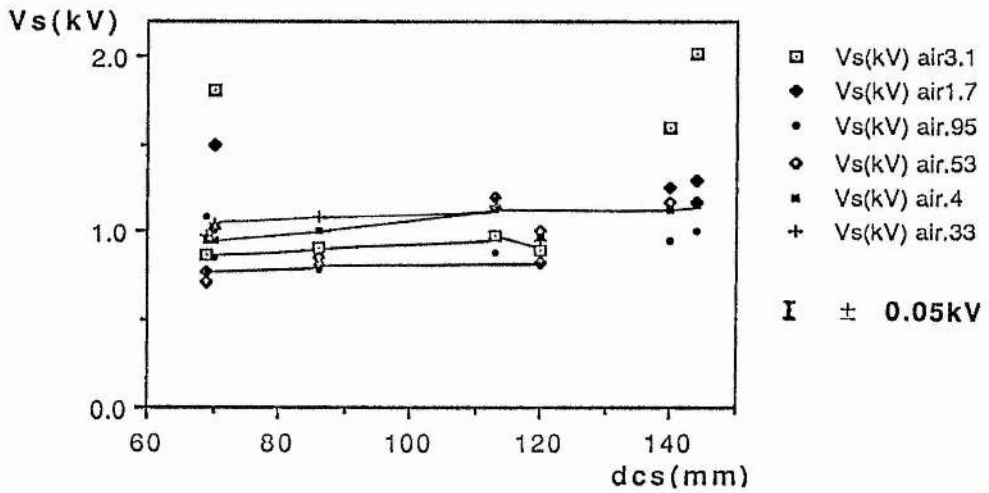

Figure 6.18 Sustaining voltage of air versus distance from cathode to dual-bore tube, at various pressures.

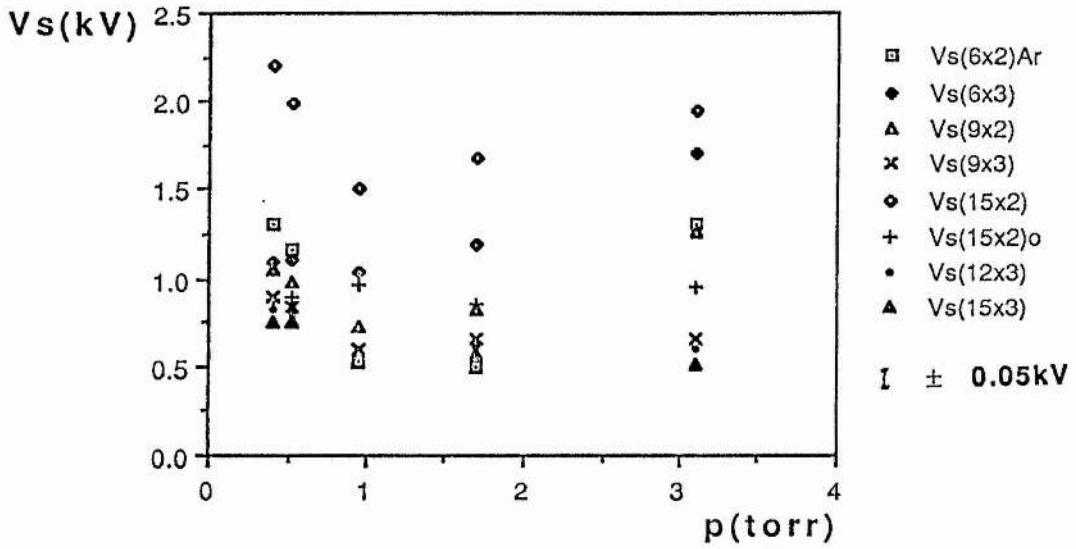

Figure 6.19 Sustaining voltage of argon versus pressure, for dual-bore tubes of different lengths.

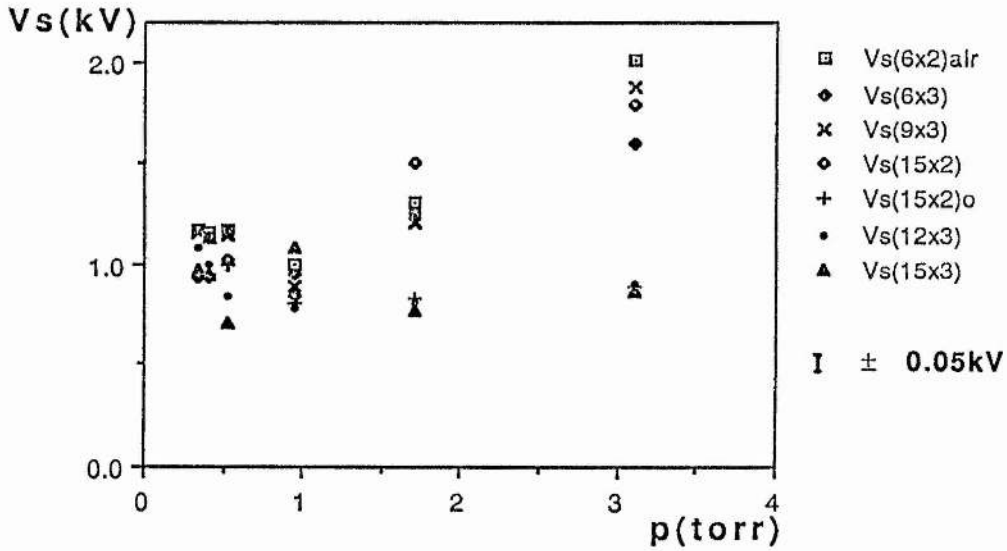

Figure 6.20 Sustaining voltage of air versus pressure, for dual-bore tubes of different lengths.

CHAPTER 7.

THE DISCHARGE CHARACTERISTICS OF AN EVACUATED TUBE CONTAINING METAL CUPS.

7.1) Introduction.

Glow discharges in dual-bore metal tubes with a quartz vacuum jacket are described in chapter 6. It is found that anode-cathode breakdown voltages depend on the length and position of the dual-bore tube between the electrodes. These dual-bore tubes are formed from interlocking brass cups (figure(6.3)).

Experiments to determine the breakdown voltage as a function of the position of a dual-bore tube of 15 brass cups are discussed. All measurements are made in atmospheric air. Results indicate that the anode-cathode breakdown voltage is equal to the sum of the breakdown voltages of gaps between the anode and the metal tube and the cathode and the metal tube.

Twelve brass cups are arranged in a quartz tube to form dual-bore tubes of various lengths and the anode-cathode breakdown voltage is measured. The relationship between anode-cathode breakdown voltage and breakdown voltage of the individual gas gaps, between the electrodes, is investigated. The tube breakdown voltage is calculated, using Paschen's law applied to the individual gas gaps, and compared with the experimental values.

Measurements of the discharge sustaining voltage give insight into the reasons for discharge penetration into the

bore of metal segments. The sustaining voltage of a glow discharge in a quartz tube is compared with that found when the quartz tube contains brass cups. The results show that the magnitude of the sustaining voltage depends on the internal surface area of the discharge tube.

7.2) Experiment.

Fifteen of the brass cups, described in chapter 6 (see figure (6.2)) are placed within a quartz tube, sealed with rubber bungs. Brass pipes, passed through the bungs act as electrodes and allow the tube to be evacuated, as described in section (6.3). Figure (7.1) shows the circuit used in the experiments. The pressure is measured at the inlet end (anode-earth) using a pirani gauge head attached to an Inficon PG 3 controller.

A symmetrical arrangement of the metal relative to the electrodes is required. A group of seven cups and a group of eight cups are placed such that the open ends of the cups face the centre of the tube and form an enclosed cylinder. Each end of the cylinder has a flat surface facing the electrodes, as shown in figure (7.2). The experiments are carried out in atmospheric air at sub-atmospheric pressures produced by a rotary pump. The distances from the end of the cathode to the cathode facing cup (d_{c-c}) and from the end of the anode to the anode facing cup (d_{a-a}) are measured. The breakdown voltage across the tube is recorded for various positions of the cylinder at several pressures. A graph of breakdown voltage (V) versus pressure (p) is shown in

figure (7.3). The variation in the breakdown voltage with position of the cup structure can be clearly seen, especially at pressures greater than 1 torr. The differences between the results obtained for the cup structure at the same segment-to-electrode separations, but with d_{cs} and d_{ss} interchanged is due to asymmetry in the electrode structure. That is to say, whether the "anode" or the "cathode" is a flat surface (a brass cup) or a cylinder (one of the tube electrodes), which will produce slight variations in the breakdown voltage. The graph shows that the results lie on the right hand side of the Paschen curve.

7.3) Explanation of results.

The variation in the breakdown voltage with the position of the cups, may be explained by the following argument. The voltage applied between the electrodes sets up various electrostatic fields in the inter-electrode gas gaps. The field in each gap must be high enough to produce the electron avalanches to initiate a self-sustaining discharge. Therefore, the breakdown voltage of the tube, assuming a uniform field in each gap, is equal to sum of the breakdown voltages of the two gaps. We may represent this mathematically, assuming that the breakdown voltage is a function only of the pressure-distance product. If V is the breakdown voltage of the discharge tube, then we have

$$V \geq V(pd_{cs}) + V(pd_{ss}). \qquad (7.3.1)$$

We deduce that

$$V \neq V(p[d_{cc} + d_{aa}]). \qquad (7.3.2)$$

The breakdown voltage cannot be a function of $(d_{cc} + d_{aa})$, as the voltage changes with cylinder position even though $(d_{cc} + d_{aa})$ remains constant.

Logically the equations for the situation with two gaps may be extended to the case for n gaps.

$$V \geq \sum_{n} V(pd_n) \qquad (7.3.3)$$

This result was proposed by G L Clark (1988) for predicting whether a discharge would take the direct route between the electrodes, through a group of metal segments, or would pass from cylinder to cylinder, dependent on which path had the lowest breakdown voltage. This is only valid if the electrostatic field can penetrate along the axis of the cylinders. Inside a cylinder, the field has fallen to 1 - 10 % of the field outside a cylinder, at a distance within the cylinder of one cylinder diameter (Maitland 1971). In the experiments described here, the metal cups each have a region of narrow bore, of length equal to the bore diameter. The electrostatic field inside the cups is reduced to a small value and breakdown must then occur between the electrodes and the cups.

7.4) Experimental verification of equation (7.3.3).

The following allows experimental verification of equation (7.3.3). Two brass cups are placed with their open ends touching. They thus form a hollow cylinder enclosed at both ends, except for the axial holes, as shown in figure (7.4). We shall call this grouping of two cups a plug. Six of these plugs may be grouped within the tube as shown in figures (7.5) a, b, c, and d, as six single plugs, three groups of two plugs, two groups of three plugs, and one group of six plugs, respectively. The breakdown voltage is measured for each grouping and all air-gap spacings are recorded.

A graph of breakdown voltage versus pressure for the various plug positions, is shown in figure (7.6). The breakdown voltages for the empty tube, at various pressures is also plotted. The individual error-bars for the breakdown voltages have been omitted to allow the trends in the variation of breakdown voltage to be viewed with greater clarity. The individual breakdown voltages show substantial scatter, but the general trends are reproducible. It can be seen that the larger groupings, (one group of six), have lower breakdown voltages relative to those for the empty tube, and that the smaller groupings have higher breakdown voltages. The results again indicate that we are on the right hand side of the Paschen curve.

7.5) Breakdown theory and Paschen's law

The results given above indicate that the breakdown voltage of the discharge tube depends on the number of gas-gaps between the electrodes. To predict the breakdown voltage of a tube with a known number of gaps and verify equation (7.3.3), we use Paschen's law. This is given by Von Engel (1965), for plane parallel, infinite electrodes (Appendix 5).

The breakdown voltage V, at pressure p, for a gap of length d, is given by

$$V = Bpd/(\ln(pd) + C). \qquad (7.5.1)$$

where we may regard B as proportional to an effective ionisation potential. The constant C is given by

$$C = \ln\{A/\ln(1 + 1/\Gamma)\},$$

where A is a saturation value for α/p at large X/p (X-axial electric field), and α and Γ are the first and second Townsend ionisation coefficients, respectively.

A typical plot of V versus pd (a Paschen curve) is shown in figure (7.7). It can be seen that the left hand side rises more steeply than the right hand side. The Paschen minimum may be found by obtaining $dV/d(pd)$ (= 0) from equation (7.5.1), which gives,

$$(pd)_{min} = (2.72/A)\ln(1 + 1/\Gamma) \qquad (7.5.2)$$

and,

$$V_{min} = B(pd)_{min}. \qquad (7.5.3)$$

Equations (7.5.2) and (7.5.3) allow the constants A and B to be calculated from a plot of the Paschen curve, by finding V_{min} and $(pd)_{min}$.

7.6) Calculation of B and C.

The constants B and C (section (7.5)) may be found by plotting a graph of pd/V versus ln(pd) for the experimental values for the empty discharge tube (figure (7.8)). The constant B is found from the gradient and then C is found from the intercept on the (pd/V) axis. Equation (7.5.1) may then be written as,

$$V = 112pd/(\ln(pd) - 1.38), \qquad (7.6.1)$$

which can be seen to hold well in the range $2.5 < \ln(pd) < 4.5$. Equations (7.6.1) and (7.3.3) are used to find the breakdown voltages for the tube when it contains the brass plugs. The calculation shows that the presence of the brass plugs effectively alters the values of the "constants" B and C. This is probably due to an increase in the surface area within the tube when the plugs are present. The increased surface area results in an increase in the surface recombination losses.

In the case of more than one gap the constants A and B cannot be found graphically and have to be estimated. The constant A is found by estimating the value of $(pd)_{min}$ from the graph of V versus p (figure (7.6)) for the "six single plugs" case and using equation (7.5.2). We have used the second Townsend ionisation coefficient Γ, (≈ 0.02) for copper (Cobine (1958)) in equation (7.5.2), and have assumed that brass should have a Γ value of the same order. We find $(pd)_{min} \approx 1.4$ torr cm, which gives $A \approx 7.6$ (torr cm)$^{-1}$ and $C \approx 0.66$. The constant B is calculated from equation (7.5.3), giving B = 260 volts/cm.torr. Equation (7.5.1) may now be written as,

$$V = 260pd/(\ln(pd) + 0.66);\ pd < 3 \qquad (7.6.2)$$

Equation (7.6.2) and equation (7.3.3) may then be used to calculate the anode-cathode breakdown voltages of the tubes containing the brass plugs. Comparison of the theoretical and experimental values of the breakdown voltage shows that they are in good agreement, when the values of pd used in equation (7.6.2) are less than 3 torr cm. When pd is greater than 8 torr cm, better agreement between theory and experiment is obtained if the value of B is taken as B = 190 volts/cm.torr. Therefore, for pd > 8 torr cm, we have

$$V = 190pd/(\ln(pd) + 0.66);\ pd > 8 \qquad (7.6.3)$$

The "constant" B effectively decreases as pd increases.

Equation (7.6.2) or (7.6.3) can be used for $3 < (pd) < 8$ torr cm, depending on the separations d, of the plugs. Equation (7.6.2) is used for larger plug separations (d greater than 6 cm), and equation (7.6.3) is used for small plug separations. Although we have used experimental data to deduce the constants of equations (7.6.2) and (7.6.3), the comparison of calculated values with experimental values is justified because the differential of equation (7.5.1) is used to calculate the constants rather than the equation itself. Also, although the constants A and B were deduced from the results of one experimental configuration they hold for the other configurations.

The decrease in the "constant" B with increased pd may be due to the presence of space charge. Von Engel (1965) discusses the influence of space charge on the breakdown voltage of uniform gaps. He concludes that the total ionisation in the gap increases through space charge being present when X/p is below a critical value. The ionisation is reduced when X/p is above the critical value. He finds the critical value $(X/p)_o$ to be

$$(X/p)_o = B/2 \text{ or } V_o = Bpd/2. \qquad (7.6.4)$$

Using equations (7.5.1) and (7.6.4) we find,

$$\ln(pd)_o = 2 - C. \qquad (7.6.5)$$

Thus with C = 0.66, the value of the pressure-distance product at $(X/p)_\infty$, $(pd)_\infty$, is 3.8 torr cm. For values of (pd) greater than $(pd)_\infty$ the presence of space charge will enhance ionisation, which means that the field necessary for breakdown is reduced. The breakdown voltage will then be lower than that found in the absence of space charge. In effect, we find that B is a function of (pd), as from equations (7.6.2) and (7.6.3) it is seen to decrease as (pd) increases. Thus equation (7.5.1) should be written with B as a function of pd, rather than as a constant.

7.7) Calculation of the anode-cathode breakdown voltage.

Equation (7.3.3) states that the breakdown voltage across the tube is (greater than or) equal to the sum of the breakdown voltages of the individual gaps. In order to verify this, we assume that the equation governing breakdown, in a tube with finite electrodes, is of the form of equation (7.5.1).

Equations (7.6.2) and (7.6.3) are used with equation (7.3.3) to calculate the anode-cathode breakdown voltages of the various plug groups.

7.8) Results.

The breakdown voltages calculated using equations (7.6.2), (7.6.3) and (7.3.3) are shown in figure (7.9) plotted against the measured breakdown voltages. As a reference the line $V_{ca} = V_{ma}$ has also been plotted. It can

be seen that most of the calculated values lie within 10% of the measured values. The agreement is excellent, even though the equations used to calculate the breakdown voltages are only approximately correct.

7.9) Constant voltage similarity

The breakdown voltage of a tube containing metal cylinders through which the electrostatic field is unable to penetrate, is approximately equal to the sum of the breakdown voltages of the gaps between the cylinders. We may use a similarity relationship (Francis 1956) to obtain an expression relating the breakdown voltage of the empty tube to the breakdown voltage of the tube when it contains metal discs which divide the tube into n gaps.

For the empty tube with electrode separation D, at pressure p, we write the breakdown voltage, $V_\infty(p)$, from equation (7.5.1) as,

$$V_\infty(p) = B.(pD)/[\ln(pD) + C], \qquad (7.9.1)$$

where B and C have been defined previously.

For a gap of length d, which is less than D, the breakdown voltage, $V_d(p)$, at pressure p is

$$V_d(p) = B.(pd)/[\ln(pd) + C]. \qquad (7.9.2)$$

We may write d as d = aD, where a is a constant, of value less than 1. For similar discharges, we scale the pressure

(p_1) to obtain the same breakdown voltage for the gap of length d, as that of the gap of length D at pressure p. We find for $p_1=p/a$,

$$V_s(p_1)=[B.(p/a)(aD)]/[\ln((p/a)(aD))+C]=V_s(p). \quad (7.9.3)$$

If we have a tube with n gaps, each of length d, we would expect, from equations (7.3.3) and (7.9.3), that the breakdown voltage, V_n, across the tube to be given by,

$$V_n(p_1) = nB.(p_1d)/[\ln(p_1d) + C] = nV_s(p). \quad (7.9.4)$$

In order to confirm this relationship, we use the same apparatus described earlier. We measure the breakdown voltages, at various pressures, of the empty tube. The breakdown voltages of the tube when a brass disc, of length 1.9 cm, is placed at the centre of the tube to produce two gaps (a=0.47), and when two discs are placed a third and two thirds along the tube to produce three gaps (a=0.29), are also measured. The breakdown voltages are plotted against pressure in figure (7.10). This graph is used to find the breakdown voltage of the tube containing one or two brass discs, at a pressure p_1 ($V_n(p_1)$), and to find the complementary value of $V_s(p=ap_1)$. The measured values of $V_s(p)$ are then multiplied by n to give $nV_s(p)$. Figure (7.11) is a plot of $V_n(p_1)$ versus $nV_s(p)$, for two and three gaps. The line $V_n(p_1) = nV_s(p)$, has also been drawn. The results start to diverge at higher pressures when space charge lowers the measured breakdown voltage ($V_n(p_1)$) of the gaps

below the calculated values ($nV_s(p)$), as mentioned in section (7.6).

7.10) Reasons for discharge penetration.

In section (7.3), it was stated that the electrostatic field at a distance of one segment diameter inside a metal segment is reduced to the order of 10 % of the external field value. This lack of field penetration prevents the formation of a direct discharge between the electrodes. Breakdown then occurs in the gaps between individual plugs. After breakdown, the discharge may be continuous between the anode and the cathode, or individual discharges may form in the gaps with conduction through the walls of the plugs.

After breakdown occurs, the discharge may move from the flat faces of the plugs to the axial hole. The narrow bore region acts as a hollow cathode. The plasma produced in the narrow bore region diffuses into the cavity of the plug and leads to breakdown on the axis. The axial path must have a lower impedance than the conduction path through the metal walls.

7.10.1) Experiment.

The breakdown voltages, sustaining voltages, and initial currents are measured, using the circuit given in figure (7.1), for the following three cases:

a) An empty quartz discharge tube.

b) A quartz discharge tube containing six separate brass

plugs, as described previously.

c) A quartz discharge tube containing six pieces of solid brass, with the same external dimensions as the brass plugs. They are arranged within the discharge tube so that the separations are the same as those in experiment (b).

All measurements are made in atmospheric air.

The glow discharge in the empty tube has a positive column approximately 24 cm in length, over the pressure range (1-5 mbar) under consideration, with an electrode separation of 27.6 cm. The "negative regions" (appendix 1) form in the remaining 3.6 cm of tube. When the brass plugs are used, the discharge is continuous between the electrodes, and appears to have a positive column of the same length as the positive column observed in the empty tube. There appears to be no positive column present in the discharges in the gaps formed by the solid brass segments, as the characteristic pink glow of the column is not observed. These gap lengths lie between 1.75 cm and 4.3 cm. Observations of the discharge in the empty tube indicate that a gap of length greater than 3.6 cm is necessary for the positive column to form, at pressures from 1 to 5 mbar. The individual gaps each contain an independent discharge, and most of these gaps are too short for a positive column to form (section (A1.2.2b)).

7.10.2) Results.

Figures (7.12) are plots of breakdown voltage and sustaining voltage versus pressure, for the three

experiments described in section (7.10.1). It is obvious that the breakdown voltages for the brass plugs and for the solid pieces of brass, are of the same order. The small differences in breakdown voltage between the two cases are probably due to the presence of contaminants, and variations in the electrode surface structure. The solid pieces of brass and the brass plugs have slightly different surface areas, due to the presence of axial holes in the latter case.

The breakdown voltages for the tube containing the brass plugs and for the tube containing the solid pieces of brass are similar for the following reasons. For the solid pieces of brass, breakdown must occur in each gap, as there is no direct path between the electrodes. A conducting plasma must form in all the individual gaps before a continuous current path is established between the anode and the cathode. When the brass plugs are used, the elecrostatic field is unable to penetrate along the axis of the plugs, and breakdown directly between the anode and the cathode cannot occur. Each (inter-segment and electrode-segment) gap must conduct in order to establish a continuous current path between the electrodes.

An empty quartz tube has the lowest sustaining voltage. A discharge in a tube containing the solid pieces of brass has a higher sustaining voltage, than a discharge in a tube containing the brass plugs. The discharge sustaining voltage is therefore lower when the conduction path is along the axis of the tube. There is less power dissipated, in the tube, along the axial path than there would be if the

conduction path were through the walls.

The discharge does not form along the axis of the plugs at pressures greater than 9 mbar. Figure (7.12) shows that sustaining voltages for the brass plugs and the solid pieces of brass appear to be converging to the same value at a pressure of about 9 mbar. Above this pressure we would expect the current to pass through the metal walls, as this produces the lowest sustaining voltage.

The sustaining voltage of the discharge in the tube containing the solid pieces of brass appears to be independent of the pressure over the range considered. The gaps between the solid pieces of brass are too short for a positive column to form (section (A1.2.2b)). The voltage measured across the discharge tube is then approximately equal to the sum of the anode falls, V_A, and cathode falls, V_C, of all of the gaps. These falls are virtually independent of pressure for a normal glow discharge. The results allow an estimate of the falls to be made which gives,

$$V_A + V_C = 347 \pm 12 \text{ volts.}$$

As the anode fall is of the order of the ionisation potential of the gas, we find the cathode fall to be,

$$V_C = 332 \pm 12 \text{ volts.}$$

The value given by Von Engel (1965) for a copper cathode in air is 375 volts, and 280 volts for a zinc cathode. Thus,

the value of 332 volts for brass is in fair agreement.

In molecular gases the axial electric field in the positive column (and, therefore the discharge sustaining potential) is known to increase as the pressure increases (Francis 1956). The increase in sustaining voltage with pressure, shown in figure (7.10), is due to the formation of a positive column on the axis of the brass plugs, and in the empty tube.

7.11) Energy balance.

The energy balance equation for the positive column is discussed in section (2.4). Here, because short segments are used, we assume that we may use the energy balance equation (positive column) derived for a tube with insulating walls (equation (2.4.2)). We equate the power input into the discharge to the power lost to the walls. The energy balance equation is then,

$$fIXL = (Vi + Ve + Vw)Aj_{+} \qquad (7.11.1)$$

where f is the fraction of the input power lost to the walls (about 0.5 at these pressures), I is the discharge current, X is the axial electric field, L is the length of the positive column, Vi is the ionisation potential of the gas, e.Ve is the energy delivered to the walls by electrons, Vw is the potential difference across the positive ion sheath, A is the wall area, and j_{+} is the random positive ion current density. The individual terms are discussed in

greater detail in section (2.4). If we now consider the cases for the empty tube and the tube containing the brass plugs, we find, approximately,

$$(IX)_E/(IX)_B \approx (IV)_E/(IV)_B \approx A_E/A_B, \qquad (7.11.2)$$

where E denotes the empty tube and B the tube containing the brass plugs. We have assumed that the electron temperature is constant for these experiments, and that $X \approx V/L$. Thus, we can calculate the voltage drop V_B, along the positive column, of the tube containing the metal plugs, by using the equation

$$V_B = (A_B/A_E)(I_E/I_B)V_E. \qquad (7.11.3)$$

The value of (A_B/A_E) is approximately 1.57. The values of the anode fall and the cathode fall must be taken into consideration in calculating the sustaining voltage, as V_B and V_E are the potential falls along the positive column. Figure (7.13) is a plot of the calculated values of the sustaining voltage for the brass plugs versus the measured values. The agreement between the two is within 10%.

7.12) Conclusions.

The breakdown voltage of a tube containing metal segments, through which the electrostatic field is unable to penetrate is approximately equal to the sum of the breakdown voltages of the inter-segment and electrode-segment gaps.

Discharges form between the anode and the cathode, either along the axis of the segments, or in the inter-segment spaces with conduction through the segments. The path taken is such that the sustaining voltage is a minimum.

The sustaining voltage of the discharges (with positive columns) under investigation has a linear dependence on the surface area in contact with the discharge. The main losses in these discharges are from electron-ion recombination at the walls. The sustaining voltage increases as the internal surface area increases.

References.

G.L. Clark, "Studies of Copper and Gold Vapour Lasers". PhD Thesis, University of St. Andrews, 1988.

A. Maitland, "Theory of Segmented Metal Discharge Tubes for Argon Lasers". J. Phys. D: Appl. Phys.,Vol. 4, 1971.

A. Von Engel. "Ionized Gases". 2nd Ed., Clarendon Press, Oxford, 1965.

J.D. Cobine., "Gaseous Conductors." Dover Publications Inc., 1958.

G. Francis. "The Glow Discharge at Low Pressure." Handbuch der Physik, Vol.22, ed. Flugge S.,Springer-Verlag, 1956.

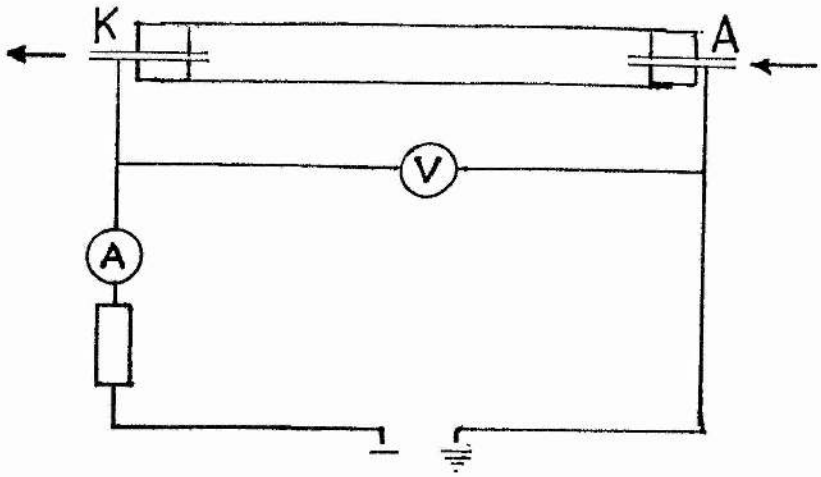

Figure 7.1 Circuit used for breakdown voltage measurements.

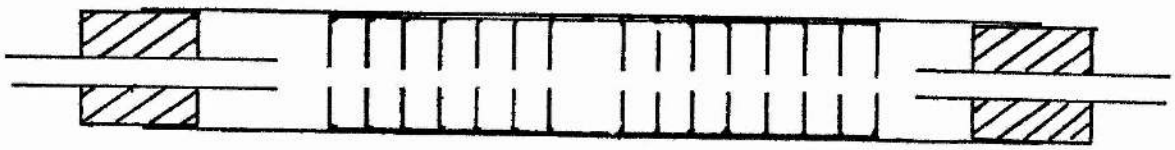

Figure 7.2 Discharge tube arrangement.

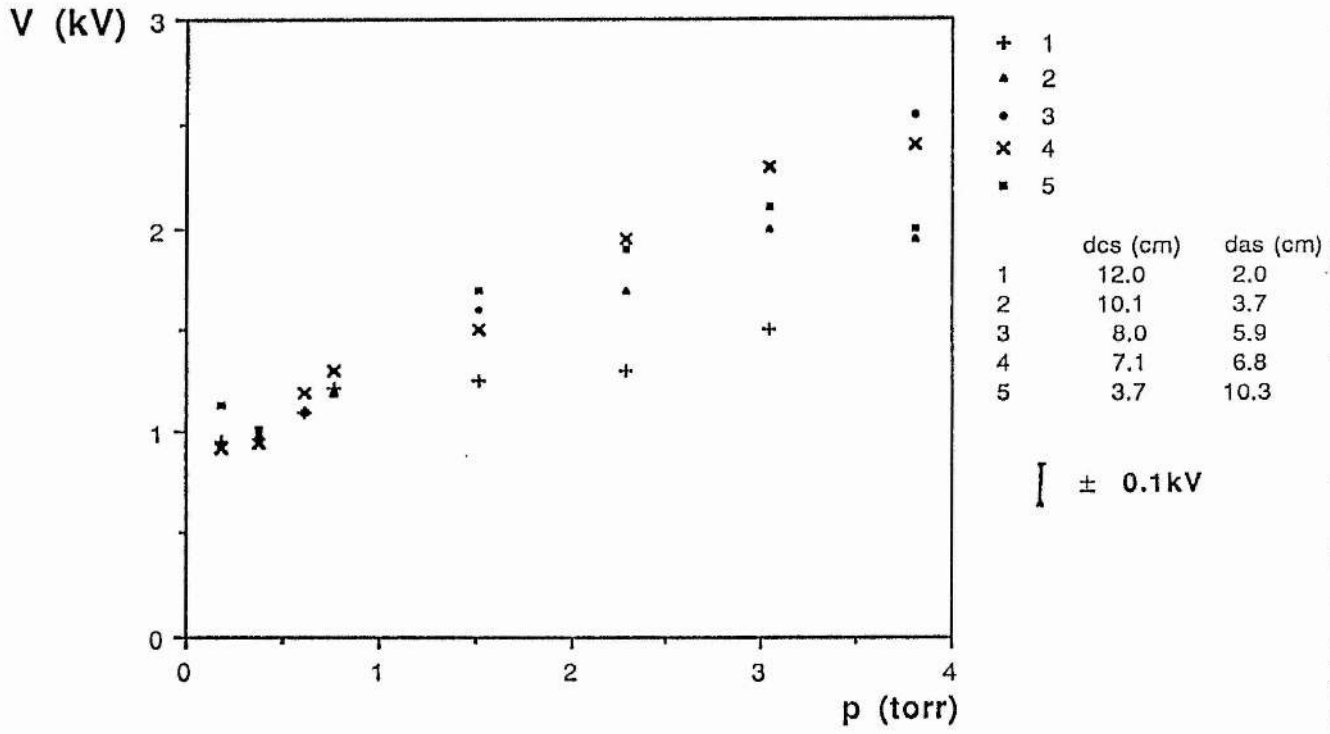

Figure 7.3 Breakdown voltage versus pressure for a group of 15 cups.

Figure 7.4 Brass "plug" (2 cups).

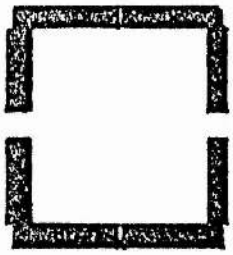

Figure 7.5 Arrangement of plugs within quartz tube.

(6x1)

a) Six individual plugs.

(3x2)

b) Three groups of two plugs.

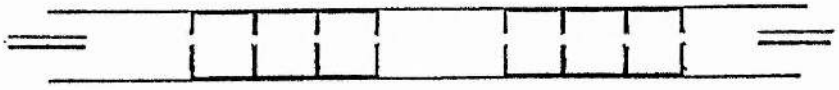

(2x3)

c) Two groups of three plugs.

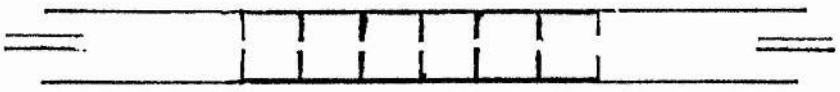

(1x6)

d) One group of six plugs.

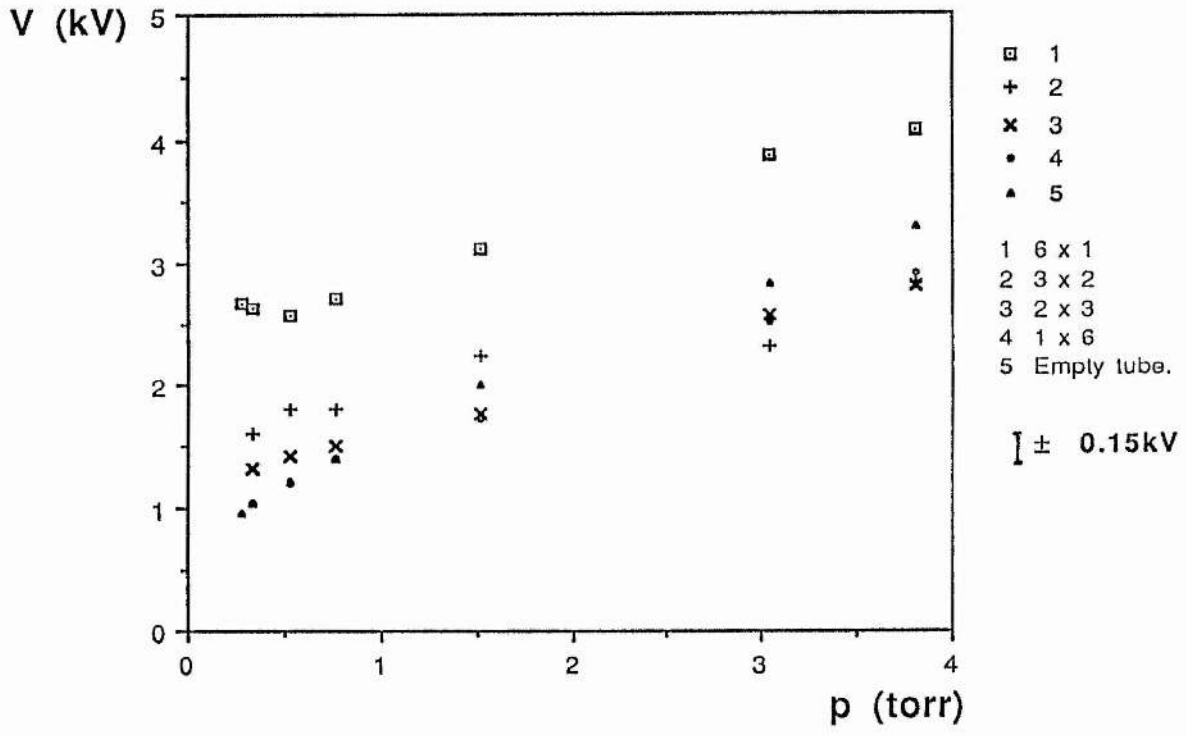

Figure 7.6 Breakdown voltage versus pressure for brass cups arranged as cylinders of various lengths.

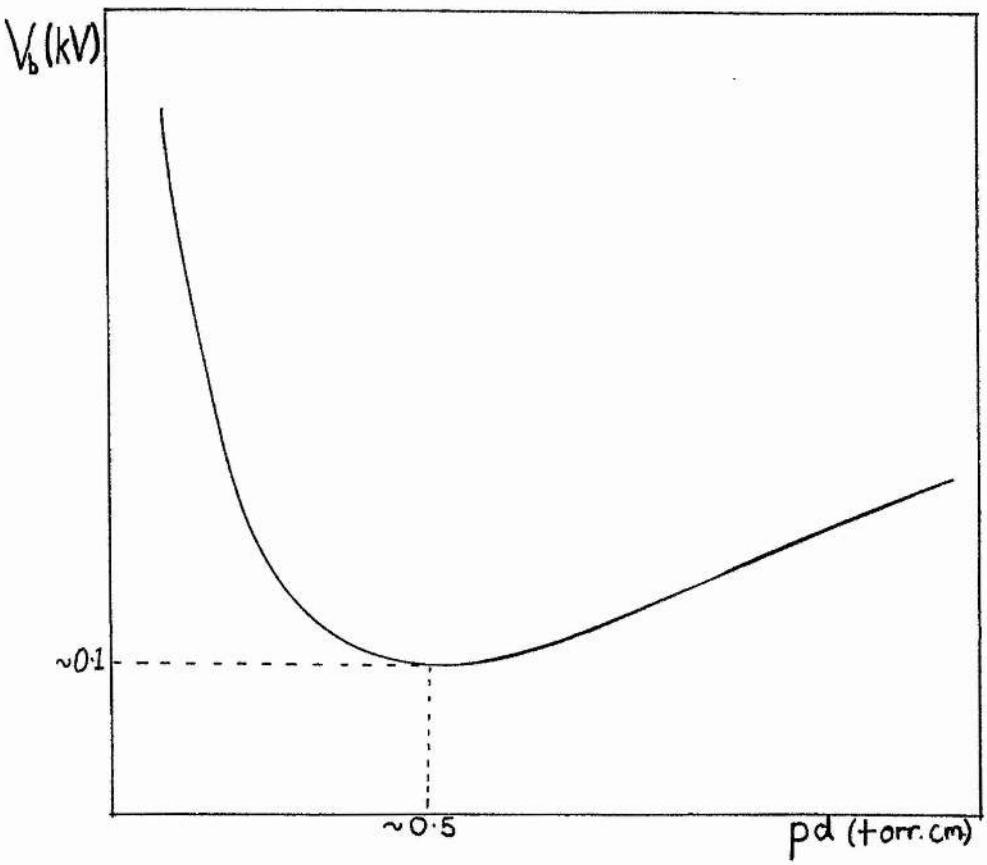

Figure 7.7 Typical breakdown curve for a low pressure gas, described by Paschens law.

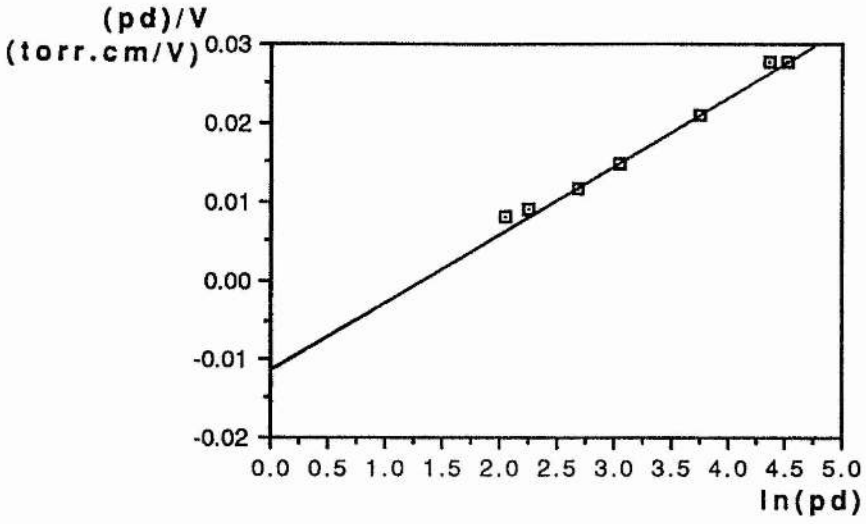

Figure 7.8 pd/V versus ln(pd)

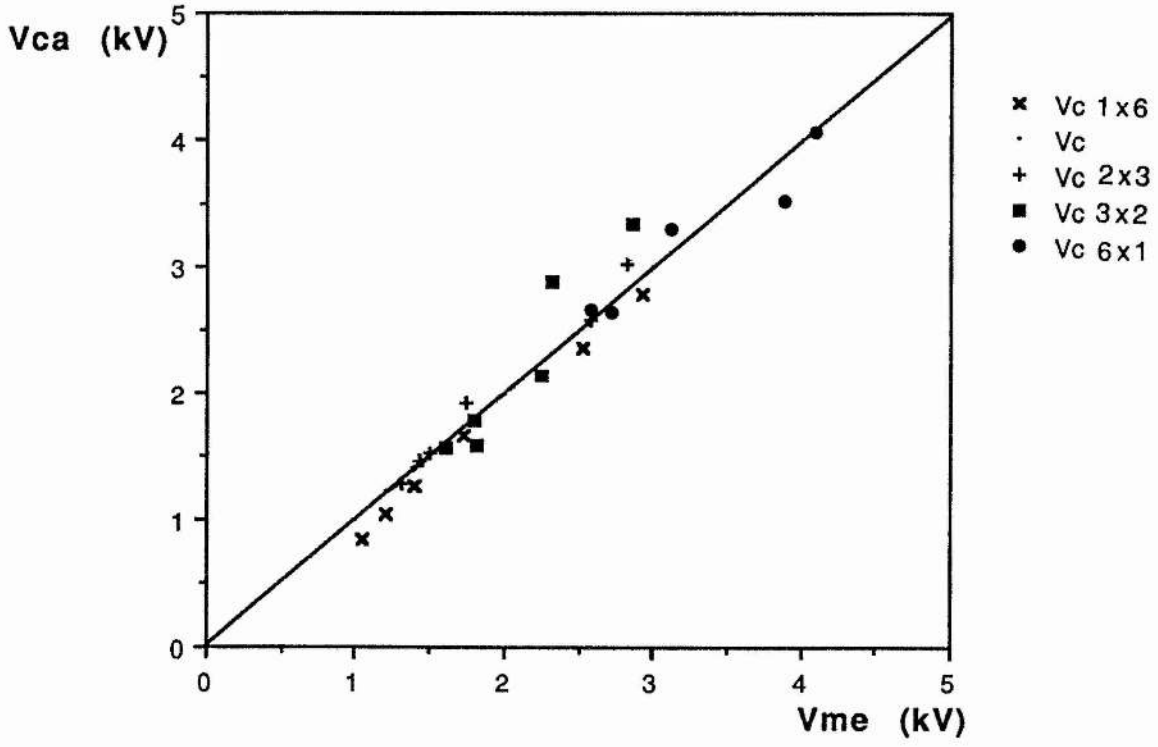

Figure 7.9 Calculated breakdown voltage (Vca) versus measured breakdown voltage (Vme).

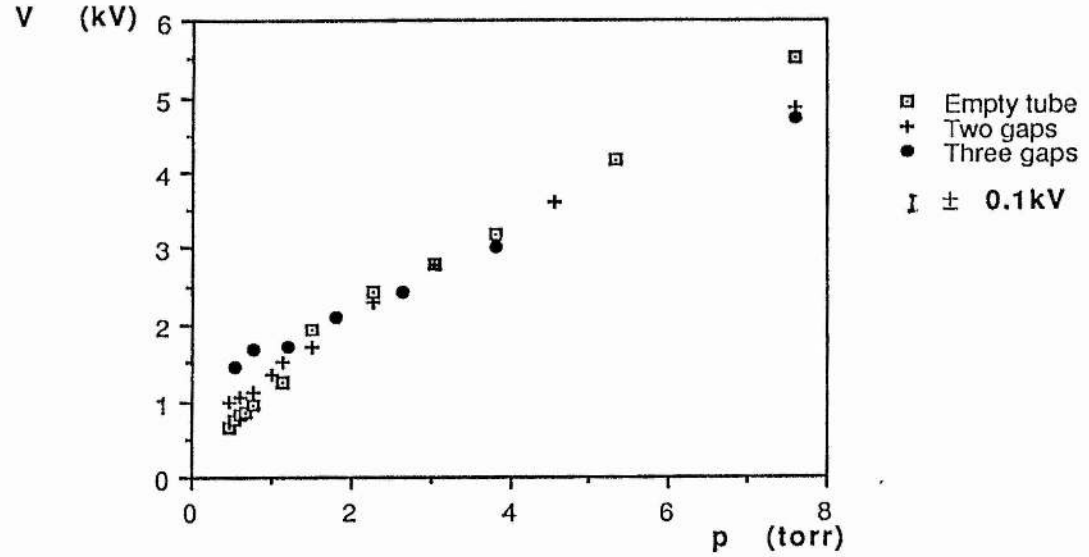

Figure 7.10 Breakdown voltage versus pressure for 1, 2, and 3 gaps.

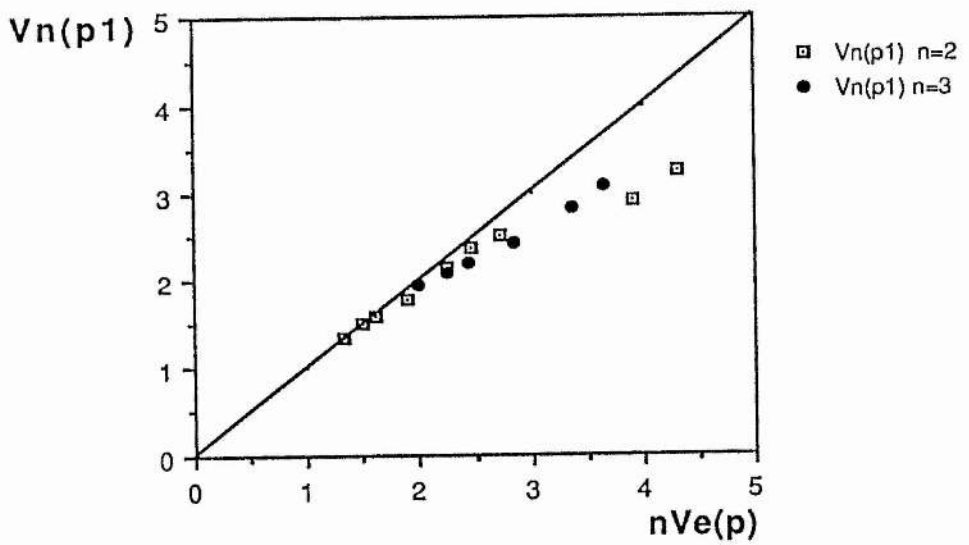

Figure 7.11 Calculated breakdown voltages from equal-voltage similarity relationship.

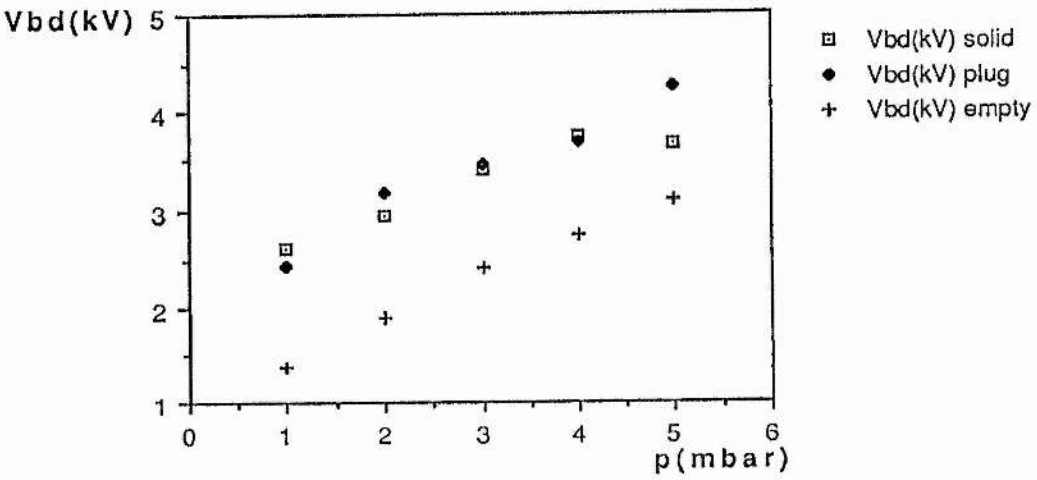

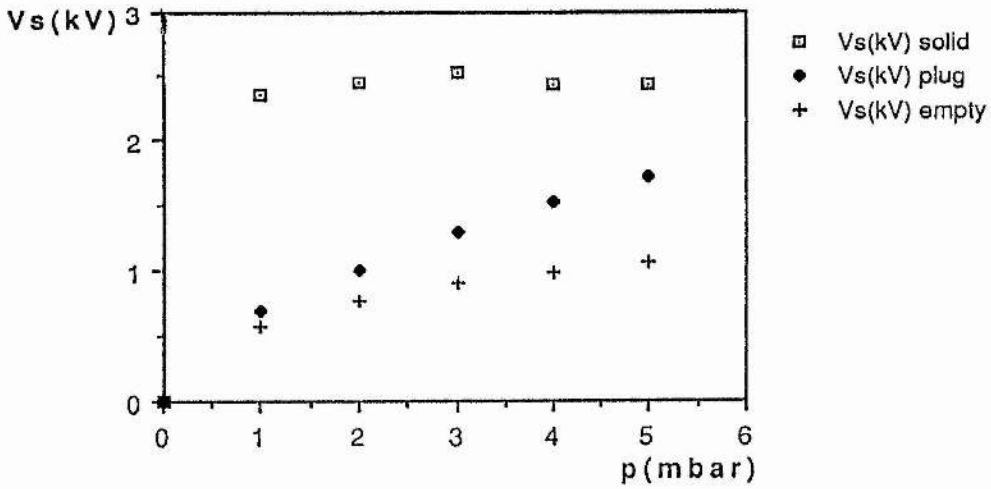

Figure 7.12 Breakdown voltage and sustaining voltage versus pressure.

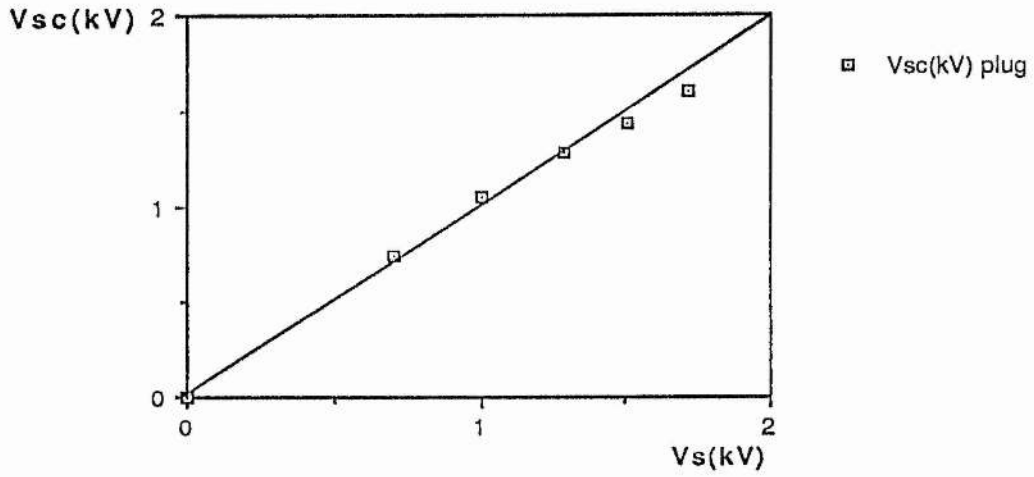

Figure 7.13 Calculated sustaining voltages versus measured values for the group of brass plugs.

CHAPTER 8.

HIGH CURRENT DENSITY DISCHARGE TUBE - MOLYBDENUM CUPS.

8.1) Introduction.

In chapter 6, brass cups are described whose design is based on the tube structure used in early argon ion lasers. In the argon ion laser, metal discs with axial holes confine the discharge. The discs are separated from each other by insulating spacers. In the metal vapour/noble gas discharge tube, under discussion, the insulating spacers and metal discs (in the ion laser) are effectively replaced by molybdenum cups (figure (8.1)). These cups fit together to form a dual-bore tube. The current density should be maintained in the wide bore regions of cups, provided that the distance between the narrow bore regions of adjacent cups is less than the electron mean free path (Halstead et al. (1968)). Experiments show that axial discharges can be maintained in long dual-bore tubes (section 6.4). Axial discharges are more likely to form when the voltage drop in the gas is less than the sum of the anode fall and the cathode fall at the metal tube and the voltage drop in the tube itself.

A dual-bore molybdenum tube (10 cups) is placed in the discharge tube arrangement described in chapter 4. Current densities in excess of 80 amps/cm^2 are obtained with argon as the buffer gas. Copper wire, contained within the wide bore regions of the molybdenum tube is vapourised through discharge heating. The copper vapour may then be ionised in

the high current density region on the tube axis.

Copper has a vapour pressure of 0.01 torr (≈ 10% of the buffer gas pressure) at approximately 1200°C (Nesmeyanov 1963). Calculation (section 8.6) shows that the axial gas temperature is of the order of 1200°C at a current density of 100 amps/cm². This current density may be high enough to obtain laser action of the copper ion. (Laser action has been obtained at low current densities (≈ 0.2 amps/cm²) in the neon-copper hollow-cathode laser at 249 nm, 260 nm and 270 nm (Gerstenberger et al. 1980)).

8.2) Molybdenum cups.

The molybdenum segments described in section (4.3.3), are used to obtain a high current density discharge in a rare gas/metal vapour mixture. One of the problems associated with their use, is the nescessity of having to separate them individually with insulating (quartz) spacers. The quartz is the weakest point in the tube and is easily damaged by metallic condensation and arcing across the conducting coated surface.

In order to reduce the amount of quartz in contact with the discharge, a new segment design was considered in the form of molybdenum cups. The molybdenum cups have a much higher melting point (2600°C) than the copper wire (1050°C), wrapped around the inside of the cups. Figure (8.1) shows a molybdenum cup. The cups interlock to give a good electrical contact, and effectively form a dual-bore tube. The outer wall of the cup is turned down to reduce the amount of metal

in contact with the quartz tube. This leaves a rim at each end of the cup. The width of the rim is the smallest thickness (≈ 2 mm) that can be machined without the metal crumbling. A small hole in the cup wall allows copper to be loaded when the cups are locked together. The diameter of the narrow bore region is 4 mm. The discharges along the axis of the molybdenum cups have lower sustaining voltages than the discharges formed along the molybdenum segments, described in chapter 4. The breakdown voltage of the tube is also lower due the the position and the length of the metal cups within the quartz tube. (The variation in breakdown voltage with dual-bore tube length and position is discussed in section (7.3) for the brass cups.)

8.3) The discharge tube.

Figure (8.2) shows the discharge tube used in the experiments. Nine molybdenum cups, each with a few strands of thin copper wound around the inside, are placed at the centre of a quartz tube, with the open end of the grouping facing the cathode. A piece of zirconia felt is wrapped around the outer walls, between the two rims. This gives added thermal insulation and also prevents copper vapour passing through the loading hole and condensing on the quartz tube. The quartz tube and cups are then placed inside the water-cooled, segmented aluminium support tube, described in chapter 4.

8.4) Circuit configuration.

A plasma jet (section (4.2)) is used as the discharge cathode. The discharge is struck between the plasma jet cathode and the support tube anode (section (4.3.1)). The electrical circuit is shown in figure (8.3). The breakdown voltage is of the order of 500 volts, at an argon pressure of 0.4 torr. A group of fire bars in series with the discharge tube and the Brentford regulator power supply (section (4.4)), act as current limiting resistors. Eighteen firebars are connected in two groups of nine to give a total resistance of 250 ohms. The sustaining voltage at 9 amps is 110 ± 5 volts.

Once the discharge is established using the Brentford supply, it is possible for the Motor Generator set, described in section (4.4), to take over. The current limiting resistors in the Motor Generator circuit have a lower resistance than those in the Brentford regulator circuit. A lower resistance may be used as the power supply output voltages are much lower when the discharge is running than at breakdown. A parallel grouping of 16 fire bars is used in the Motor Generator circuit, with a total resistance of 3.2 ohms. Currents up to 20 amps can be passed. The current limiting resistors stabilise the discharge when it has a negative dynamic resistance (appendix 7). If the discharge is operated at currents where the dynamic resistance is positive, it is not nescessary to use resistors, which waste energy.

8.5) Experiment - Nine cups.

Voltage and current measurements are made. The V-I characteristic curves, at various pressures, are shown in figure (8.4). Comparing the current-voltage characteristic curves in figure (8.4) with those in figure (5.2) shows that the discharge voltages in the tube containing the molybdenum cups (section (8.2)) are lower than those in the tube containing the molybdenum segments (section (4.3.3)). (The active lengths of the cups and the segments are similar. The active length of 9 cups is approximately 11.7 cm while 4 segments have an active length of 10 cm). The lower sustaining voltages obtained in the tube containing the molybdenum cups, are due to the smaller surface area of the cups (in contact with the discharge (section (7.11)), in relation to the surface area of the molybdenum segments. Figure (8.5) shows a V-I characteristic obtained at higher currents. The reduction in discharge voltage at currents above 10 amps may be indicative of copper entering the discharge since copper has an ionisation energy of 7.7 eV compared with 15.7 eV for argon. Thus, less energy is needed for ionisation when copper vapour is present.

When the light from the discharge is viewed through a hand held spectrometer a series of green argon ion lines are observed. At currents of the order of 15 amps a strong yellow line appears which may be the copper line at 578.2 nm.

8.6) Copper vapour density.

At currents of less than 20 amps we may estimate the copper vapour density by calculating the gas temperature. Chester (1968) has proposed an impirical formula for the longitudinal gas temperature, T_g(K) in an argon ion laser,

$$(T_g/300) = (1 + 0.02[JD^{1/2}]) \qquad (8.6.1)$$

where J is the current density in amps/cm^2 and D is the tube diameter in mm. Figure (8.6) shows a plot of T_g versus I (current). We can see that at a current of 14 amps the gas temperature is 1336 ^{o}C. At this temperature copper has a vapour pressure of approximately 0.1 torr, which is the same as the argon pressure for the discharge characteristics shown in figure (8.5), where the discharge impedance is seen to fall at currents above 10 amps. The discharge impedance starts to fall, when the copper vapour pressure is of the order of 0.1 % of the buffer gas pressure.

8.7) Power delivered to the tube walls.

The distribution of the power delivered to the walls, along the cup structure (figure (8.2)), may be inferred from the amount of copper wire which has melted in each cup. The amount of melted wire increases as the power delivered to a cup increases. The cups are labelled 1 - 9 from cathode end to anode end of the cup structure. The amount of melted copper wire in each cup is as follows. (Cup 1 has its open

end facing the cathode, and therefore does not contain copper.) The copper wire in cups 2 to 4 had melted at its ends (a few mm). The copper in cup 5 had only melted slightly. In 6 approximately half the copper wire had melted. The wire in cups 7, 8, and 9 had completely melted. Figure (8.7a) shows the approximate axial distribution of the power delivered to the cups.

The small amount of melted wire in the fifth cup may be due to poor electrical contact between cup 4 and cup 5. If these two cups are not electrically connected, the grouping of nine cups then behaves as two dual-bore tubes, one of four cups and one of five cups. Figure (8.7b) shows the wall potential (of the cups) relative to the axial potential of the plasma, in this case.

Metal segment theory (section (2.2)) predicts a larger potential difference between the plasma and the segment, across the positive ion sheath, at the anode end of a long metal segment than at the cathode end. The ions at the anode end therefore impact with greater energy. The variation in the potential difference across the sheath produces an equivalent variation in the distribution of the power delivered to the walls along the length of a segment. The above suggests that there may may be a higher copper vapour density at the anode end of the metal tube.

8.8) Lasing considerations.

To increase the probability of observing laser action, the active length of the discharge is approximately doubled

by using a further 10 cups to form another tube. This gives a total active length of 24.7 cm. The cups are placed in a group of nine and a group of ten in the quartz tube. The groups are separated by 2 cm. The cups are not placed in one large grouping as this may exceed the maximum length of metal segment which will sustain an on-axis discharge.

We assume that to obtain lasing we require similar conditions to those found in argon ion laser discharges. These conditions are an operating pressure of about 0.1 torr and current densities in excess of 100 amps/cm^2. With a bore diameter D, of 4 mm the optimum pressure is 0.125 torr. ($p_{optimum}$(torr)D(mm) $\approx$ 0.5 (JD < 100 amp/cm) Dunn and Ross (1976).)

8.9) Discharge characteristics - 19 segments.

The molybdenum cups are each loaded with four, 1 cm pieces of 1 mm copper wire. The discharge characteristics at low currents are shown in figure (8.8). The discharge voltages are higher than those shown in figure (8.4) due to an increase in the number of metal cups (and hence an increased surface area in contact with the discharge.(section 7.11))

At the optimum pressure of 0.125 torr (section (8.8)) and at a current of 12 amps, the discharge sustaining voltage is about 250 volts. This voltage is the maximum output voltage of the Motor Generator. The current density at 12 amps is only 95 amps/cm^2, which may be less than the current density required for laser action.

A metallic coating is formed on the quartz tube, in the region between the dual-bore molybdenum tubes, and over a few centimeters at each end of the molybdenum tubes. This coating did not lead to arcing, as occured in the tube containing the molydenum segments (section (5.3.3)).

8.10) Argon ion power supply.

A high power stabilised DC supply is used to obtain higher current densities than those attainable using the Motor Generator (section (4.4)). The DC supply, originally designed for use with a 2.3 metre argon ion laser, can operate at currents in excess of 100 amps at 500 V. However, because of wiring limitations the maximum current available is 40 amps. The supply is connected to the mains through an isolating transformer, which allows the negative terminal to be earthed. Figure (8.9) shows the circuit diagram. The diodes protect the argon ion supply from high voltage spikes produced at breakdown. Two sets of sixteen fire bars in parallel, in series with the supply ensure that the supply "sees" a total positive resistance (Appendix 7).

Only a few tentative results have been obtained using this supply, which indicate that at currents of 30 amps (current density of 240 amps/cm^2) at 0.16 torr, the sustaining voltage is only 260 volts. Equipment problems, which include damage to the tube anode and the power supply, have resulted in the experiments being postponed at this tantalising point.

8.11) Conclusions.

Dual-bore tubes formed from molybdenum cups have been described. Discharges can form along the axis of long (10 cups) dual-bore tubes. Copper wire contained within the cups is found to have melted, indicating that the cups have reached a temperature in excess of 1100°C. A high current density discharge has been obtained in an argon-copper vapour mixture.

High current densities (greater than 200 amps/cm^2) are reached at sustaining voltages of only a few hundred volts. The discharge sustaining voltage is found to decrease at currents above about 12 amps. This may indicate that copper vapour, at a pressure of the order of the buffer gas pressure ($\approx$ 0.1 torr), is entering the discharge.

The high current density/high copper vapour pressure should lead to large quantities of copper ions being present, with the possibilty of population inversions produced by excitation by direct electron impact.

References.

A.S. Halsted, W.B. Bridges, G.N. Mercer. "Gaseous Ion Laser Research.", Technical report AF-5237, Hughes Research Laboratories, 1968.

M.H.Dunn and J.N.Ross. "The Argon Ion Laser." Prog. Quant. Elec. Vol. 4. 1976, p 233.

A.N.Chester. "Experimental measurements of gas pumping in an argon discharge." Phys. Rev. 169(1), 1968, p 184.

D.G. Gerstenberger, R.Solanki, G.J. Collins. "Hollow cathode metal ion lasers." IEEE J.Quant.El., QE-16, 1980, p 820.

An.N. Nesmeyanov. "Vapour pressure of the elements." Translated and edited by J.I. Carasso, Infosearch Ltd., 1963.

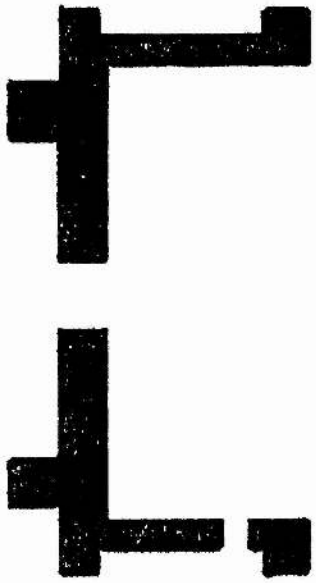

Figure 8.1 Molybdenum cup.

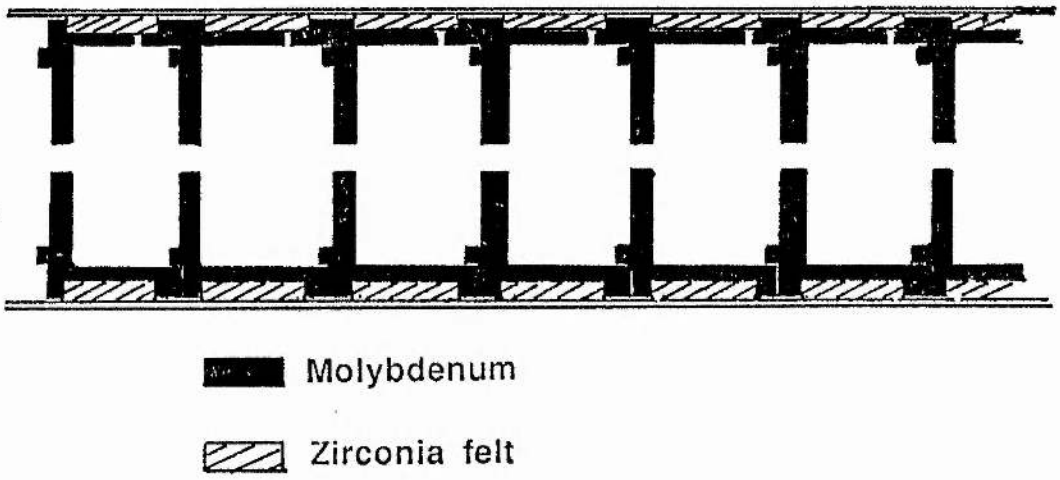

Figure 8.2 Quartz tube containing molybdenum cups.

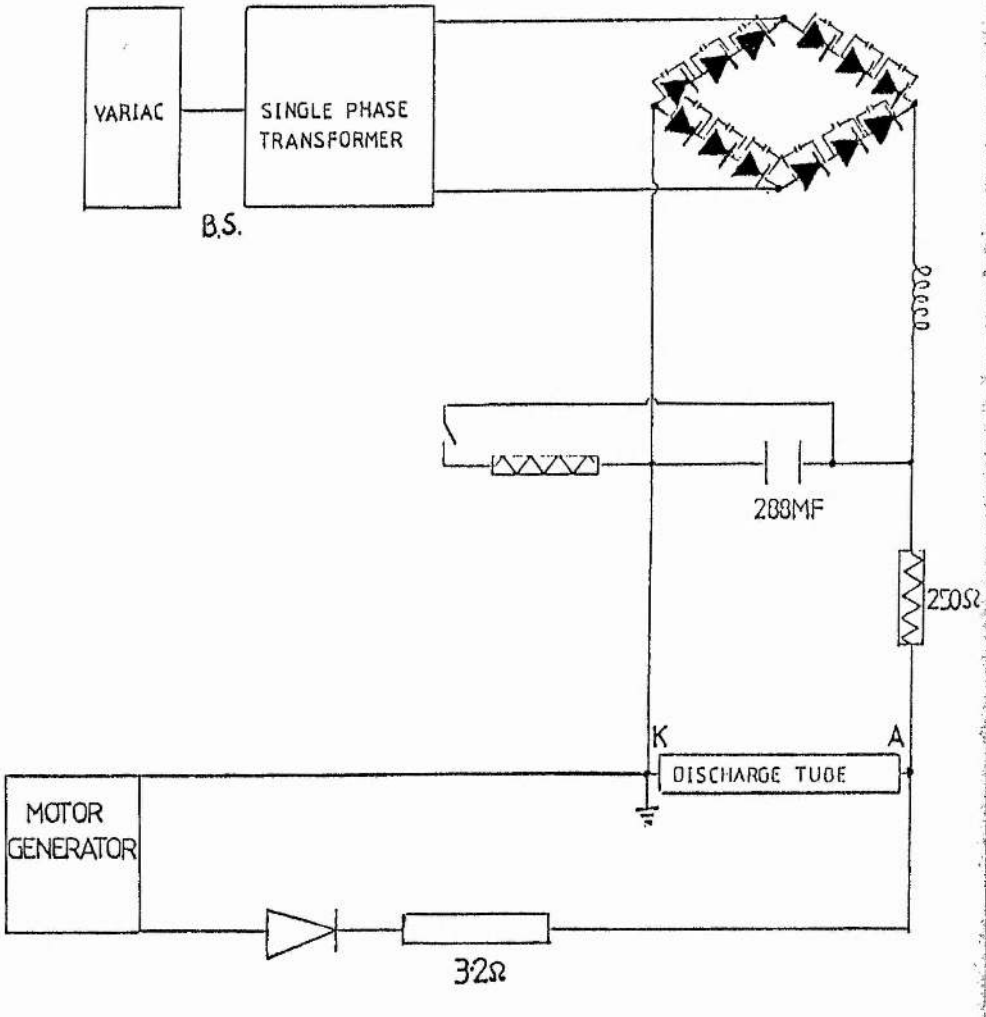

Figure 8.3 Power supplies used for the argon-copper discharge in the molybdenum cups.

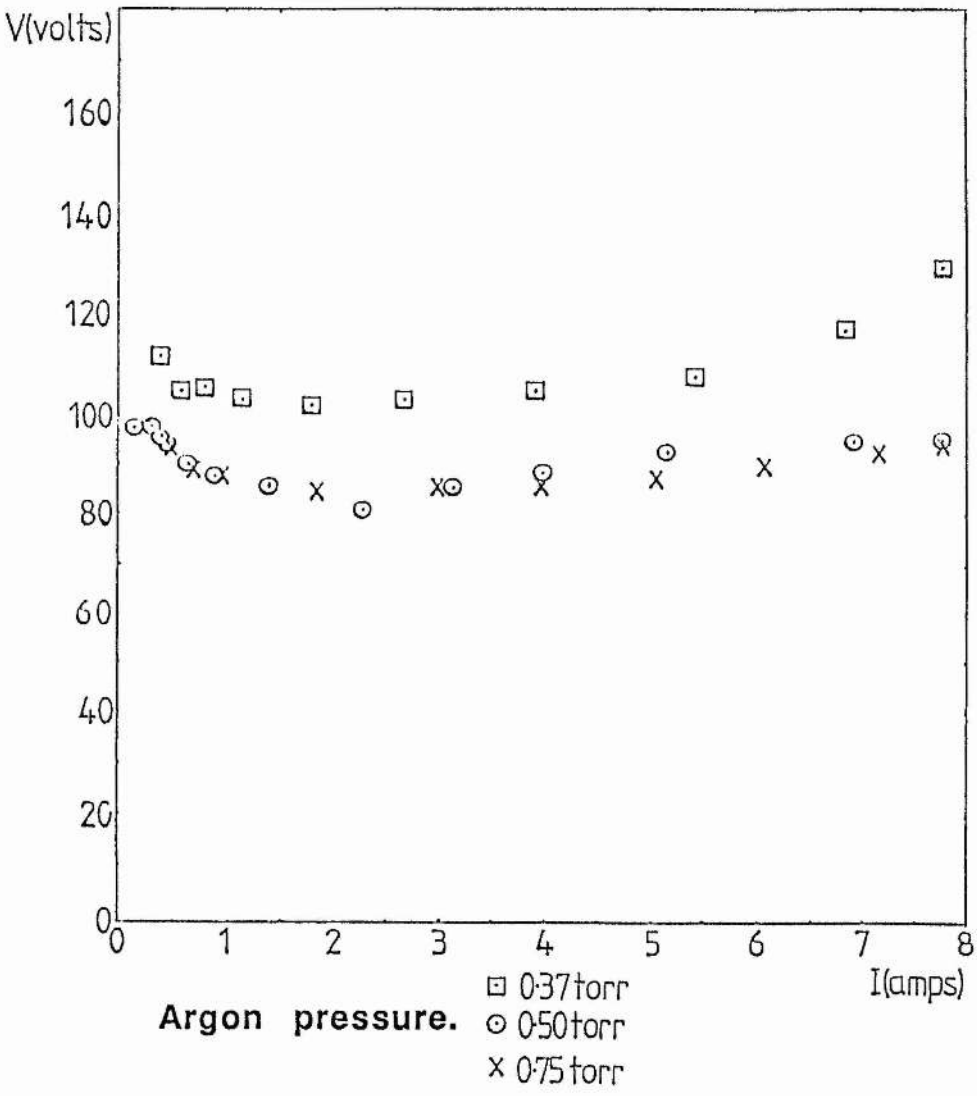

Figure 8.4 Voltage-current characteristics for argon-copper discharge. (Nine molybdenum cups.)

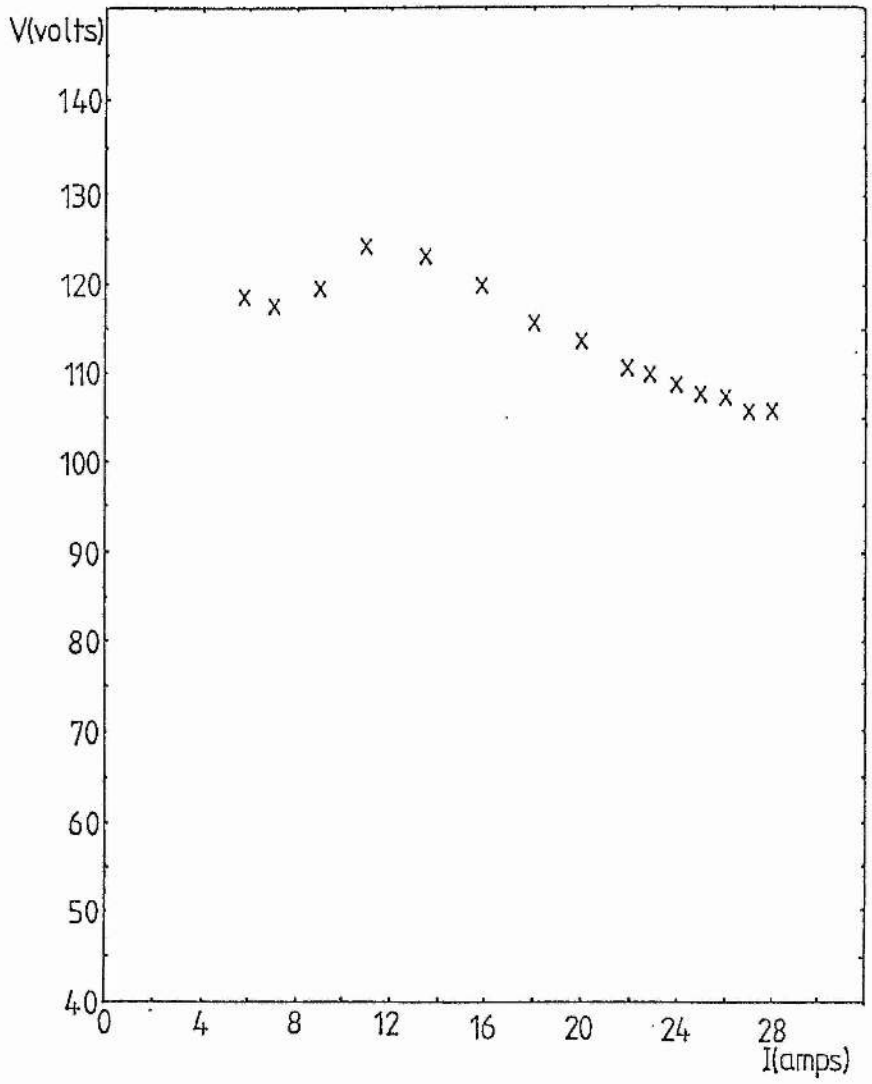

Figure 8.5 Voltage-current characteristic for argon-copper discharge at higher currents. (Nine molybdenum cups). (Argon pressure 0.1 torr.)

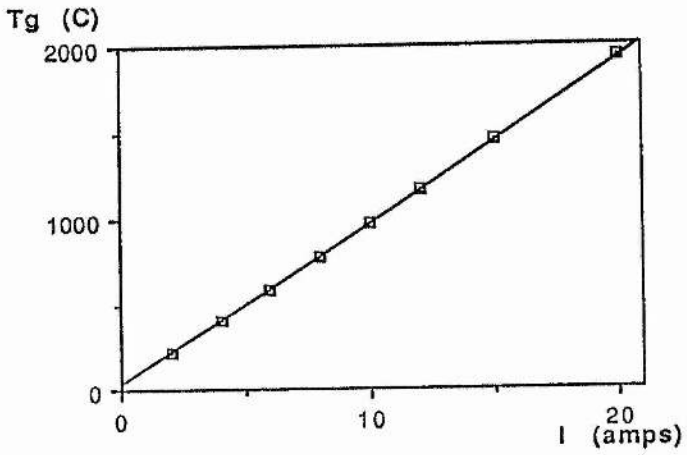

Figure 8.6 Plot of gas temperature (Tg) versus current (I).

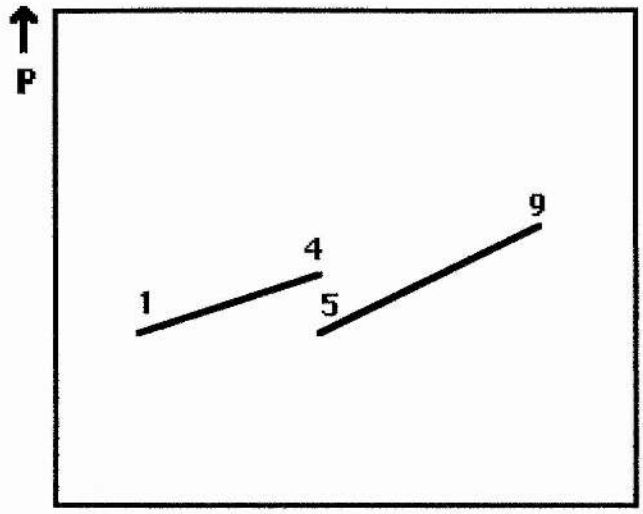

Figure 8.7a Approximate distribution of the power delivered to the cups.

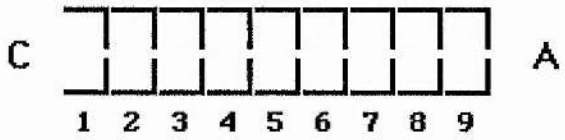

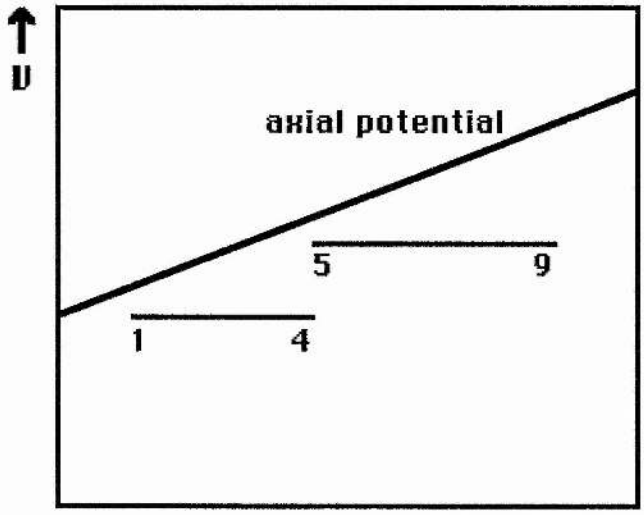

Figure 8.7b Potential of cups relative to the axial discharge potential.

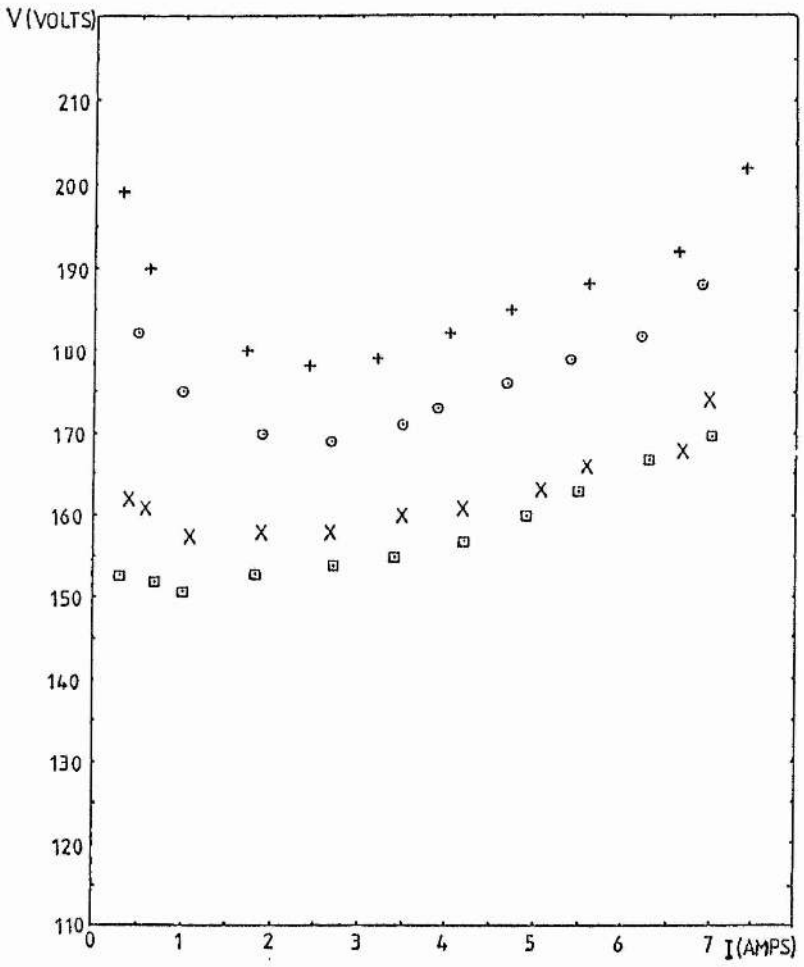

Figure 8.8 Voltage-current characteristics for argon-copper discharge. (19 cups).

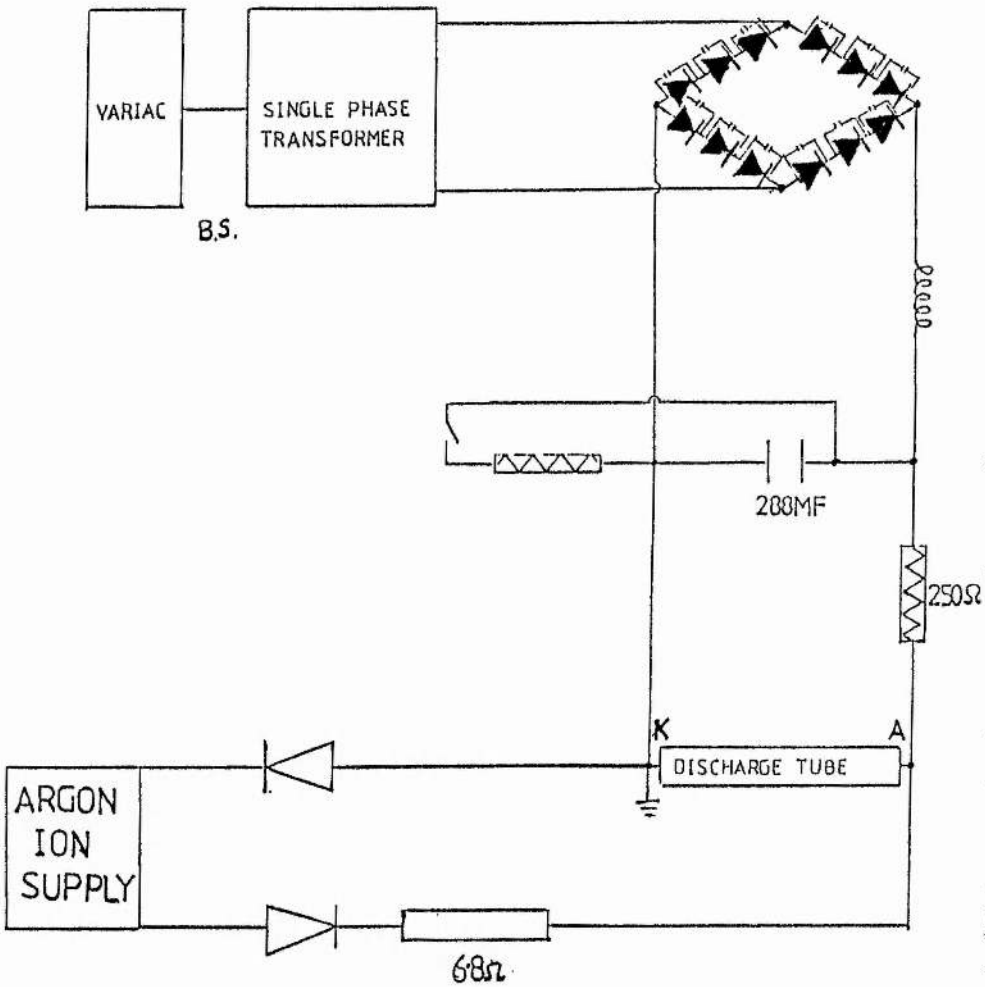

Figure 8.9 **Power supplies used at higher currents for argon-copper discharge.**

CHAPTER 9.

CONCLUSIONS.

9.1) Maximum segment length.

Various criteria have been used to find relationships between the maximum length of a metal segment and the axial electric field (and hence the tube radius and the tube pressure). These criteria are;

a) The cathode end of a metal segment attains plasma potential.(section (2.3.2))

b) The radial field at one end of the segment is equal to a critical breakdown field. (section (2.9))

c) The potential drop along the axis of the segment has the same value as the sum of anode and cathode falls at the segment.(section (6.4))

Criteria a, b, and c provide the basis for a method to estimate the maximum usable length. Calculation of the maximum segment length in each case will yield a minimum value, which may be used when considering segment lengths in discharge tube design.

All the criteria indicate that the maximum length is inversly proportional to the axial electric field and hence in the pressure range from 1 - 10 torr is proportional to the tube radius and inversly proportional to the pressure.

9.2) Positive ion sheath thickness.

The thickness of the positive ion sheath which forms between the plasma and the wall of a discharge tube is a function of the potential differnce across the sheath (section (2.8)). Hence, for a metal segment (conducting wall) the sheath is thicker at the anode end of the metal segment than at the cathode end. In low current density discharges (10^{-3} amps/cm^2), the sheath thickness at the anode end of the segment can become an appreciable fraction of the tube radius and the resulting reduction in the conduction path may lead to an increased axial field in the plasma.

9.3) Energy balance.

The energy balance equation has been determined, for the case of conducting walls, by equating the power lost at the tube walls to the input power to the discharge (section (2.4)). Measurements of the axial field in metal tubes at low current densities shows an increase of the order of 20% over the field in a tube with insulating walls (section (3.3.2)).

9.4) Longitudinal wall currents.

The longitudinal wall current (the current in a direction from end to end of a segment) in a metal segment increases on moving from the anode end to the cathode end of

a metal segment (section (3.6)), while at the same time the axial discharge current decreases. An indication of the magnitudes of the longitudinal wall currents was obtained by measuring the current between adjacent metal segments in a suitable external circuit connecting the two segments. Measurements of the current between the inter-connected metal segments (section (3.5)) (equivalent to the current at the central section of a segment) show an increase in the ratio of the inter-segment current to the anode-cathode current with increasing pressure and decreasing anode-cathode current.

9.5) Breakdown voltages.

The anode-cathode DC breakdown voltage of a discharge tube containing isolated cylindrical metal segments (through which the axial field is unable to penetrate) is approximately equal to the sum of the breakdown voltages of the inter-segment and electrode-segment gaps (sections (7.3) and (7.8)). The anode-cathode breakdown voltage can be increased, when metal segments are present, above the breakdown voltage of the empty tube. This increase is due to the nonlinearity of the relationship between the breakdown voltage of a gap and the pressure-electrode separation product (appendix 5). Considerably higher breakdown voltages are obtained at low pressures if the gaps between the metal segments are small enough to result in breakdown on the left hand side of the Paschen curve.

9.6) High current density metal vapour discharges.

High current density discharges have been produced in a metal vapour - noble gas mixture (sections (5.3) and (8.5)) Dual-bore (alternate narrow and wide bores) metal tubes (chapter 6) are used to confine the discharge. The narrow bore sections determine the current density of the discharge, and if the length of the wide bore sections is less than a value which depends on the electron mean free path the high current density will be maintained in the wide bore sections.

In multi-segment tubes arcing may occur between adjacent segments, and therefore the use of long dual-bore metal tubes reduces the number of arc sites and results in stable gas discharges. The high current densities obtainable may lead to excitation of the copper ion by direct electron impact resulting in ultra-violet laser transitions. The laser system would be inherently more efficient than conventional noble gas ion lasers, due to the lower excitation and ionisation energies in the former case.

APPENDIX 1

The Glow Discharge.

A1.1) Introduction.

The following is a brief discussion of the low pressure, low current discharge, known as the glow discharge. When a potential is applied between two electrodes (assumed planar) at each end of a glass tube containing a low pressure gas, a very small current is seen to flow. As the potential is increased the current also increases slowly, until the breakdown potential is exceeded and then a large current will flow, which is circuit limited. Light is emitted by the excited gas. If the current is constrained between 10^{-4} and 10^{-1} amps, at a pressure of the order of a torr, a "normal" glow discharge is formed. The potential difference between the electrodes of a normal glow discharge is independent of the current. Figure (A1.1) shows the variation of the discharge voltage as the current increases, in a typical low pressure gas discharge.

A1.2) Appearance of the discharge.

A1.2.1) Regions of the discharge.

The normal glow discharge consists of regions of dark and light, as shown in figure (A1.2). These regions have a specific appearance and exhibit different physical characteristics.

The negative regions.

The negative regions lie between the cathode and the Faraday Dark Space (FDS)-Positive Column boundary. It is known that the negative zones have beam like properties. When a planar cathode is rotated around a fixed anode, within a spherical container, the negative zones remain "fixed" to the cathode, while the positive "column" fills the remainder of the vessel.

As we move from the cathode the following regions may be observed.

a) The Aston Dark Space. The Aston dark space is a thin dark layer adjacent to the cathode

b) The First Cathode Layer. The first cathode layer is a thin band of light. The electrons from the cathode have gained enough energy to excite the gas in this layer.

c) The Cathode Dark Space (CDS). The cathode dark space is also known as the Crookes or Hittorf dark space. This is actually the region bounded by the cathode and the negative glow. It is a region of high positive space charge which produces a large electric field. The field decreases linearly from the cathode to the edge of the glow. The cathode dark space is essential to the maintainance of the discharge, and is where the electrons emitted from the cathode acquire most of their energy.

d) The Negative Glow (NG). The negative glow is a highly luminous region. The light from the glow reaches a maximum in the centre of the region, then gradually fades towards the anode end of the glow into the FDS.

e) The Faraday Dark Space (FDS). The Faraday dark space emits very little light in relation to the regions which form its boundaries. The length of the Faraday dark space increases as the tube radius increases (constant pressure). The electric field is very small (almost zero) in the negative glow and the Faraday dark space.

All the negative regions (a to e) have boundaries which are parallel to the surface of the cathode and are concave towards the cathode in regions close to the walls. The boundaries of the regions lie along equipotential surfaces. This suggests that the walls are at a positive potential with respect to the adjacent ionised gas, in these regions.

The positive regions.

The positive regions of the normal glow discharge lie between the Farday dark space-positive column boundary, and the anode. (The metal segment theory presented in this thesis concerns the positive column.) The theory of the positive column is discussed in section (A1.3). In the positive regions the boundaries are convex towards the cathode showing that the walls are charged negatively with respect to the plasma in these regions.

f) The Positive Column (PC). The positive column fills the tube from the Faraday dark space almost to the anode. In general it has a low axial electric field which is constant along its length. The column may be divided into regions of varying brightness, and non-uniform field, known as striations. These may be stationary or moving. The formation conditions for striations are complicated functions of pressure and current.

g) The Anode Dark Space and Anode Glow. The anode dark space and the anode glow lie between the positive column and the anode. The anode dark space is a region of space charge, which may be positive or negative. The glow is formed adjacent to the anode by excited atoms.

The electron current collected by the anode is directly proportional to the anode area. The electron current at the anode is equal to the current in the external circuit. For small anodes, a region of negative space charge forms in front of the anode. The positive potential difference produced across this region, leads to an increase in the electron current arriving at the anode surface. Large anodes may collect a random electron current in excess of the external circuit current. A region of positive space charge may develop and produce a negative potential difference in front of the anode (Francis 1956). The electron current to the anode therefore decreases and current continuity between the discharge and the external circuit is maintained.

A1.2.2) Variations in appearance due to changes in the ambient physical conditions.

The appearance of the discharge is affected by the physical conditions, for example, the pressure, and the electrode separation.

a) Pressure. An increase in pressure causes the negative regions (A1.2.1) to decrease in thickness. They move closer to the cathode, leaving the positive column to fill the remainder of the tube. Eventually it appears to fill the

whole tube (≈ 100 torr). With further increase in the pressure the column starts to contract radially.

When the pressure is reduced to values below about one torr, the negative regions become larger, and the boundaries between them become more diffuse. The positive column disappears, followed by the anode glow as the Faraday dark space moves towards the anode. When the negative glow finally disappears, the discharge is extinguished, unless the applied voltage is increased. The discharge is said to be "obstructed". At these low pressures (≈ 0.01 torr) the length of the cathode dark space (for the normal glow discharge) is greater than the electrode separation. If the voltage is increased in order to maintain the discharge, beams of high energy electrons are observed to come from the cathode. These cause the tube walls to fluoresce and produce soft X rays. Beams of positive ions (canal rays) may also be produced, which travel towards the cathode.

b) Electrode separation. When the electrode separation is increased, at constant pressure, the positive column expands to fill the tube and is accompanied by a slight increase in the sustaining voltage. When the electrode separation is reduced, the potential falls until the separation is of the order of the CDS, then the voltage rises rapidly. If the external circuit will not allow this increase, the discharge is extinguished (obstructed discharge).

c) Current and Potential. For the normal glow discharge, the voltage remains constant as the current increases. The

cathode glow expands over the surface of the cathode, thus the current density at the cathode remains at a constant value. Once the glow covers the whole of the cathode any further increase in current leads to an increase in voltage. This is the region of the "abnormal" glow discharge.

d) Gas. The colour of the discharge depends on the gas used. The colours of the negative glow and the positive column are usually different (Francis 1956). In air, for example, the glow is purple and the column is pink (see cover plate). These colours depend on the purity of the gas and are different in the two regions due to the different electron energy distributions in the glow and the column.

Atomic gases tend to have lower sustaining voltages than molecular gases. The normal cathode and anode falls also depend on the gas, the anode fall being of the order of the ionisation potential of the gas.

e) Cathode material. The cathode material is one of the factors which determine the cathode fall in potential. In general, materials which emit electrons easily (they have a low work function) have the lower values of cathode fall. For example, the work functions of Sodium and Copper are 2.3 volts and 4 volts, respectively; for discharges in air the normal cathode falls are (Na) 200 volts and (Cu) 370 volts (Francis 1956).

A1.3) Theory of the positive column.

The energy balance equation in chapter 2 is derived from the equivalence of the power input to the power lost to the walls, in the positive column of the discharge. The axial electric field referred to throughout is that in the column. It is therefore appropriate to give the simple theory of the positive column. The following assumptions are made;

a) The electron and positive ion number densities (in the main body of the column) are approximately equal, that is to say we are dealing with a quasi-neutral plasma.

b) A Maxwellian distribution is used for the electron energy, which allows an electron temperature to be assigned to the discharge.

c) The electron temperature is independent of radial position within the plasma.

d) The rate of ion production is proportional to the electron number density.

e) The Boltzmann equation for energy distribution is valid.

f) The discharge current and the tube radius are known quantities.

A1.3.1) The radial electron/ion number density distribution.

Under the conditions in the positive column in the low current glow discharge, Schottky diffusion theory is used to determine the radial electron/ion number density

distribution. Electrons and ions diffuse to the walls at the same rate - ambipolar diffusion.

A1.3.1.1) Ambipolar diffusion coefficient.

The continuity of particle flux equations for ions and electrons are given by

$$Nv = -D_e(dN/dr) - N\mu_e E, \quad \text{electrons}$$

$$Nv = -D_i(dN/dr) + N\mu_i E, \quad \text{ions}$$

where D represents the diffusion coefficient, μ the mobility, v the ambipolar velocity and E the radial electric field, produced by charge separation due to the higher mobility of the electrons. Eliminating E from the equations we find,

$$Nv = -D_a(dN/dr),$$

where D_a is the ambipolar diffusion coefficient given by

$$D_a = (D_e\mu_i + D_i\mu_e)/(\mu_i + \mu_e).$$

Using Einstein's relationship ($D/\mu = kT/e$) and noting that in the positive column we have $T_e >> T_i$, and $\mu_e >> \mu_i$ we obtain an approximation for D_a,

$$D_a = \mu_i kT_e/e.$$

A1.3.1.2) Number density distribution.

Using assumption (a) we have

$$dN_+/dr \approx dN_-/dr = dN/dr. \qquad (A1.1)$$

The ambipolar diffusion equation gives,

$$Nv = -D_a\, dN/dr, \qquad (A1.2)$$

where v is the ambipolar velocity and D_a is the ambipolar diffusion constant. The number of ion pairs entering a volume element of thickness dr, and unit length, at a distance r from the axis, per second, is,

$$-2\pi r D_a (dN/dr)_r \qquad (A1.3)$$

and the number of pairs leaving the volume, at a distance (r + dr) from the axis is,

$$-2\pi(r + dr)D_a(dN/dr)_{(r + dr)}. \qquad (A1.4)$$

$$\approx -2\pi(r + dr)D_a(dN/dr + dr.(d/dr)(dN/dr)).$$

The net number leaving the shell, y_1, is,

$$y_1 \approx -2\pi D_a r[(d^2N/dr^2 + (1/r)dN/dr)]dr. \qquad (A1.5)$$

From assumption (d), the number of ion pairs, y_o, created in the shell, per second, is

$$y_o = 2\pi r(dr)Nz, \qquad (A1.6)$$

where z is the number of ionising collisions an electron makes each second. In equilibrium, we can equate (A1.5) to (A1.6), and we derive the equation,

$$d^2N/dr^2 + (1/r)dN/dr + (z/D_a)N = 0 \qquad (A1.7)$$

The solution of equation (A1.7) is a zero order Bessel function J_o, thus we find,

$$N/N_o = J_o(r(z/D_a)^{1/2}). \qquad (A1.8)$$

Where N_o is the electron/ion number density on the axis (r=0). We assume that at the walls (r=R) the number density is zero. The first zero of the zero order Bessel function Jo(x) is at $x \approx 2.4$. Therefore we have,

$$R(z/D_a)^{1/2} \approx 2.4 \qquad (A1.9)$$

Substituting (A1.9) into (A1.8) gives

$$N = N_oJ_o(2.4(r/R)). \qquad (A1.10)$$

This radial dependence has been measured experimentally, and is valid up to the region of the positive ion sheath.

A1.3.2) The electron temperature.

The relationship between the electron temperature and the tube radius and gas pressure has been derived by Von Engel (1965). He starts by finding the rate of ionisation per electron, z, used previously,

$$z = FpW(1 + x/2)\exp(-x). \qquad (A1.11)$$

where $F = 2am_e/\pi^{1/2}$, $W = (2kT_e/m_e)^{3/2}$ and $x = eV_i/kT_e$, p is the pressure, a is a constant, and V_i is the ionisation potential. The ionisation rate is also given by equation (A1.9) and the ambipolar diffusion coefficient is given approximately by=-09,

$$D_a = \mu_+ kT_e/e, \qquad (A1.12)$$

where μ_+ is the ionic mobility. Assuming that $eV_i/2kT_e$ is much greater than 1, equations (A1.9), (A1.11) and (A1.12) give a relationship between the electron temperature, and the radius and pressure. We find,

$$(kT_e/eV_i)^{1/2}\exp(eV_i/kT_e) \approx C(pR)^2. \qquad (A1.13)$$

C is a constant whose value depends on the units used.
(Note: The above theory fails at small values of pR (free-fall regime) and large p (constricted column), and has ignored the effects of recombination and multistage ionisation.)

A1.3.3) The axial electric field.

In chapter 2 we used the energy balance equation to determine differences in the plasma parameters in tubes with insulating or conducting walls. Another form of the energy balance equation may be obtained by equating the energy that electrons gain from the field with that which they lose by collision with gas particles. It is assumed that the electrons lose a fraction f, of their energy at each collision, therefore we have,

$$eXv_d \approx f(mc^2/2)(c/\Gamma_e) \approx f[(3/2)(kT_e)(c/\Gamma_e)], \quad (A1.14)$$

where X is the axial field, v_d is the drift velocity, c is the mean velocity, c^2 is the mean square velocity, Γ_e the electron mean free path, thus c/Γ_e is the collision frequency. Von Engel (1965) has found (for, $c>>v_d$), that,

$$v_d/c \approx (f/2)^{1/2} \quad (A1.15)$$

In many cases, for example Helium at several torr, with T_e = 60,000 K and X/p = 400 V/cm.torr (Cherrington 1979), the condition that the mean velocity is very much greater than the drift velocity is valid ($v_d \approx 0.02c$). However measurements by Stephens and Allen (1976) have found values of $v_d \approx 0.1c$ in argon discharges.

From (A1.14) and (A1.15) we find,

$$X \approx 3(f/2)^{1/2}(kT_e/e\Gamma_e) \qquad (A1.16)$$

With $\Gamma_e = \Gamma_1/p$, where Γ_1 is the mean free path at one pascal, we find an expression for the electric field in terms of the electron temperature and the gas pressure.

$$X/p \approx 3(f/2)^{1/2}(kT_e/e\Gamma_1) \qquad (A1.17)$$

In the rare gases, at low electron temperatures, we would expect there to be few inelastic collisions and $f \approx 2m_e/M$, where M is the atomic mass ($f < 10^{-3}$). This gives small values of the electric field. As the pressure falls the electron temperature increases and more inelastic collisions occur, f increases, and thus the elecric field is larger. The (average) fraction f can be of the order 0.5 in exciting and ionising collisions.

In molecular gases the electron temperatures are low because of the numerous inelastic collisions between electrons and molecules. However the fraction of energy f, lost per collision may be large ($f>2\times10^{-3}$). Hence, X/p is larger in molecular gases, than the values in rare gases, by a factor of ten or more.

A1.3.4) Electron temperature when $\Gamma_+ \geq R$.

In ion laser discharges at low pressure (and small tube radius) the ions and electrons move to the walls making few

collisions with neutral molecules. The collisions are, however, numerous enough to replace the charges lost to the walls, and to produce a Maxwellian energy distribution of electrons. The walls are negatively charged with respect to the plasma.

We assume that the ions have a velocity v_i, in the direction of the walls (appendix 3) given by,

$$v_i \approx (2kT_e/M)^{1/2}. \qquad (A1.18)$$

We equate the rate of creation of charge to the rate of loss to the walls. The rate of loss, z_i, is given by,

$$z_i \approx v_i/R = (2kT_e/M)^{1/2}/R. \qquad (A1.19)$$

The rate of creation is given by (A1.11) (with $eV_i/2kT_e >> 1$), and equating this with (A1.19) we find,

$$(eV_i/kT_e) = \ln(apR(4M/\pi m_e)^{1/2}.eV_i) \qquad (A1.20)$$

References.

K.G. Emeléus. "The conduction of electricity through gases." Methuen and Co. Ltd. 1951.

G. Francis. "The Glow Discharge at Low Pressure". Handbuch der Physik, Vol. 22, ed. Flugge S.,Springer-Verlag, 1956.

A. Von Engel. "Ionized Gases". 2nd Ed., Clarendon Press, Oxford 1965.

B.E. Cherrington. "Gaseous electronics and gas lasers"

Pergamon Press Ltd., Oxford, 1979.

F.D. Stephens and J.E. Allen. "Axial wall currents in cylindrical metal discharge vessels." Gas Discharges IEE Conference Publication 143, 1976, p 331

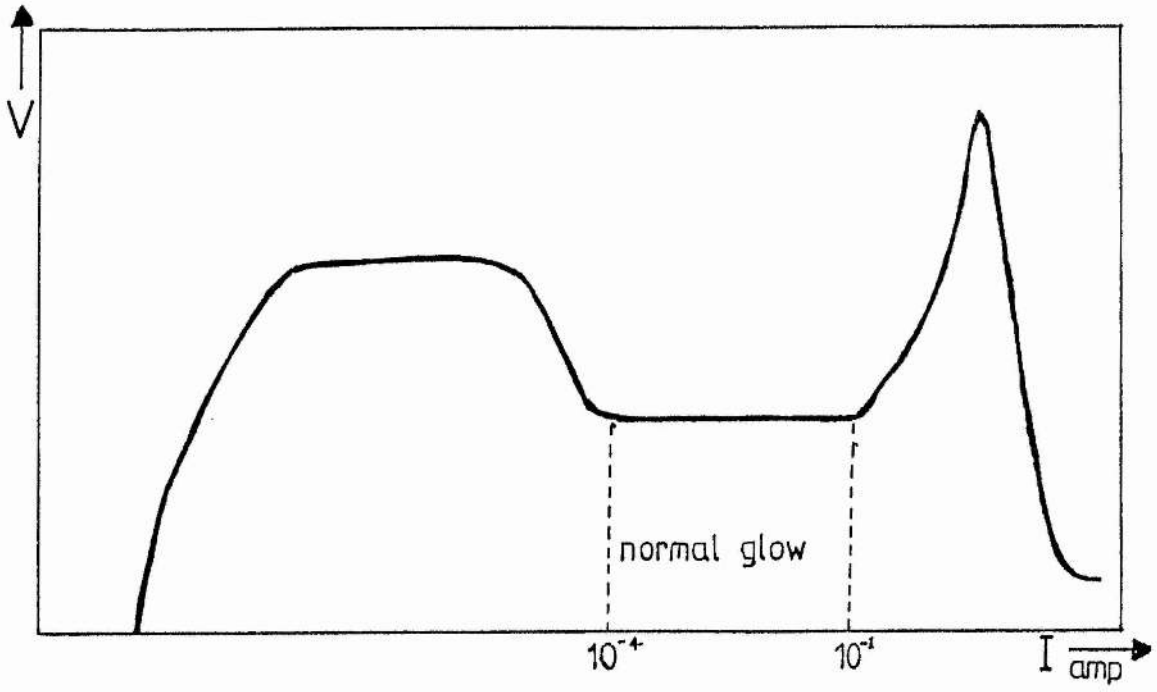

Figure A1.1 Variation of tube potential with current in a gas discharge.

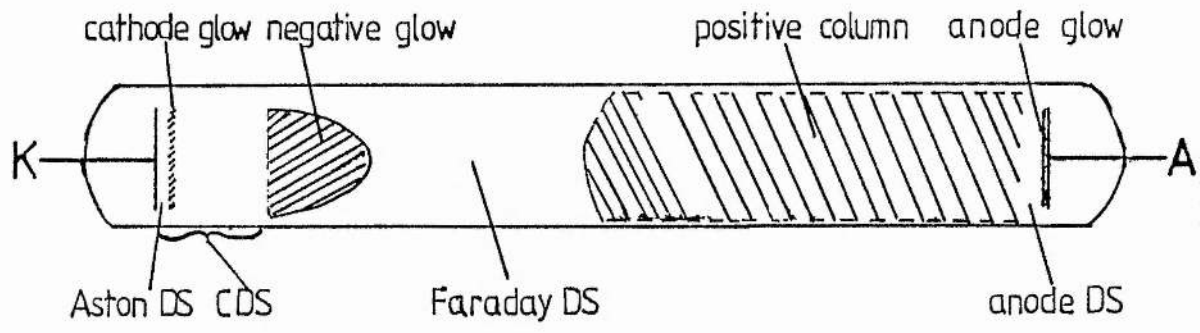

Figure A1.2 Structure of a glow discharge.

APPENDIX 2.

The Debye shielding length.

The Debye length is defined as the distance at which the potential of a charge perturbation (where the neutrality of a plasma is disturbed) falls to 1/e (e is the base the natural log) of its initial value. A sheath of opposite charge forms around a charge perturbation. The perturbation is screened by the sheath and the potential of the perturbation is attenuated by the charges of opposite sign. Debye sheaths form between the plasma, and the walls of a gas discharge vessel. (An ionised gas may be regarded as a plasma if the Debye length is a lot less than the dimensions of the discharge vessel.)

Let us consider a perturbation in the charge neutrality of the plasma caused by an electron grouping situated at x=0, at a potential V(0) (negative in this case) with respect to the plasma. We want to calculate how the potential varies with distance x. If the perturbation is fast, and only remains for a short time then the density of the ions remains constant, whereas the electrons assume a Boltzmann distribution about the charge. Poisson's equation may be written as,

$$d^2V/dx^2 = -(en/\epsilon_\infty)[1 - \exp(eV(x)/kT_\infty)], \qquad (A2.1)$$

where we have assumed that the electron number density is equal to the positive ion number density (n) at infinity.

This equation may be solved in the limit $eV(x) << kT_e$, that is to say, for small perturbations in potential. (This limit is invalid close to x=0 where V(x) varies rapidly). Expanding the exponential in (A2.1) we have,

$$d^2V/dx^2 \approx (en/\epsilon_0)[eV(x)/kT_e] \qquad (A2.2)$$

We may solve (A2.2) and find

$$V(x) = V(0)\exp(-x/l_D). \qquad (A2.3)$$

Where l_D is the Debye screening length, given by

$$l_D = (\epsilon_0 kT_e/ne^2)^{1/2}. \qquad (A2.4)$$

Shielding by the plasma becomes incomplete when the electrostatic potential energy reduces to the thermal energy of the electrons and ions. The electrons and ions are then able to escape from the sheath region around the perturbation. Therefore, at the edge of the sheath where $|eV(x)|$ is of the order of kT_e, voltages of $\approx kT_e/e$ can penetrate into the plasma. This value of $|eV(x)|$ violates earlier assumptions in the derivation of equation (A2.4), therefore care must be taken when using the shielding length.

References.

B. Chapman "Glow discharge processes." John Wiley and Sons, New York, 1980.

J.D. Swift and M J R Schwar. "Electrical probes for plasma diagnostics." London ILIFFE Books Ltd, 1970.

APPENDIX 3.

The Bohm criterion.

The positive ion current density at the wall is defined in section (2.3.1). It can be seen that the current density is a function of the electron temperature in the plasma. As this dependence on the electron temperature is not obvious, the following theory is given to explain the relationship.

Any surface in contact with a plasma acquires a negative charge, which leads to a positive ion sheath forming adjacent to the surface (region 2, figure (A3.1)). Between the plasma and the sheath is a quasi-neutral region (region 1, figure (A3.1)) penetrated by a low electric field. This tends to give a small directed velocity to ions entering the sheath.

We shall make the following assumptions in the derivation of the criterion;

a) At $x = 0$, the sheath boundary, (see figure (A3.1)) the number of ions ($n(0)$) is equal to the number of electrons.

b) The sheath is collisionless, therefore there are no ionisation processes, and the ion current density j_+, is constant

$$j_+ = en(x)u(x). \qquad (A3.1)$$

The positive ion flux is constant even though the velocity and number density might change.

From the conservation of energy for the ions, we find that the velocity at a point x, u(x), is given by,

$$u(x) = (u(0)^2 - (2e/m_+)[V(x) - V(0)])^{1/2}, \qquad (A3.2)$$

where V(0) is the potential of the sheath boundary with respect to the plasma and V(x) is the potential at the point x, within the sheath.

From the conservation of ion flux, we have

$$n_+(x) = n(0)u(0)/u(x)$$
$$= n(0)(1 - (2e/m_+)[V(x) - V(0)]/u(0)^2)^{-1/2}. \qquad (A3.3)$$

The electrons assume a Boltzmann distribution given by

$$n_-(x) = n(0)\exp[e(V(x) - V(0))/kT_-]. \qquad (A3.4)$$

Poisson's equation may be written as,

$$d^2V/dx^2 = -(e/\epsilon_0)[n_+(x) - n_-(x)]. \qquad (A3.5)$$

For a positive-ion space-charge sheath, d^2V/dx^2 is negative. Therefore, from equations (A3.3), (A3.4) and (A3.5) we have,

$$(1-(2e/m_+)[V(x)-V(0)]/u(0)^2)^{-1/2} > \exp[e(V(x)-V(0))/kT_-]$$

Squaring and inverting, we find

$$(1-(2e/m_+)[V(x)-V(0)]/u(0)^2) < \exp[-2e(V(x)-V(0))/kT_-].$$

We can expand the potential at points where V(x)-V(0) is small. This finally leads to,

$$m_+u(0)^2 > kT_e. \qquad (A3.6)$$

The Bohm criterion (Bohm 1949) states that there is a minimum value of the initial velocity of the ions u(0), for the formation of a positive ion sheath. This minimum value is given by

$$u(0) > (kT_e/m_+)^{1/2}. \qquad (A3.7)$$

Thus the ions must acquire this directed velocity as they travel across the quasi-neutral pre-sheath region. The potential across this region is thus

$$|V(0)| \approx m_+u(0)^2/2e \approx kT_e/2e, \qquad (A3.8)$$

where we have assumed that the directed velocity at the boundary of the pre-sheath region and the plasma is zero. As potentials of the order of kT_e/e may "leak" into the plasma (see Debye shielding), this does not contradict the assumption that $n_e(0)=n_+(0)=n$.

The ion flux at the sheath boundary may be found from the following. At the boundary, the electron density is given by,

$$n_e(0) = n_e\exp(-eV(0)/kT_e), \qquad (A3.9)$$

where n_- is the electron number density in the plasma. We know V(0) from equation (A3.8), therefore we have for $n_-(0)$,

$$n_-(0) \approx 0.6n_- \qquad \text{(A3.10)}$$

As we have already assumed that $n_-(0) = n_+(0)$, from equation (A3.8) we find the ion flux at the boundary to be,

$$n_+(0)u(0) \approx 0.6n_-(kT_-/m_+)^{1/2}. \qquad \text{(A3.11)}$$

Thus we can see that the ion flux at the sheath boundary depends on the electron temperature and not on the ion temperature in the plasma.

References.

D. Bohm "The characteristics of electrical discharges in magnetic fields." ed. A. Guthry and R.K. Wakerling, McGraw-Hill, New York, (Ch. 3, p 77) 1949.

B. Chapman "Glow discharge processes." John Wiley and Sons, New York, 1980.

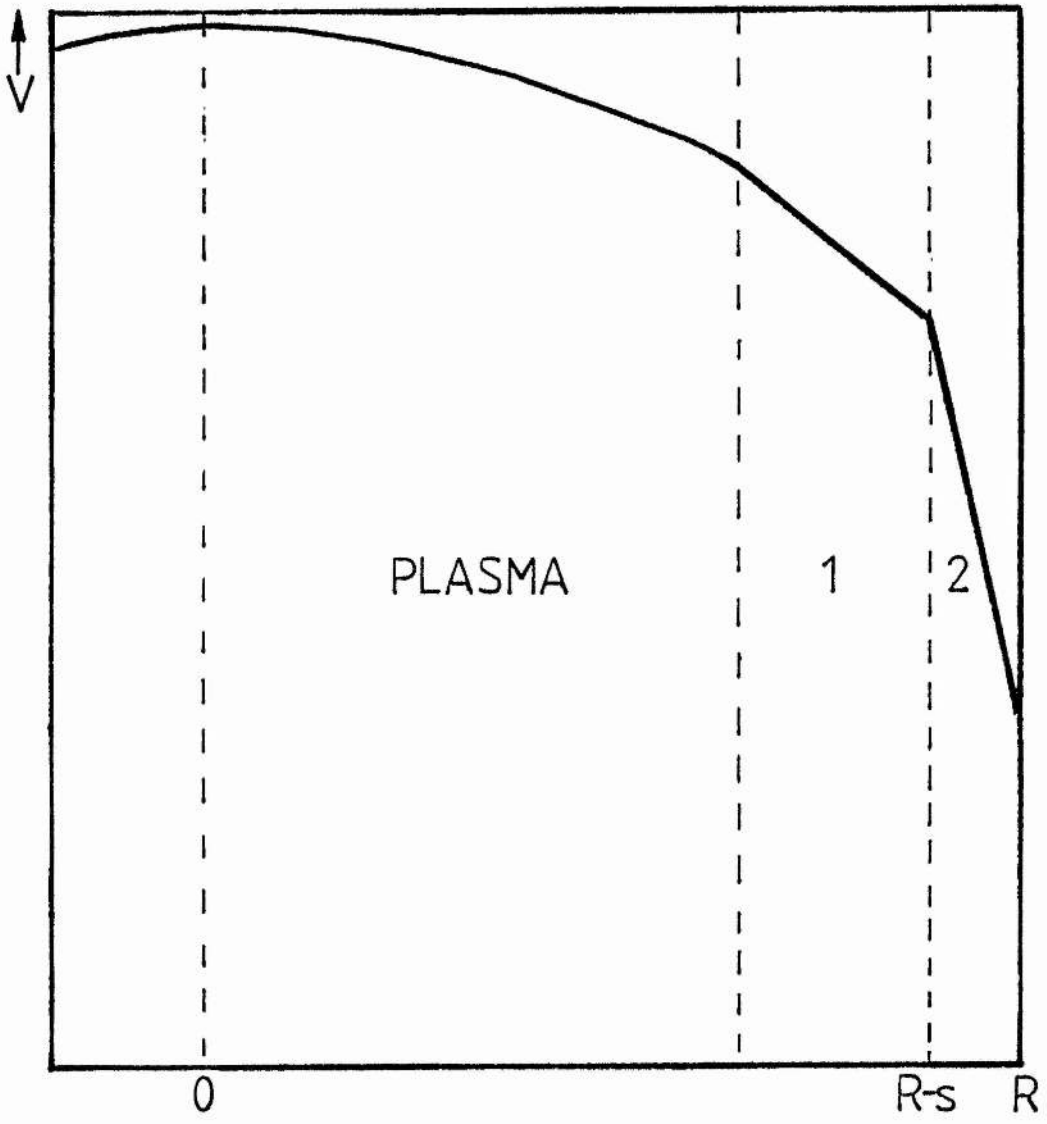

Figure A3.1 Radial potential distribution (not to scale).
1 - Quasi-neutral pre-sheath region.
2 - Positive ion sheath.

APPENDIX 4.

Solution of Poisson's equation in the positive ion sheath.

A4.1) Charged particle number density within the sheath.

In low pressure gas discharges, at high current densities, we have a thin (≈0.1mm) positive ion sheath between the plasma and the walls of the discharge vessel. The sheath thickness is very much smaller than the mean free paths for electron-neutral (λ_{en}) and ion-neutral (λ_{in}) collisions (Dunn and Ross 1976). We also assume that recombination is negligible within the sheath. A thin sheath, between the plasma and the wall, in a vessel with cylindrical geometry, may be approximated by a sheath with planar geometry. This is because the surface area of the plasma-sheath boundary is approximately equal to the surface area of the wall for a thin sheath.

The wall charges negatively with respect to the plasma to equalise the electron and ion currents to it. Any potential V(r), within the sheath, is negative with respect to the potential at the plasma-sheath boundary, $V(r_s)$. The electron number density assumes a Boltzmann distribution,

$$n_e(r) = n.\exp(-c(V(r_s)-V(r))), \qquad (A4.1)$$

where n is the electron/ion number density in the plasma and $c = e/kT_e$.

The ion flux at any point in the sheath (radially

outwards towards the wall) is determined by the ion flux at the plasma-sheath boundary, so, we have

$$n_+(r)v_+(r) = nv_+(r_m). \qquad (A4.2)$$

Also, by conservation of energy,we get

$$v_+^2(r) = v_+^2(r_m) + (2e/m_+)(V(r_m)-V(r)). \qquad (A4.3)$$

Using the Bohm criterion (Bohm (1949) and Appendix 3), we take $v_+^2(r_m) \approx (kT_e/m_+)$. Thus, using equations (A4.2) and (A4.3) we can solve (A4.2) for $n_+(r)$ in terms of the potential and we get,

$$n_+(r) = n\{1 + 2c(V(r_m)-V(r))\}^{-1/2}. \qquad (A4.4)$$

Approximations for $n_+(r)$ may be found for the following cases;

a) $(V(r_m)-V(r))$ small.(Near the plasma-sheath boundary.)

In this case we find,

$$n_+(r) \approx n\{1 - c(V(r_m)-V(r))\}. \qquad (A4.5)$$

b) $(V(r_m)-V(r))$ large.(Near the walls.)

The positive ion density approximates to

$$n_+(r) \approx n(2c(V(r_m)-V(r))^{-1/2}\{1-[4c(V(r_m)-V(r))]^{-1}\} \qquad (A4.6)$$

However if the difference $(V(r_\infty)-V(r))$ is very large, we have

$$n_+(r) \approx n\{2c(V(r_\infty)-V(r))\}^{-1/2}. \qquad (A4.7)$$

We may use the above approximations to determine the electric field and, in some cases, the "radial" potential distribution (with respect to the plasma) within the sheath.

A4.2) Solution of Poisson's equation within the sheath.

Let $V'(y)$ be the first derivative of V with respect to y and let $V''(y)$ be the second derivative. The one-dimensional form of Poisson's equation may be used, as for a thin sheath, the geometrical decrease of number density with radius is small. Poisson's equation may be written as

$$V''(y) = f(V). \qquad (A4.8)$$

To calculate the field distribution, we multiply both sides of equation (A4.8) by $2V'(y)$ and integrate with respect to y to get,

$$[V'(y)_y]^2 - [V'(y)_o]^2 = \int_{V(0)}^{V(y)} 2f(V)dV, \qquad (A4.9)$$

where $V'(y)_o$ is the electric field, E_o, at y=0. We may now solve Poisson's equation using equation (A4.9).

i) Solution in the general case.

Poisson's equation, (A4.8), may be written as,

$$V''(r) = -K(n_+(r) - n_-(r)), \qquad (A4.10)$$

where we have $K=e/\epsilon_0$ and $\epsilon_0(=8.85\times10^{-12}$ F/m) is the permitivity of free space. Writing $r \equiv y$, $r_m \equiv (y = 0)$ and $V(r_m) \equiv 0$, using equations (A4.1) and (A4.4) we get,

$$V''(y) = Kn\{ \exp(cV(y)) - (1 - 2cV(y))^{-1/2}\}. \qquad (A4.11)$$

Using equations (A4.9) and (A4.11) we get,

$$(V'(y))^2-E_0^2 = (2Kn/c)\{ \exp(cV(y))+(1-2cV(y))^{1/2} -2\}. \qquad (A4.12)$$

We assume a pre-sheath region of radial dimension equal to the Debye length, $l_D=(kT_e\epsilon_0/ne^2)^{1/2}$ and potential $\approx (kT_e/e)$. This gives an approximate value for E_0, the radial electric field at y=0.

$$E_0\approx(kT_e/el_D) \approx 1.2\times10^{-8}(nT_e)^{1/2} \text{ V/m}.$$

Since this value of E_0 is equivalent to $(Kn/c)^{1/2}$, equation (A4.12) becomes,

$$V'(y) = E_0\{2[\exp(cV(y)) + (1-2cV(y))^{1/2}]-3\}^{1/2}. \qquad (A4.13)$$

This equation cannot be solved analytically so we can use the approximations previously derived (equations (A4.5), (A4.6) and (A4.7)).

(ii) $|V(y)|$ is small.

In this case we expand to terms in $V(y)^3$ to obtain,

$$V'(y) \approx E_\infty\{1 - 2(cV(y))^3/3\}$$
$$\approx E_\infty. \qquad (A4.14)$$

Thus, we find,

$$V(y) \approx E_\infty y. \qquad (A4.15)$$

Therefore, near to the plasma-sheath boundary the potential varies linearly.

iii) $|V(y)|$ is large.

In this case we assume that the electron term is approximately equal to zero and we are left with the much larger ion term. Equation (A4.13) becomes,

$$V'(y) \approx E_\infty\{2(-2cV(y))^{1/2} - 3\}^{1/2}. \qquad (A4.16)$$

We may integrate this further by the substitution, $(-V(y))=Y^4$, which finally gives,

$$y \approx A^{1/2}[4(-V(y))^{3/4}/3 + 6A(-V(y))^{1/4}]/E_\infty, \qquad (A4.17)$$

where we have put $A = [2(2c)^{1/2}]^{-1}$.

For large V, we find,

$$y^2 \approx (8\epsilon_0/9n)(2ekT_e)^{-1/2}(-V(y))^{3/2}, \qquad (A4.18)$$

or

$$y^2 \approx (4\epsilon_0/9j)(e/2m_+)^{1/2}(-V(y))^{3/2}, \qquad (A4.19)$$

where the current density j is given by $j=(ne/2)(kT_e/m_+)^{1/2}$. Equation (A4.19) is the well-known Child-Langmuir law (Child 1911, Langmuir 1913). When V(y) is equal to the wall potential V(R), then y is equivalent to the positive ion sheath thickness s. We may use equations (A4.16) to (A4.19) where V is large, that is to say, in regions close to the wall.

References.

M.H. Dunn and J.N. Ross. "The Argon ion laser." Prog. Quant. Electr., 4, 1976, p 233.

D. Bohm "The characteristics of electrical discharges in magnetic fields." ed. A. Guthry and R.K. Wakerling, McGraw-Hill, New York, (Ch. 3, p 77) 1949.

C.D. Child. Phys. Rev.I, 32, 1911, p 492.

I. Langmuir. "The effect of space charge and residual gases on thermionic currents in high vacuum." Phys. Rev.II, 2, 1913, p 450.

APPENDIX 5.

Paschen's law.

In chapter 7 we use an expression for Paschen's law (Paschen 1889), to calculate the breakdown voltage of a tube containing brass cups. Paschen's equation for plane parallel, infinite electrodes is given by Von Engel (1965). His derivation of the equation is as follows.

A simple expression for the first Townsend ionisation coefficient, α (the number of ionising collisions per cm of path) is,

$$\alpha/p = A\exp(-B/(X/p)), \qquad (A5.1)$$

where p is the gas pressure (torr), X is the axial electric field (V/cm), and we have

$$A = 1/l_1 \; ; \quad B = Vi/l_1,$$

where l_1 is the free ionising path at 1 torr, and Vi the ionisation potential in volts. The assumptions used in the derivation are:-

a) An electron is certain (probability 1) to produce an ionising event once its energy has exceeded the ionisation energy.

b) An electron starts each free path with an energy small compared with the ionisation energy.

c) Non-ionising collisions are ignored.

These assumptions mean that the experimental and theoretical

values of A and B differ. (Rather than consider the theoretical values of A and B, we should consider their physical meaning. We may regard A as a saturation value for α/p at large X/p, and B is proportional to an effective ionisation potential, which takes other collision processes into account.)

From breakdown theory, the criterion for a self sustaining discharge is

$$\gamma(\exp(\alpha d) - 1) = 1, \qquad \text{(A5.2)}$$

where γ is the second Townsend ionisation coefficient (the number of secondary electrons produced by each positive ion arriving at the cathode). Replacing α in equation (A5.2) by (A5.1) gives,

$$X_b/p = B/(\ln(pd) + C), \qquad \text{(A5.3)}$$

where X_b is the field at breakdown and C is given by

$$C = \ln\{A/\ln(1 + 1/\gamma)\}.$$

If we assume a uniform electric field we may write $X_b=V/d$, where V is the breakdown potential, and we rewrite (A5.3) as,

$$V = Bpd/(\ln(pd) + C). \qquad \text{(A5.4)}$$

References.

F. Paschen. Wied. Ann. 37, 1889, p 69.

A. Von Engel. "Ionized Gases". 2nd Ed., Clarendon Press, Oxford, 1965.

APPENDIX 6.

Negative dynamic impedance - Its causes in gas discharges.

The gas discharges described in chapters 5 and 8, have a negative dynamic impedance at low currents. The discharge voltage is seen to decrease as the current increases. To see how this may occur, we consider the basic discharge processes.

Ionisation in gases may proceed via two processes, either:

a) Direct ionisation, see equation (A6.1) where the rate of increase of electrons (or ions) is directly proportional to the current. OR

b) Cumulative ionisation, for example two step ionisation as in equation (A6.2), where the rate of increase of charged particles is proportional to the square of the current. Thus for n step ionisation the production rate is proportional to the n^{th} power of the current.

Direct ionisation $(dN_e/dt) \propto N_eN \propto IN.$ (A6.1)

Cumulative ionisation $(dN_e/dt) \propto N_eN^* \propto N_e^2N \propto I^2N.$ (A6.2)

Where N is the neutral particle density, N_e is the electron (ion) density, N^* the density of excited particles and I is the current.

When direct ionisation is the dominant process, the voltage remains approximately constant as the current

increases, at a level whereby the electrons have enough energy to ionise at each collision.

For two step ionisation the production rate is proportional to the square of the current. It can be seen that if the current doubles then the rate quadruples; four times as many electrons are produced in the case of 2I as opposed to I.

If we ignore loss processes, we may apply the following argument. The discharge current I, is proportional to the voltage V, across the discharge and the electron density N_e. That is to say, we have

$$I = KN_eV, \qquad \text{(A6.3)}$$

where K is a constant. For two currents I_1 and I_2, equation (A6.3) gives

$$(I_1/I_2) = (N_{e1}/N_{e2})(V_1/V_2). \qquad \text{(A6.4)}$$

As the electron density is proportional to the rate of electron production, we use equations (A6.2) and (A6.4), and get,

$$(I_1/I_2) = (I_1/I_2)^2(V_1/V_2)$$

or

$$(I_2/I_1) = (V_1/V_2). \qquad \text{(A6.5)}$$

If we let I_2 equal $2I_1$ in equation (A6.5), we find

$$V_2 = (V_1/2). \qquad (A6.6)$$

Thus, we see that for two stage ionisation the discharge voltage falls as the current increases.

From equation (A6.5) we have,

$$VI = \text{constant} = F. \qquad (A6.7)$$

Differentiating equation (A6.7) we find

$$dV/dI = -F/I^2. \qquad (A6.8)$$

As F and I^2 are positive then dV/dI is always negative.

Usually both direct and cumulative ionisation are present in a gas discharge, the relative amounts of each determining the actual shape of the Voltage-Current characteristic.

General Reference.

W. Elenbaas. "Light sources." (Phillips) The Macmillan English Press Ltd., 1972.

APPENDIX 7.

Discharge stabilisation.

In order to obtain stable discharges, it may be necessary to include resistors in series with the discharge tube. These are generally high wattage resistors whose total resistance must be such as to give a total impedance (including the discharge impedance) which is positive. This is because discharges can sometimes exhibit a negative dynamic impedance (appendix 6), where the gradient of the V-I characteristic, dV/dI, may be negative. (When resistors are absent, the discharge tube or the power supply may be severely damaged by a runaway current situation.) Unstabilised and stabilised discharges are considered in the following paragraphs.

Consider the negative characteristic of a discharge obtained without a resistor present, see figure (A7.1a). (The following is based on the work of Elenbaas (1972), Ross (1974) and Papoular (1965).) If the discharge has a voltage V_o applied, then the current will be I_o. This point represents unstable equilibrium, as can be seen from the following argument. If the current increases to I_1 the voltage nescessary to maintain the discharge is V_1, but the voltage is held at V_o, thus an excess voltage dv is applied, and the current increases further. This is a runaway situation which must be avoided, as severe damage may result.

Figure (A7.1b) shows the DC discharge characteristic

plotted with the load-line of a resistor of R ohms. The load-line may be plotted by considering the two points where it intersects with the axes. When there is no current flowing, the power supply voltage E is dropped across the tube, giving the intersection with the V-axis. At the other extreme, when the tube resistance goes to zero, the current flowing through the circuit would be given by E/R, the load-line intersection with the I-axis. The vertical distance from the dashed line (V = E) to the load line gives V_R, the voltage dropped across the resistor at a particular current.

The load-line intersects the curve at two points. The point at A is unstable. Between the points A and B on the curve the power supply voltage is greater than the sum of the voltages, across the resistor, V_R, and the voltage necessary to maintain the discharge, V_D at a particular current, that is to say

$$E = V_R + V_D + dv,$$

where dv is the voltage mismatch.

The other intersection at B is found to be stable from the following considerations. A small increase in current, dI, at B causes a voltage DG to be dropped across the resistor leaving only a voltage GF available for the discharge at this point, therefore dv is negative. This voltage (GF) is not great enough to maintain the discharge at this current so it returns to point B, and then the discharge is stabilised.

Looking at the problem from a mathematical point of view, we may represent the discharge characteristic as:

$$V_D = f(I), \qquad \text{(A7.1)}$$

and the load line by:

$$V_L = E - RI. \qquad \text{(A7.2)}$$

Let V_1, I_1 be the point at which $V_L = V_D$. Near the point (V_1, I_1) we may expand equation (A7.1), thus we obtain

$$V_D = V_1 + (dV/dI)_1 dI + ... \qquad \text{(A7.3)}$$

$$V_D = V_1 + r_1 dI + ... \qquad \text{(A7.4)}$$

Where r_1 is the dynamic impedance $(dV/dI)_1$, and dI is assumed to be positive.

For small fluctuations in current, $(I_1 \rightarrow I_1+dI)$ about (V_1, I_1) we find,

$$E = V_D + V_R + dv$$

$$E = V_1 + r_1 dI + R(I_1 + dI) + dv \qquad \text{(A7.5)}$$

From equations (A7.2) and (A7.5) with $V_L = V_1$ and $I = I_1$ we can calculate the small voltage, dv, produced by the current fluctuation.

$$dv = -(r_1 + R)dI. \qquad \text{(A7.6)}$$

If $(r_1 + R) > 0$, the mismatch voltage, dv, is negative and opposes the current fluctuation, and the discharge is stable.

If $(r_1 + R) < 0$, the mismatch voltage, dv, is positive and reinforces the current fluctuation, and the discharge is unstable.

A load line may be plotted for each output voltage from the power supply, the intersection of each with the discharge characteristic gives the discharge condition for

that supply voltage. In our experiments, with argon-metal vapour discharges, it is at low currents, less than 1 amp, that the discharge tends to become unstable. Figures (5.2), (5.7), and (8.4) show typical discharge characteristics.

General References.

W. Elenbaas. "Light sources."(Phillips) The Macmillan English Press Ltd., 1972.

J.N. Ross. "Oscillation Phenomena in Argon laser discharges." PhD thesis, 1974.

R. Papoular, "Electrical phenomena in gases." Trans. B. Jeffrey, ed. D.L. Jones, London ILIFFE Books, 1965.

Figure A7.1 DC gas discharge V-I characteristics.

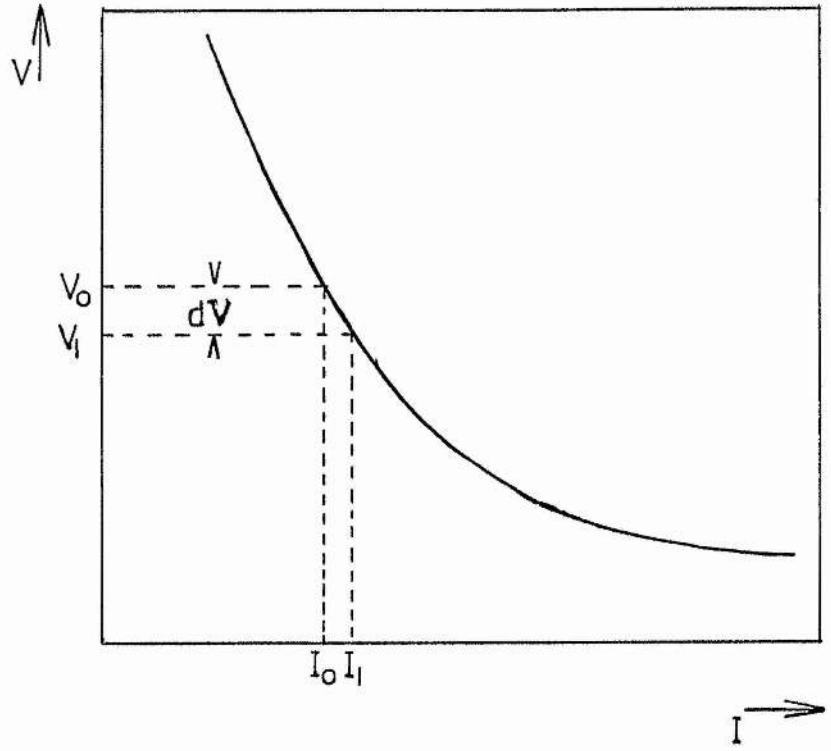

a) V-I characteristic of a gas discharge exhibiting a negative dynamic impedance.

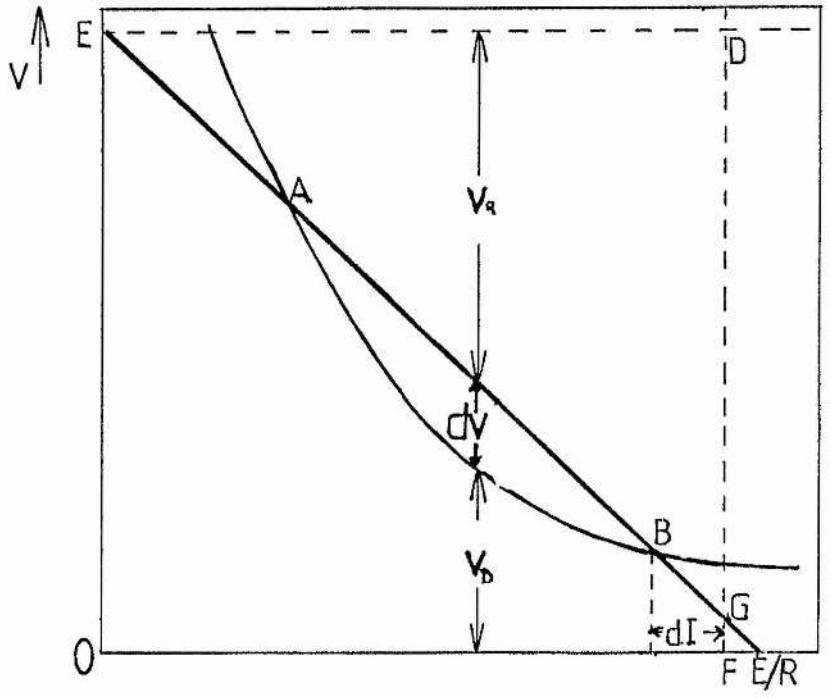

b) V-I characteristic of a gas discharge and load-line of stabilising resistor.

APPENDIX 8.

Electron temperatures in conducting walled tubes.

A8.1) Introduction.

In the theory given in chapter 2 (high current density discharge) we assumed that the electron temperature (T_{ee}) in a discharge with insulating walls is the same as the electron temperature (T_{em}) in a discharge with conducting walls (at the same current and pressure). Von Engel (1965) has found that the electron temperature is proportional to the axial electric field (constant pressure) in the discharge. The axial electric field in a discharge in a metal tube has been shown to be higher than that in an insulating tube so we can expect that the electron temperature is also higher. We can now modify the theory of sections (2.3.3) and (2.5) to account for this difference in electron temperature.

A8.2) Equivalence of wall potentials.

In section (2.3.3) we found the axial position (x) at which the potential difference V(x), across the positive ion sheath, at the wall of a metal segment, is equal to the potential difference V_w, across the sheath at an insulating wall. If we now take into consideration the fact that the electron temperatures in the metal-walled and ceramic-walled discharges are not equal, we can find, from equations

(2.3.4) and (2.3.10), the position at which $V_w = V(x)$. Thus we find,

$$(x/L)=(1/Y_m)[(1-(T_{eo}/T_{em}))(\ln(M))+\ln((\exp(Y_m)-1)/Y_m)], \qquad (A8.1)$$

where Y_m equals (eX_mL/kT_{em}) and M equals $(2m_+/\pi m_e)^{1/2}$. It can be seen that equation (A8.1) reduces to equation (2.3.11) when T_{em} is equal to T_{eo}. In section (2.3.3) we showed that x/L is greater than or equal to 0.5, that is, that the second term of equation (A8.1) is greater than or equal to 0.5. As the first term of equation (A8.1) is always greater than or equal to zero, then the position where we have V(x) equal to V_w is closer to the cathode end of the segment (that is x/L > 0.5) than the position given by equation (2.3.11).

A8.3) Energy balance.

In section (2.5), we stated (equation (2.5.1)) that

$$I_mX_m = I_mX_o + S,$$

where we have written I_mX_o after assuming that the electron temperatures, T_{em} and T_{eo}, are equal (section (2.7)). As the electron temperatures are not equal, due to their dependence on the axial electric fields, we must reconsider equation (2.5.1) and write it as,

$$I_mX_m = (I_mX_o)_m + S, \qquad (A8.2)$$

where $(I_mX_o)_m$ (for argon) is given by

$$(I_mX_o)_m = 7.2\times10^{-10}\ RnT_{em}^{1/2}(15.7+7.2\times10^{-4}T_{em}). \qquad (A8.3)$$

If we now take the ratio, G, of $(I_mX_o)_m$ (equation (A8.3)) to (I_mX_o) (equation (2.4.9)) we find that

$$G=(T_{em}/T_{eo})^{1/2}(B_m/B_o), \qquad (A8.4)$$

where we have

$$B_p=[Vi+(3kT_{ep}/e)+(kT_{ep}/e)\ln(M)], \quad p = m,c.$$

We can make an estimate of G by assuming the following values; T_{em} = 40000K, T_{eo} = 35000K and Vi = 15.7 volts (Argon), which give G = 1.16. In section (2.5) we showed that S (equation (A8.2)) is always greater than or equal to zero and as $(I_mX_o)_m$ is greater than or equal to (I_mX_o), we can state,

$$(I_mX_m) \geq (I_mX_o). \qquad (A8.5)$$

References.

A. Von Engel. "Ionized Gases." 2nd Ed., Clarendon Press, Oxford, 1965.